Institut für Bio- und Geowissenschaften 2 (IBG-2) Pflanzenwissenschaften
Forschungszentrum Jülich

Remote sensing of crop parameters using UAV-based multispectral imaging and radiative transfer models

Dissertation
zur Erlangung des Grades
Doktor der Agrarwissenschaften (Dr. agr.)
der Agrar-, Ernährungs- und Ingenieurwissenschaftlichen Fakultät
der Rheinischen Friedrich-Wilhelms-Universität Bonn

von

Erekle Chakhvashvili

aus
Tbilissi, Georgien

Bonn 2025

Referent:
Prof. Dr. Uwe Rascher, University of Bonn, Germany

Korreferent:
Prof. Dr. Zbyněk Malenovský, University of Bonn, Germany

Tag der mündlichen Prüfung: 25. April 2025

Erscheinungsjahr: 2025

Angefertigt mit Genehmigung der Agrar-, Ernährungs- und Ingenieurwissenschaftlichen Fakultät der Universität Bonn

For my mom, Eliso

დღისით ჩემს ფიქრებში დასეირნობ,
ღამით ჩემს სიზმრებს აფხიზლებ,
ხოდა, ნუ გამიწყრები

By day, you wander through my thoughts,
By night, you awaken my dreams,
So, please—don't take it to heart.

Eliso Shanidze

Abstract

In the face of climate change and a growing global population, it's important to increase the output of agricultural systems and improve crop resilience to challenging environmental conditions. Achieving these objectives requires monitoring crop health in the field, as well as breeding more resilient crop varieties. However, these tasks are labor-intensive and not economically sustainable. Remote sensing tools, such as uncrewed aerial vehicles (UAVs), have demonstrated their potential to successfully measure crop parameters while minimizing the need for human and financial resources.

The mapping of crop parameters has been widely studied in both the satellite and UAV research communities. The UAV community typically uses data-driven and parametric models to predict crop parameters, while satellites rely on physical models called radiative transfer models (RTMs) to retrieve these variables. However a key drawback of using satellites is their low spatial and temporal resolution for applications in precision agriculture.

This thesis explores the use of radiative transfer model PROSAIL to retrieve crop variables with UAVs and multispectral imaging. First, we examine the reflectance calibration workflows of the optical sensor, vital for time-series image analysis. We propose a multi-panel approach for calibrating reflectance of a multispectral sensor, which our analysis shown to perform better than the one-point calibration. Next we address the challenges of retrieving structural and biochemical variables in complex and homogeneous crop canopies. Our findings confirm that the higher spatial resolution provided by UAVs doesn't disrupt the fundamental assumptions of the PROSAIL, which was originally developed for simpler canopies. Finally, we investigate the sensor synergies for crop stress detection. In one study we explore the synergy between terrestrial laser scanner, multispectral imaging, and RTMs to track drought-induced leaf movement in soybean. We show that it's possible to track leaf orientation using just multispectral cameras. Another study discusses the challenges associated with using multiple sensors together to detect crop stress.

Zusammenfassung

Der fortschreitende Klimawandel und die wachsende Weltbevölkerung erfordern sowohl eine Steigerung der landwirtschaftlichen Produktivität als auch eine verbesserte Widerstandsfähigkeit von Nutzpflanzen gegenüber sich wandelnden Umweltbedingungen. Um diesen Herausforderungen zu begegnen, sind eine zielgerichtete Überwachung von Pflanzenbeständen im Feld als auch die Züchtung widerstandsfähigerer Sorten unverzichtbar. Herkömmliche Methoden der Pflanzenüberwachung sind jedoch zeit- und ressourcenintensiv sowie ökonomisch ineffizient. Fernerkundungstechnologien, wie der Einsatz von Drohnen, bieten großes Potential Pflanzenparameter objektiv und effizient zu erfassen und dabei den Bedarf an personellen und finanziellen Ressourcen zu reduzieren.

Die Anwendung von Satelliten- und drohnenbasierten Ansätzen zur Erfassung von Pflanzenparametern ist bereits intensiv erforscht. Drohnenbasierte Methoden nutzen häufig datengetriebene oder parametrische Modelle, während satellitenbasierte Ansätze physikalische Modelle, sogenannten Strahlungstransfermodelle, einsetzen. Allerdings sind Satelliten durch ihre begrenzte räumliche und zeitliche Auflösung limitiert, was ihre Anwendung in der Präzisionslandwirtschaft erschwert.

Diese Arbeit untersucht die Integration des Strahlungstransfermodells PROSAIL mit drohnengestützter multispektraler Bildgebung zur Bestimmung von Pflanzenvariablen. Im ersten Teil charakterisieren wir das Reflexionsvermögen des optischen Sensors, eine wesentliche Voraussetzung für die zuverlässige Zeitreihenanalyse von Bilddaten. Unsere Studie stellt einen Multi-Panel-Ansatz zur Kalibrierung der Reflektanz eines multispektralen Sensors vor, der sich in unseren Analysen als präziser im Vergleich zur herkömmlichen Einpunktkalibrierung erwiesen hat. In zwei darauf folgenden Publikationen beleuchten wir die Herausforderungen bei der Anwendung von PROSAIL zur Erfassung struktureller und biochemischer Variablen in komplexen und homogenen Pflanzenbeständen. Unsere Ergebnisse zeigen, dass die höhere räumliche Auflösung von Drohnenbildern die Modellannahmen in PROSAIL nicht beeinträchtigt, obwohl das Modell ursprünglich für wenig komplexe Pflanzenbestände entwickelt wurde. Abschließend untersuchen wir die Synergien zwischen verschiedenen Sensortypen zur Detektion von Pflanzenstress. Eine Publikation widmet sich den Synergien zwischen terrestrischem Laserscanning, multispektraler Bildgebung und RTMs zur Untersuchung dürrebedingter Blattbewegungen in Sojabohnen. Unsere Ergebnisse zeigen, dass die Blattorientierung allein durch multispektrale Kameras erfasst

werden kann. Eine weitere Publikation adressiert die Herausforderungen bei der kombinierten Nutzung verschiedener Sensoren zur Detektion von Pflanzenstress.

Acknowledgements

I would like to express my deepest gratitude to the individuals who have played an important role in this project: First and foremost I would like to thank my supervisors Professor Uwe Rascher and Dr. Juliane Bendig for supporting me throughout the PhD project. Their guidance throughout my academic journey has been truly exceptional. They've supported me not only in tackling academic challenges but also in helping me grow both personally and professionally, and I'm deeply grateful for their encouragement every step of the way. I would also like to thank my co-supervisors Dr. Onno Muller and Dr. Bastian Siegmann for always being there to extend a helping hand, literally and figuratively. I am grateful for PhenoRob commmunity that has provided me with plenty of resources that made this project possible.

I would like to give heartfelt thanks to the team of technicians: Nils Müller, Ilgaz Askin, Angelina Steier and Michael Quarten without whom carrying out measurement campaigns would have been impossible. To my fellow PhD students: Oliver Knopf, Sofia Choza Farias, Deepthi Konche and Vera Krieger, I would like to thank them for their unconditional support. Special thanks go to my office-mate Julie Krämer who was always there for me.

I extend my heartfelt thanks to my partner, Shtefan, for his unwavering support and guidance throughout my academic journey. I am especially grateful for his patience in handling the numerous questions I constantly bombarded him with.

And most importantly, to my dearest mom, without whom I would not be where I am today, and who has supported the path I chose since childhood, I am immensely grateful.

My sincere thanks go out to all those I have acknowledged, and to anyone whose name I may have unintentionally missed. Your support, guidance, and contributions have been essential to the success of this project.

This work was funded by the Deutsche Forschungsgemeinschaft (DFG, German Research Foundation) under Germany's Excellence Strategy – EXC 2070 – 390732324.

Contents

Chapter 1

Introduction

Remote sensing platforms and sensors allow monitoring of crop performance, vital for implementing sustainable farming practices and breeding new crop varieties. Uncrewed Aerial Vehicles (UAVs) are an emerging technology in agriculture. Their potential in agricultural research and practical applications has been extensively studied. A key use of UAVs in agriculture is phenotyping, deriving plant charachteristics from the image data. These parameters often relate to the plant performance. However, there is a challenge in ensuring the reproducibility and the interpretation of approaches used to obtain these plant parameters from the UAV data.

In Section 1.1, the motivation of this thesis is stated. In Section 1.2, a list of publications that constitute this thesis is provided, and lastly, in Section 1.3, the main contributions of this thesis are outlined.

1.1 Motivation

In the face of the rising global population [72], degradation of soil and water resources [193] and climate change-induced extreme environmental events, global food security is compromised. To ensure that agricultural production is resilient to adverse environmental effects, intensification of farming, and rising food demand, we need to adopt sustainable farming practices and develop resilient crop varieties [105]. In this effort, remote sensing plays a vital role. It can assist farmers and plant breeders in monitoring crop parameters and quickly identify high-performing crop varieties through the means of phenotyping.

Plant phenotyping refers to describing a plant's outer characteristics either using the human eye and/or various tools. These characteristics can be important agronomic variables, such as biomass, the number of grains in the wheat head, or the leaf area. Some variables are indicative of stress, such as changes in chlorophyll content and leaf angle, stunted growth, etc. The standard practice in the past has been to record and monitor these plant characteristics using human labor. Since the task of measuring large fields or different crop varieties in breeding trials is labor-intensive, technologies have been developed to assist the farmers and breeders in this task. These are called high-throughput phenotyping platforms. While some platforms operate close to the plants in the greenhouse setting, monitoring plant characteristics in the field to cover large areas is practically only possible with aerial platforms.

Among aerial platforms, UAVs have demonstrated strong monitoring and phenotyping capabilities due to their versatility, high spatial and temporal resolution, and ease of use [224]. UAVs can deliver very high-resolution image data over large areas which enables the high-throughput phenotyping of various crops and crop varieties within the breeding trials. UAVs can carry different sensors (RGB, multispectral, thermal, lidar. etc.) [1] at the same time and these sensors can capture different information on the crop parameters (structural or biochemical). In this thesis the focus is on optical multispectral sensors that capture images in different wavelengths. There are different ways of getting to crop parameters from such sensors.

The most widely used approach uses so called vegetation indices (VIs), quantities derived from the optical measurements performed in separate spectral bands to relate to the plant parameter such as chlorophyll content. While VIs are powerful tools for mapping relationships with various plant parameters, they often lack transferability to different scenarios, such as across different growth stages, different crops or even varieties. Another widely used approach is machine learning, which has demonstrated promising retrieval capabilities. However, a significant drawback of this method is its reliance on the training data used to develop the model. Applicability of ML models may be limited when the training set lacks relevant information about the crop of interest. A third approach, radiative transfer models (RTMs), simulate the interaction of light with vegetation canopies, modeling how radiation is absorbed, reflected, and transmitted by leaves and other canopy elements and how vegetation parameters affect the distribution of this radiation. Inversion of these models enables retrieving crop parameters. RTMs address the problem of transferability, but they introduce several challenges. One major issue is their complexity; RTMs, especially 3D RTMs require detailed information about canopy parameters, which can be difficult to obtain. More complex

RTMs can be computationally intensive, especially for large-scale applications. Nevertheless, because RTMs simulate the physical processes of radiative transfer, they can be applied to a wide range of scenarios without requiring recalibration. This contrasts with empirical models, which are often site-specific or limited to the conditions under which they were developed. Hybrid retrieval combines RTMs with ML models. ML algorithms can be trained on RTM simulations to create fast and accurate retrieval models. This approach uses the physical basis of RTMs while benefiting from the speed and generalization capabilities of ML.

RTMs have been developed for satellite-level imaging data and extensively applied in that context. However, their use in UAV applications remains relatively unexplored, raising questions about how high-resolution UAV data would perform with RTMs. Addressing this knowledge gap is the primary motivation for this thesis. We have identified several research questions:

- What are the necessary steps before attempting crop parameter retrieval via RTMs? Before generating satellite products, rigorous radiometric calibration is typically performed, which is often not the case with consumer-grade UAV sensors. Additionally, research on the radiometric calibration of UAV sensors is limited. Proper calibration is crucial for ensuring accurate comparisons with other sensors and datasets collected throughout the measurement season.
- How does spatial resolution impact the retrieval? Since RTMs were originally designed for satellite-level, spatially coarse data, it is unclear whether high-resolution image data from UAVs will perform similarly, better, or worse.
- Which crop parameters can potentially be retrieved, and how can these results be interpreted? Is it easier to retrieve biochemical parameters, such as chlorophyll content, using UAV data, given that sun-lit leaves can be more easily identified in high-resolution images compared to those from satellites?
- Can the retrieved products be used for stress detection? If so, does the use of multiple sensors improve retrieval results, and what are the best scientific practices for utilizing multiple sensors? Crop stress is a significant research topic in the context of climate change, and it has been established that employing multiple sensors enhances the detection of specific and/or early signs of crop stress.

Based on these research questions, the thesis is grouped in three main topics. The

first topic introduced in 3.1, explores the importance of high-quality reflectance calibration of multispectral UAV sensors, which is an essential step before crop parameter retrieval. The second topic covered in section 3.2, examines the application of high-resolution UAV imagery in crop parameter retrieval using the PROSAIL model. Finally, the third topic presented in section 3.3, investigates the synergistic use of UAV-based optical sensors in crop stress detection.

1.2 Publications

Parts of this thesis have been published in peer-reviewed conferences and journal articles. The research questions are addressed in the next chapters.

- **Publication 1** (Peer-reviewed, conference proceedings)
  E. Chakhvashvili, B. Siegmann, J. Bendig and U. Rascher, "Comparison of Reflectance Calibration Workflows for a UAV-Mounted Multi-Camera Array System," 2021 IEEE International Geoscience and Remote Sensing Symposium IGARSS, Brussels, Belgium, 2021, pp. 8225-8228,
  doi: 10.1109/IGARSS47720.2021.9555143.

- **Publication 2** (Peer-reviewed, conference proceedings)
  E. Chakhvashvili, J. Bendig, B. Siegmann, O. Muller, J. Verrelst and U. Roscher, "LAI and Leaf Chlorophyll Content Retrieval Under Changing Spatial Scale Using a UAV-Mounted Multispectral Camera," IGARSS 2022 - 2022 IEEE International Geoscience and Remote Sensing Symposium, Kuala Lumpur, Malaysia, 2022, pp. 7891-7894,
  doi: 10.1109/IGARSS46834.2022.9883446

- **Publication 3** (Peer-reviewed, Journal)
  E. Chakhvashvili, B. Siegmann, O. Muller, J. Verrelst, J. Bendig, T. Kraska, U. Rascher, "Retrieval of Crop Variables from Proximal Multispectral UAV Image Data Using PROSAIL in Maize Canopy". Remote Sens. 2022, 14, 1247. doi: 10.3390/rs14051247

- **Publication 4** (Peer-reviewed, Journal)
  E. Chakhvashvili, L. Stausberg, J. Bendig, L. Klingbeil, B. Siegmann, O. Muller, H. Kuhlmann, U. Rascher, "Multispectral imaging and terrestrial laser scanning for the detection of drought-induced paraheliotropic leaf movement in soybean", International Journal of Applied Earth Observation and Geoinformation, 2024a, 135, p.104250.
  doi: 10.1016/j.jag.2024.104250

- **Publication 5** (Peer-reviewed, Journal)
  E. Chakhvashvili, M. Machwitz, M. Antala, O. Rozenstein, E. Prikaziuk, M. Schlerf, P. Naethe, Q. Wan, J. Komárek, T. Kloucek, S. Wieneke, B. Siegmann, S. Kefauver, M. Kycko, H. Balde, V. Sobejano Paz, J. A. Jimenez-Berni, H. Buddenbaum, L. Hänchen, N. Wang, A. Weinman, A. Rastogi, N. Malachy, M.L. Buchaillot, J. Bendig, U Rascher, "Crop stress detection from UAVs: best practices and lessons learned for exploiting sensor synergies", Precision Agriculture, 2024b, 25, pp. 2614–2642,
  doi: 10.1007/s11119-024-10168-3

1.3 Main Contributions

In the following, we state the main scientific contributions of each part of the thesis:

Reflectance calibration

Calibration of images acquired from the aerial platforms is an initial and essential step before analyzing and deriving products from them. Reflectance calibration ensures that the datasets acquired on different dates can be compared with one another and that comparisons can be made with other sensors. Most of the consumer-grade multispectral cameras that are equipped for vegetation research come with a single panel with known reflectance. The image of the panel is taken before the flight at the ground and used later to calibrate each image channel using the known reflectance values of the panels. While this approach has been tested to deliver sufficiently good information for vegetation research, it does not account for atmospheric scattering. A more robust approach would be to use multiple panels with varying reflectance factors and take the images from the flight altitude to remove any atmospheric effect. In our first publication (Chakhvashvili et. al, 2021), we applied this method and showed that the multi-panel approach produces better calibration results, compared to the single-panel approach, especially in red-edge and NIR regions, which were relevant bands for the 4th publication.

Crop parameter retrieval

Crop parameters can be retrieved with various methods from UAV platforms. The most widely used approaches either are data-driven, such as VIs or ML, and lack transferability. ML methods are dependent on data that is being trained to retrieve the variable of interest. If the training dataset never contained e.g.

a specific growing stage of the plant, it will fail to estimate the parameter. As empirical models, VIs lack a strong physical basis. They are typically developed and calibrated for specific conditions, which can limit their transferability to other scenarios. This empirical nature means they may not always accurately represent the underlying biophysical processes. Additionally, VIs typically use only a few spectral bands, potentially overlooking important information contained in other parts of the electromagnetic spectrum. Radiative transfer models, owing to their physical nature overcome the pitfall of transferability. RTMs have been mostly applied to low spatial resolution satellite data. They have not been well-tested for UAV applications. The most widely used RTM is PROSAIL (refer to Chapter 2 for more information on it). In publication 2 (Chakhvashvili et al. 2022), we explored the application of PROSAIL on high-resolution UAV imagery in soybeans to retrieve leaf area index (LAI) and leaf chlorophyll content (LCC). Our results show that PROSAIL can be used to successfully retrieve both of the variables and that high-resolution images allow us to accurately remove the soil to retrieve the LCC. Also, the method could be applied to different dates without the need to tweak the model. In publication 3 (Chakhvashvili et al. 2022), PROSAIL was applied to the maize dataset. The results showed that, while PROSAIL may not be ideal for complex canopies due to factors like leaf clumping and shading, it still allowed for reliable retrieval of LAI and LCC. For row crops, where greater detail is needed, more advanced RTMs would provide better accuracy.

Sensor synergies for crop stress detection

Crop stress is posing an increasing threat to agricultural systems in face of the growing number of extreme weather events. For example, the largest share of negative economic impacts on European agriculture has been caused by drought and heat, and this is expected to persist in the future [60]. Crop stress monitoring, especially early stress detection and stress attribution to a certain event, are vital to managing agricultural systems. Stress can be detected using various optical or non-optical sensors at different stages. It has been shown that sensor synergies, the usage of multiple sensors, delivers more robust results [29]. Early stress detection as well as attribution of stress to certain biotic or abiotic events is a challenging task. The plant response to the stressors is not necessarily visible to the naked eye. Additionally plants might be affected by several stressors at the same time.

Some crops have developed an evolutionary mechanism to combat various adverse biotic or abiotic stressors. One of such mechanisms is paraheliotropism, a movement of the leaf parallel to the incoming radiation to combat water scarcity. This is also a process that has been overlooked in the scientific community for a

long time due to difficulty of measuring it. In Publication 4 (Chakhvashvili et. al 2024a.) we explored the application of a multispectral sensor and terrestrial laser scanner to track the diurnal changes of leaf angles in the soybean varieties under drought stress. We found critical regions in the spectrum that correlate well with the leaf angle and successfully developed a simple ratio index for this purpose. PROSAIL was also used to retrieve leaf angle from the data but it was not as good as a simple relationship between the developed vegetation index and the leaf angle.

Since sensor synergy provides a better understanding of plant responses to stress, it is important to consider the potential challenges in collecting data from different UAV platforms. In the 5th publication (Chakhvashvili et al. 2024b) sensor synergies for crop stress detection were discussed in terms of practical recommendations. How multiple sensors could be used successfully to observe the stress at different stages and what aspects of data collection and processing have to be taken into account to have a successful measurement campaign using UAVs.

Chapter 2

Basic Techniques

2.1 Remote Sensing of Crops

Remote sensing is a technique for observing objects or phenomena without direct physical contact [41]. It uses various methods to detect and measure different types of signals, mainly electromagnetic radiation (EMR). Imaging sensors are the predominant type of RS technology due to their ability to generate data that is easily interpretable across various scientific fields. Early image capture relied on hot air balloons, kites, and pigeons [52]; today, we use sensors mounted on satellites, airplanes, and UAVs. These sensors fall into two main categories: passive and active. Passive sensors, like multispectral, hyperspectral, and thermal sensors, measure energy that is naturally available from the environment, e.g. reflected sunlight. Active sensors, such as radar and lidar, provide their own energy source for illumination of targets and measure the radiation that is reflected back [41]. Unlike passive sensors they can operate day or night and in most weather conditions.

Passive sensors record EMR that is reflected or emitted from an object's surface. In case of this thesis the surface is a crop canopy. These waves vary in wavelengths and frequency, which includes ultraviolet, visible, infrared, and other bands of electromagnetic spectrum [147]. Before reaching the canopy, light has to pass through different parts of atmospheric layers, where it is reflected, scattered, or absorbed by different atmospheric constituents such as ozone and water. Only a fraction of light reaches the canopy after this process. Upon reaching the canopy, EMR follows different paths: some is reflected from the top of the canopy, some is absorbed, and some is transmitted through the leaves before either being

absorbed, transmitted, or reflected to other canopy layers. The sensors record this combination of reflected light.

Remote sensing platforms

The era of modern vegetation research using RS began with satellite technology, specifically the launch of the Landsat satellite mission in 1972, which employed a multispectral scanner to capture the optical properties of the Earth's surface using just four spectral bands. The foundational work established by Landsat 1 has paved the way for over fifty years of continuous monitoring and innovation in remote sensing technologies. E.g the data from Landsat 1 led to the development of the normalized difference vegetation index (NDVI) [174], a widely used vegetation index (VI) that correlates well with, many agronomic parameters. The creation of NDVI prompted the exploration of other vegetation indices and later facilitated the development of hyperspectral sensors with more spectral bands to study Earth's surface. Nowadays, satellite constellations such as Sentinel 2 [30] and Planet Labs [79] provide frequent, high-resolution Earth observation data. While traditional satellites faced limitations, these modern constellations now offer significantly improved spatial resolution (down to 30 cm) and revisit rates as frequent as multiple times per day, addressing many of the historical constraints.

Satellite-based imaging sensors provide essential data for global and regional research. They cover large swaths of the Earth's surface and deliver well-calibrated products with automated pipelines. However, satellites face limitations such as coarse resolution, infrequent revisit times, and an inability to see through the clouds. Improving one of these factors often requires compromising on others. For example, increasing spatial resolution (i.e., pixel size is decreased) will impact signal-to-noise ratio (SNR). As spatial resolution increases, each pixel covers a smaller ground area, capturing less energy and reducing signal strength relative to noise. Similarly, higher spectral resolution (narrower bandwidths) also means fewer photons per band. In this context, UAVs are playing an important role in filling the gap between satellite and ground-based RS measurements. UAVs can achieve much higher spatial resolution than satellites, usually in the range of centimeters per pixel. They also offer the flexibility of being deployed frequently and on-demand allowing for high temporal resolution. While satellite imagery may be affected by cloud cover, UAVs can often fly below cloud level, providing clear imagery more consistently.

UAVs have occupied their niche within the RS community. They are compact, portable, accessible, and much cheaper than traditional aerial surveys or satellite imagery acquisition. UAVs can be launched close to fields and experimental plots.

They allow for sensor data collection from various angles, that enable 3D modeling of crop canopies. They can be equipped with different sensors, be it spectral imaging sensors (multispectral, hyperspectral, thermal) or laser scanners. They can be combined with ground-based sensors for comprehensive data collection. For the review and the history of UAVs the reader is referred to [50].

While UAVs offer the flexibility mentioned above, they also come with trade-offs. Increasing spectral resolution in UAVs comes at the cost of spatial resolution. Still, their ability to fly at lower altitudes helps mitigate this trade-off at the expense of the coverage area. Low-altitude flights also increase the flight times. This can be problematic due to limited battery life and may require multiple flights or battery changes to complete a mapping mission. Additionally, the perspective distortion in images can increase, potentially affecting the accuracy of photogrammetry and 3D modelling. As a result, UAV operators must carefully balance these factors based on their specific research or operational needs.

Remote sensing sensors

RGB cameras are among the most prevalent and accessible sensors used in UAV-based remote sensing. They offer high spatial resolution at a relatively low cost, making them an attractive option for many applications. However, RGB sensors are limited in their spectral performance, capturing only three channels—red, green, and blue. This means they do not provide information beyond the visible spectrum, such as near-infrared which is often crucial for vegetation analysis and other applications.

Despite these limitations in spectral information, RGB sensors and their products are widely used due to their high spatial resolution. One notable application is the Structure from Motion (SfM) technique, which relies on overlapping 2D images to reconstruct three-dimensional structures. SfM is particularly effective with RGB images because it prioritizes spatial detail over spectral information. As a result, UAVs equipped with RGB cameras can produce detailed digital elevation models (DEMs), 3D models and orthomosaics that are valuable for deriving structural crop parameters, such as canopy height and volume.

While most UAVs are currently equipped with RGB sensors, more advanced crop trait estimation relies on multispectral or hyperspectral imaging. This data offers better insights into the structure and biochemistry of the canopy, providing more detailed information on plant performance. As light interacts with a crop canopy, its behaviour is largely determined by the canopy's structural and biochemical properties. Vegetation exhibits a distinct reflectance profile, with high absorption in the blue and red spectral regions and high reflectance in the green and

near-infrared regions (Figure 2.1). These characteristics are valuable for deriving various crop parameters. For example, in denser canopies the absorbance of red and blue light is higher due to more leaves, hence the reflectance is lower.

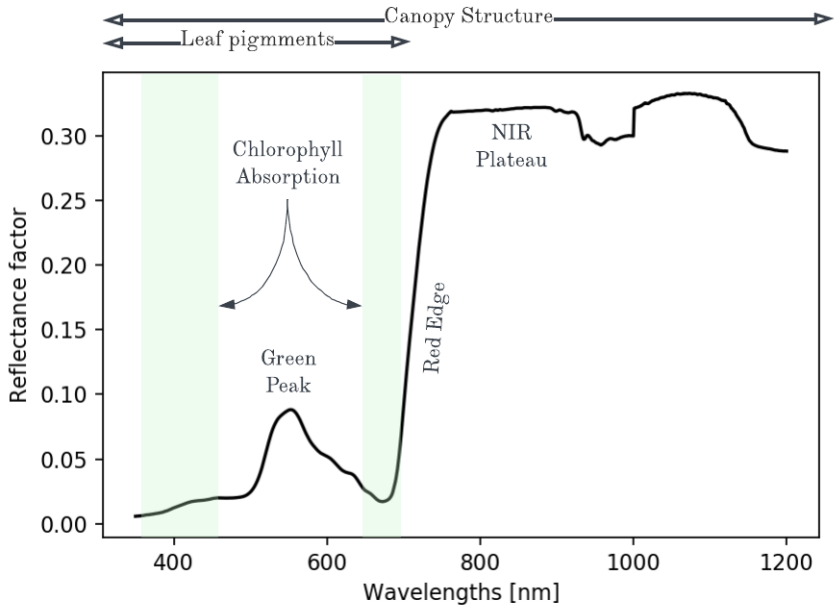

Figure 2.1: Typical reflectance profile of a vegetation canopy with highlighted features.

Relevant crop parameters

Among the crop parameters leaf area index (LAI), leaf chlorophyll content (LCC) and average leaf inclination angle (ALIA) are interesting from RS perspective (Figure 2.2). LAI is defined as the total one-sided area of a leaf per unit of ground surface area. It's a key biophysical parameter that characterizes plant canopies and is critical for understanding various ecological processes such as photosynthesis and primary productivity [12, 10]. It is widely used in climate modelling and crop yield estimations. Similarly, LCC provides valuable information on photosynthetic capacity, overall primary production, and the nitrogen status of the plant [91, 47, 53]. ALIA refers to the angle between a leaf and the horizontal plane. It's an important structural parameter that affects light interception, canopy reflectance, water use efficiency and plant adaptations to various stressors. These three parameters are often interrelated in their effects on plant functioning and remote sensing observations. They contribute to the overall signal in different wavelengths and sometimes this contribution overlaps. For example, leaf area index significantly impacts canopy reflectance in visible and NIR range, while ALIA impacts the red edge and NIR part of the spectrum.

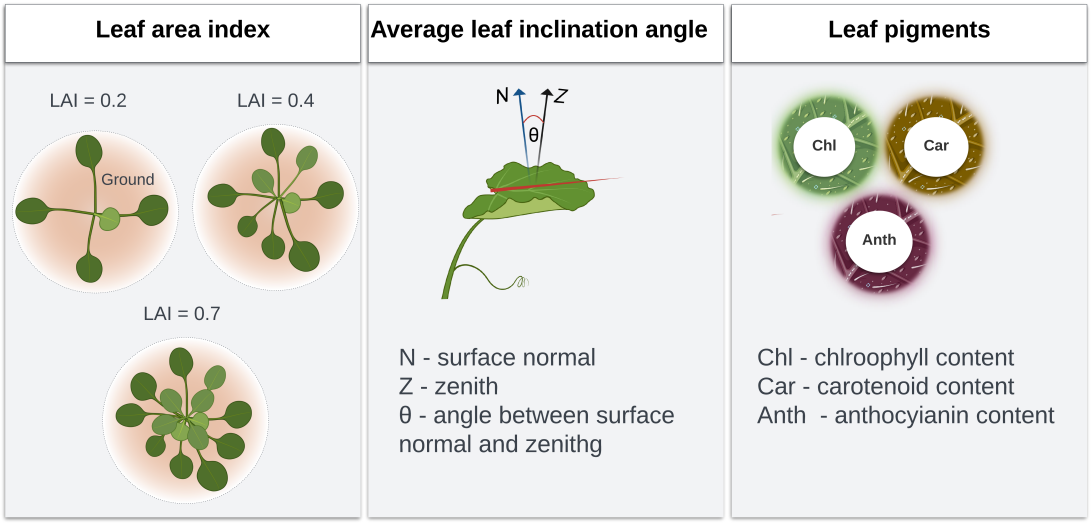

Figure 2.2: Crop parameters that were explored in this thesis. Only chlorophyll content was studied form the leaf pigments.

Structure from motion pipeline

Single images usually are not the end product of UAV campaigns. They are used to create a larger image of the area, known as an orthomosaic. Orthomosaics are created in specialized SfM software where images are uploaded and stitched together. Image stitching is a complex process and involves several steps. In the first step, key points, such as edges or other noticeable geometrical features are identified in overlapping images and across the whole image dataset to create a sparse point cloud [195]. If the key point identification is successful, a more precise point cloud can be calculated, followed by the creation of a digital elevation model, upon which all the images can be overlayed to create an orthomosaic. A significant part of this pipeline involves georeferencing the orthomosaics by providing points with known geographical coordinates (latitude, longitude, and altitude) measured before or after the flight. This ensures that the orthomosaic is correctly placed on the Earth's surface, usually with centimetre accuracy.

2.2 Trait Retrieval Problem

How can one extract plant structural and biochemical traits from imaging data? There are various methods to retrieve crop parameters from optical data, which can be classified into four categories: parametric, non-parametric, physical and hybrid [207].

Parametric methods

Parametric methods use simple calculations on measured spectra to derive vegetation indices such as NDVI, which is a ratio of NIR and red band. Compared to single bands VIs are more sensitive to the variable of interest and enable comparisons across different time points. E.g NDVI is sensitive to leaf area index (LAI) more than just the reflectance in red and NIR bands, especially when compared across datasets. Standard practice is measuring variable of interest and relating it to the VI to create a simple model, be it linear, exponential etc. The pitfall of the VI-based models is that they are not transferable to other conditions: to different sensors, crops, maybe even varieties, so the new models have to be created for each application. Despite this, VIs hold immense importance in RS and vegetation monitoring.

Non-parametric methods

The second retrieval family includes non-parametric models. These are data-driven machine learning (ML) models that take large amounts of training data to predict the variable of interest. In this case, both spectra and the ground observations are used to train the model and test it on the test sample. There are many machine learning models. Random forests and support vector machines, neural networks, have been widely used in the RS community to predict different crop parameters. The primary limitation of data-driven models is their dependence on the quality and availability of data [207]. As long as the models are trained on sufficiently large amount of data, predictions can be accurate, but oftentimes this is not the case. E.g if a training set does not contain different soil shading due to the water content or different stages of the plant growth, variable estimation may not be robust.

RTMs and hybrid methods

The physical retrieval family includes radiative transfer models (RTMs). RTMs simulate the interaction of the light with the canopy. They are based on the principles of radiative transfer which describe how a photon is propagated in different media such as crop canopy: absorbed, transmitted, scattered or reflected. The transfer of the light is dependent on the biochemical and structural properties of the canopy. The biochemical properties include the leaf pigments such as chlorophyll, carotenoids, anthocyanins, leaf optical thickness, leaf water and dry matter contents. The structural variables include the leaf orientation, leaf area index, height etc. The combination of these parameters determines how the light will be transferred within the canopy. E.g with LAI of 5 the reflectance in the near-infrared region will be much higher compared to LAI of 1. This

is explained by the fact that vegetation does not absorb the light in the NIR spectrum as much, so with more leaves stacked on top of each other the reflected signal will be much larger compared to areas with low LAI where the soil is more exposed. Canopy RTMs operate in two modes: forward and inverse. In forward mode, RTMs simulate canopy reflectance based on input parameters describing the canopy structure and leaf properties. In inverse mode, RTMs are used to estimate canopy properties from observed reflectance data.

RTMs can simulate a wide range of scenarios by adjusting input parameters, allowing for the exploration of hypothetical conditions. RTMs developed for one sensor can often be adapted for use with other sensors by accounting for differences in spectral response function. Unlike empirical models that are often site-specific, RTMs can be applied to different vegetation types and environmental conditions with appropriate parameterization. They require knowledge on the state variables and the choice and the complexity of the RTMs depend on the canopy architecture: heterogeneous canopies cannot be modelled in simple RTMs like PROSAIL, while complex RTMs like DART require knowledge on large amount of input parameters. The hybrid retrieval family combines RTMs with non-parametric models. In this case MLs are used to predict variables based on the RTM simulations.

Radiative transfer model PROSAIL

RTMs can have a very simple representation of the canopy e.g. turbid medium of PROSAIL or can have a large amount of the input parameters and near-real world 3D representations of objects like 3D RTM DART [81]. PROSAIL has been widely used in the RS community. The model combines leaf optical property (PROSPECT) with structural property (SAIL - Scattering by Arbitrarily Inclined Leaves) models (Figure 2.3). PROSPECT was designed to simulate the directional-hemispherical reflectance and transmittance of plant leaves across the optical spectrum, typically ranging from 400 to 2500 nm [113]. It relies on several key parameters to model leaf optical properties. The leaf structure parameter (N) represents the number of compact layers within the mesophyll. Leaf chlorophyll, carotenoid and anthocyanin content charachterize the leaf pigments. Equivalent water thickness, and dry matter refer to leaf's water content and the dry mass. The PROSPECT model has gone through several versions, including PROSPECT-4, PROSPECT-5, PROSPECT-D, and PROSPECT-PRO. Each new version added capabilities or refined existing ones. For example PROSPECT-PRO added protein content (related to nitrogen) and cellulose + lignin content(constituents of dry matter other than proteins). SAIL is a one-dimensional radiative transfer model that simulates the interaction of

light with plant canopies. Key input parameters for SAIL include LAI, ALIA, soil reflectance and observation and illumination parameters. LAI represents the total one-sided area of leaf tissue per unit ground surface area; ALIA describes the average leaf inclination angle in the canopy; soil reflectance represents the optical properties of the background; parameters such as solar zenith angle, observer zenith angle and relative azimuth angle between the sun and the observer describe illumination and viewing geometries. The model assumes a horizontally homogeneous canopy structure, which is represented as a turbid medium of randomly distributed leaves. This is a very simplistic representation and often does not apply to the real world. PROSAIL has been mostly used in satellite applications, but the usage is increasing in the UAV community [202, 172].

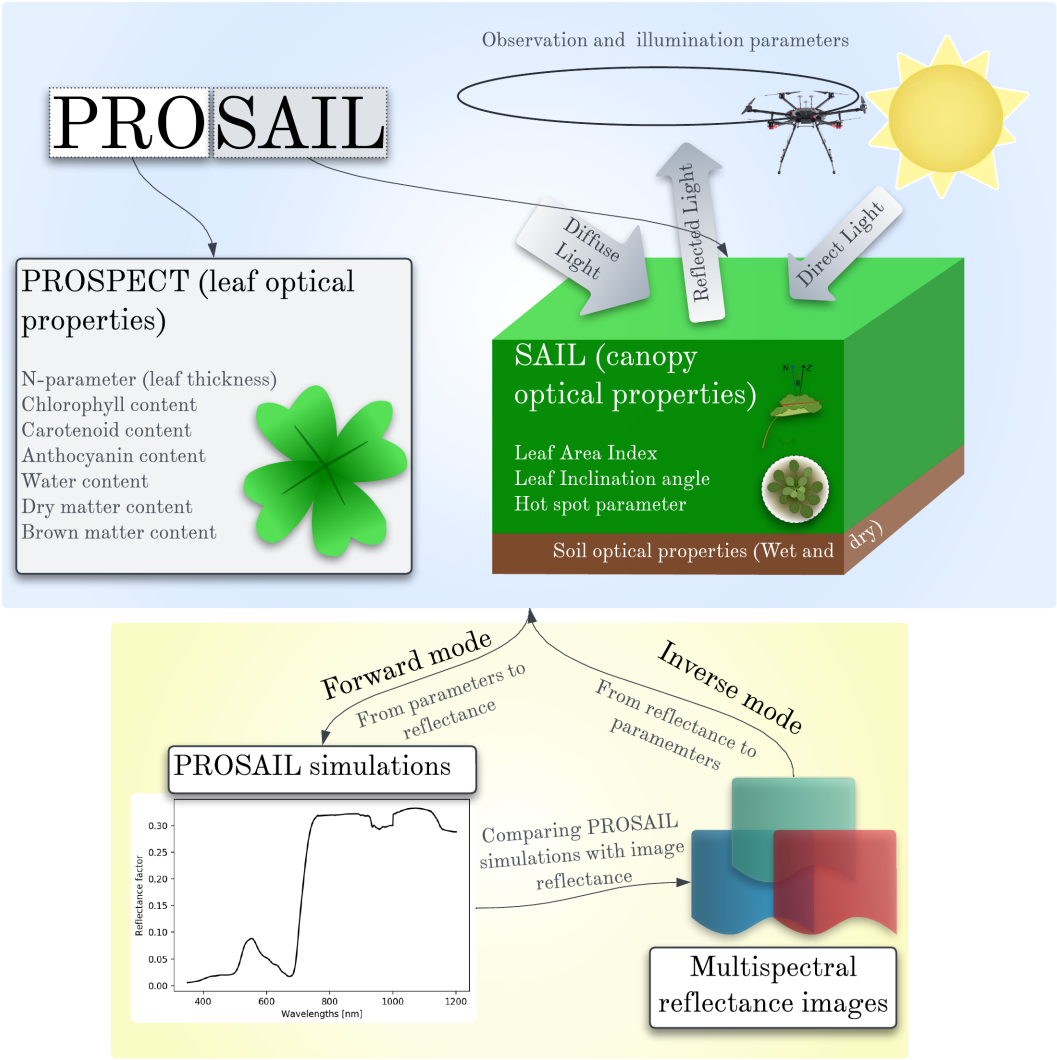

Figure 2.3: Graphical representation of the PROSAIL model. PROSAIL is a coupling of leaf PROSPECT model (on the left) and canopy SAIL (on the right) models. Parameters that are needed to run the PROSAIL simulations are listed for each model.

PROSAIL inversion

In this thesis we focus on the inversion of the PROSAIL model to retrieve the parameters. There are different inversion methods. The Look-Up Table (LUT) approach uses a database of simulated spectra which is generated using PROSAIL with various parameter combinations. The measured spectrum is then compared to the LUT to find the best matching simulated spectrum and its corresponding parameters. Optimization methods involve iteratively adjusting model parameters to minimize the difference between simulated and measured spectra. ML approaches like neural networks or support vector regression are trained on simulated PROSAIL data to learn the relationship between reflectance and biophysical parameters.

The inversion of PROSAIL faces several challenges. Multiple combinations of input parameters can produce very similar canopy reflectance spectra, leading to non-unique solutions. This is known as an ill-posed problem and makes it difficult to reliably retrieve specific vegetation parameters. Uncertainties in both the model assumptions/simplifications and the remote sensing measurements propagate through the inversion process, affecting the accuracy of retrieved parameters. Many inversion approaches, especially optimization methods, can be computationally demanding when applied to large datasets or when using complex models. Strong correlations between some vegetation parameters (e.g., LAI and ALIA) can make it difficult to separately retrieve these properties. Simplified assumptions in PROSAIL may not accurately represent complex real-world canopies, leading to inversion errors. There are several strategies to address some of these challenges. E.g. Isolating spectral bands most sensitive to the parameters of interest or using prior information or constraints to limit the parameters has shown to help with the ill-posed problem.

2.3 Validation

An important aspect of crop parameter retrieval is the validation. For this purpose the variables of interest are measured close (during, before or after) to the overflights. In this thesis we have focused on the ground validation of three main variables: LAI, LCC and ALIA. LAI and LCC can be measured destructively (taking plant samples) or non-destructively (without damaging the plant). ALIA can only be measured non-destructively.

For destructive LAI measurements, a small representative area within the exper-

mental plot, typically 40x40 cm, was selected, and the above-ground biomass was collected. The leaves were then analyzed using a LI-3100C leaf scanner (LI-COR, Lincoln, Nebraska, USA) to measure the total leaf area. Leaf scanner features two transparent conveyor belts that rotate to move leaves across a scanning bed. As leaves pass through, the instrument uses an electronic method to scan and measure the leaf area. LAI was calculated by dividing the total leaf area by the soil area of the selected plot. Non-destructive measurements were conducted with the SunScan Canopy Analysis System (Delta-T Devices, Cambridge, United Kingdom), which consists of two main components: a sunshine sensor that measures total incident PAR above the canopy (both diffuse and direct light components), and a probe that measures PAR along its length 1m length using 64 PAR sensors. The standard procedure involves placing the rod beneath the canopy and comparing the PAR levels under the canopy with those above it, as measured by the sunshine sensor. The LAI calculation in the SunScan system is based on an inversion of Beer's Law, which describes light attenuation through a medium. However, the system uses a more complex model to account for the intricacies of plant canopies: information on canopy architecture such as leaf angle distribution, solar position and different light components (diffuse and direct). This approach allows the SunScan system to provide LAI estimates that are more accurate and robust across a range of canopy types and lighting conditions compared to simpler light transmission models.

Non-destructive LCC measurements were taken using a SPAD meter (Konica Minolta, Tokyo, Japan). The SPAD device measures the transmittance of red (650 nm) and near-infrared (NIR, 940 nm) light through the leaf, providing a value related to chlorophyll content [198]. The procedure involves taking multiple readings from the leaf and averaging the results. It is essential to collect as many measurements as possible within the experimental plot to obtain a representative value. Since the SPAD reading is not a direct measure of chlorophyll content, it must be converted using a calibration formula, typically linear or exponential, as found in the literature.

For ALIA measurement we used a terrestrial laser scanner. The plots were scanned from different positions, which resulted in 3D point clouds. These 3D point clouds were then meshed and average leaf inclination angle per plot was calculated. For more detailed description of the measurements refer to Chapter 5.

All sensor and ground measurements discussed in this thesis have been acquired in the PhenoRob Central Experiment, at Campus Klien-Altendorf, near the city of Bonn, Germany. The measurements were conducted in various experiments in

the span of 2020-2022 vegetation seasons.

Chapter 3

Summary of Relevant Publications

This thesis is structured in three main topics. The distribution of publications to their respective topics can be seen in Figure 3.1. Publication 4 falls into both 'Retrieval of crop parameters' and 'Sensor synergies for crop stress detection' topics.

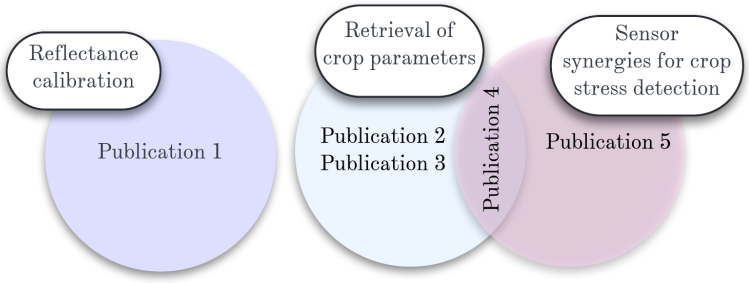

Figure 3.1: Publications and their allocation to respective topics.

3.1 Reflectance Calibration

Scientific context

Reflectance calibration of the optical sensors is an important step to preparing image data for analysis and ensuring the accuracy and reliability of final re-

sults [46]. It also allows for the comparison of datasets acquired throughout the measurement season with one another and with the datasets derived from other optical sensors. Many UAV sensors that have recently flooded the market lack proper reflectance calibration pipelines. Even when such pipelines are provided, the accuracy assessment of these calibrations is often overlooked, inadequately addressed or is not transparent enough. This oversight can lead to unreliable data, as users may not be aware of the limitations or potential errors in their sensor measurements. Additionally, it hinders the development of large-scale, multi-sensor remote sensing projects. Before the reflectance calibration, raw images have to be converted to radiance ($W \cdot sr^{-1} \cdot m^{-2} \cdot nm^{-1}$). This requires correcting for sensor-specific parameters, including variations in exposure times, the vignetting effect, and dark current levels.

Next step involves the relation of radiance images to reflectance of a known object. Calibration is done using spectrally flat surfaces also known as lambertian surfaces. This means that the reflectance across the electromagnetic spectrum remains nearly constant. Generally, for UAV applications small aluminium panels coated with special paints with varying shades of gray from white to black are used and the reflectance of these panels are measured in the lab. Before the take-off the panel images are taken and used to calibrate images to reflectance. Calibration is then performed by applying a simple linear function to relate the radiance of the image to the reflectance of the panel (see Figure 3.2). The assumption is that the relationship between the radiance and reflectance is linear, but since that is not always the case due to the characteristics of different sensors, it's recommended to use several panels with varying reflectance factors to inspect for the linearity [186].

Many optical imaging sensors come with the reflectance calibration pipelines using just one panel. This approach neglects the effect of atmospheric scattering and assumes that the target with 0% reflectance will produce 0 at sensor-radiance. Several studies have shown that single panel approach for UAV-mounted multispectral cameras overestimates the reflectance especially in red edge and NIR bands [74, 164]. The cause of this overestimation could be attributed to the absolute radiometric calibration of the camera or 'spectral pollution' of the dark panels by the surrounding vegetation.

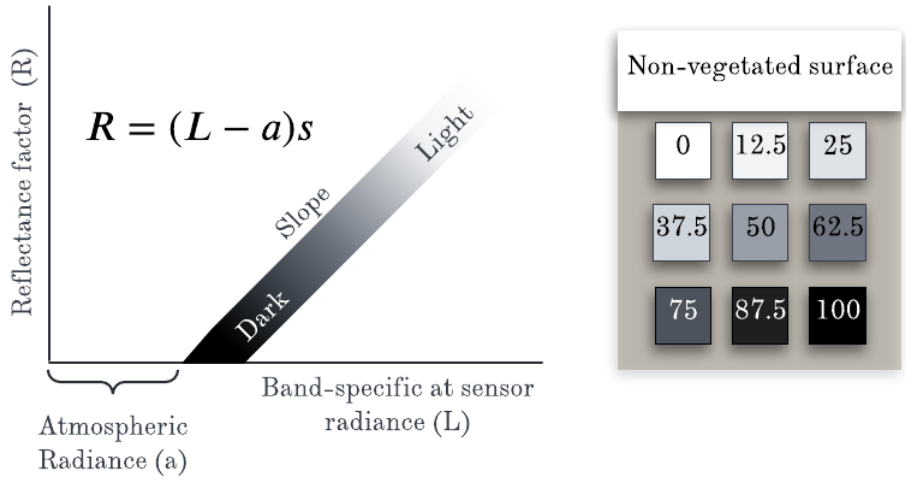

Figure 3.2: Depiction of linear relationship between band-specific at sensor radiance (L) and reflectance of factors of the calibration panels (left). The usage of contrasting (dark and light) panels confirms that the relationship is indeed linear. Figure is adapted from Smith et al. (1999); Representation of reflectance panels with different reflectance factors depicted in percentages (%). a is radiance caused by atmospheric scattering between sensor and the target.

Publication 1 (Peer-reviewed, conference)

Chakhvashvili, E., Siegmann, B., Bendig, J., & Rascher, U. (2021, July). Comparison of reflectance calibration workflows for a UAV-mounted multi-camera array system. In 2021 IEEE International Geoscience and Remote Sensing Symposium IGARSS (pp. 8225-8228). IEEE.

In this publication we explored different calibration approaches: the one used by the camera manufacturer which involves taking close images of the single panel before and after the flight and the approach that we developed which involves taking images of multiple panels from the flight altitude. Our approach ensured that atmospheric column and thus the effect of atmospheric scattering would be accounted for while flying the UAV. While our results show that single panel approach is good enough for visible bands, it delivers less accuracy in the NIR and red edge bands compared to multiple panel approach. These are the bands that are vital for vegetation research so they should be well calibrated. We propose to use gray-gradient panels with varying reflectance factors (at least 3 in the range of 5-40% reflectance factor) to ensure the linearity of the calibration model. Additionally we inform the future users that panels with reflectance factors higher than 60% are often oversaturated in visible bands and can't be used for the calibration for the MicaSense Dual camera system used in this study. This is not

the case for Red Edge and NIR bands.

3.2 Retrieval

Scientific Context

Once the image processing chain is established and reflectance products (orthomosaics) are finished, it is time to test the retrieval of crop variables using PROSAIL. For the description of PROSAIL please refer to Chapter 2.

The applicability of PROSAIL to UAV data has been explored in various studies and for various crops. The most widely retrieved variables are green fraction (GF), LAI, LCC and canopy chlorophyll content (CCC) [172, 202, 117, 3, 63, 191]. In the majority of these studies, UAVs were either flown at high altitudes to produce coarse-resolution imagery that mimics airborne or satellite data [172, 202, 63], or the resolution of the final orthomosaic was artificially reduced [172]. This reduction was done to meet the assumption of a turbid medium model such as PROSAIL. While reducing the spatial resolution might be sensible for structural variable retrieval, it has an adverse effect on the estimation of biochemical variables: image data become affected by mixed pixels, meaning that it is no longer possible to separate shaded and soil pixels from vegetation (leaves). This blending effect in turn influences the proper estimation of leaf variables per plot. Images of higher spatial resolution allow the separation of only vegetated pixels from the scene to better estimate the leaf variables. Additionally, in the majority of the above-mentioned studies, hyperspectral sensors were employed. While these sensors deliver spectrally contiguous data, their applicability in breeding and precision agriculture is currently limited due to their high cost and complex data post-processing. Multispectral sensors, on the other hand, are much cheaper and provide information of important spectral regions, which proved to be sufficient to retrieve crop biophysical variables of comparable quality [202].

A common method of retrieving vegetation variables at plot level is averaging the measured spectra per plot and applying the inversion scheme to it. While this method works well for coarse-resolution imagery and for structural variables, we assume that leaf biochemical variables could be better estimated by applying the inversion scheme to the reflectance maps and then averaging the variables per plot. In this way, valuable information on each canopy feature can be obtained.

Publication 2 (Peer-reviewed, conference)

Chakhvashvili, E., Bendig, J., Siegmann, B., Muller, O., Verrelst, J., & Rascher, U. (2022, July). LAI and leaf chlorophyll content retrieval under changing spatial scale using a uav-mounted multispectral camera. In IGARSS 2022-2022 IEEE International Geoscience and Remote Sensing Symposium (pp. 7891-7894). IEEE.

PROSAIL was created for spatially coarse satellite data. One of our primary objectives was to test whether PROSAIL could be effectively applied to UAV data. For this purpose we have resampled orthomosaics to lower spatial resolutions to simulate flights at maximum 100 m altitude, without simulating the effect of the atmosphere between the sensor and the crop. We collected ground measurements of LAI and SPAD in two soybean varieties, extracted the spectra from their respective plots and applied the RTM inversion scheme. For chlorophyll content retrieval we tested two approaches: where soil and shaded pixels were removed from the scene and where soil and shade were intact.

In this study, we have demonstrated that with decreasing spatial resolution the retrieval accuracy of both structural and biochemical parameters slightly decreases. The results show that coarsening spatial resolution had less impact on the retrieval of LAI. However, it had a significant impact on the retrieval of LCC, especially when soil and shaded areas were masked from the orhtomosaics. This study confirmed that UAVs can be successfully used for pigment retrieval as its' high spatial resolution allows for the discrimination of different canopy constituents, such as soil, sun-lit leaf and shaded leaf.

Publication 3 (Peer-reviewed, Journal)

Chakhvashvili, E., Siegmann, B., Muller, O., Verrelst, J., Bendig, J., Kraska, T., & Rascher, U. (2022). Retrieval of crop variables from proximal multispectral UAV image data using PROSAIL in maize canopy. Remote sensing, 14(5), 1247.

The third publication tests PROSAIL's application in more complex row crop: maize. It explores the retrieval of LAI, LCC and CCC from two distinct maize types: silage and sugar corn, with complex architectures. The row structure of maize canopies creates gaps and a non-uniform distribution of plant material, which conflicts with the turbid medium assumption of the PROSAIL model. Additionally, row crops typically have a pronounced vertical stratification of leaf area and other canopy components, which affects the distribution of light and nutrients throughout the canopy. In this publication we tested LUT-based retrieval on differently processed reflectance data with soil and shade removed. We first averaged the reflectance per plot and inverted the model. The second approach involved applying the inversion scheme to each pixel.

Compared to spatially lower-resolution satellite and airborne imagery, high-resolution UAV images allowed the separation of soil, shaded and sunlit pixels. Thus, it was possible to retrieve the leaf chlorophyll content (LCC) by applying the inversion scheme only to green sunlit pixels. The LCC retrieval yielded promising results in comparison to ground measurements when using both retrieval approaches and led to higher accuracies compared to satellite or airborne studies. The measurement uncertainties associated with LCC retrieval could be further reduced by acquiring destructive chlorophyll measurements for a more accurate SPAD to LCC conversion equation. The retrieval accuracy of LAI was differed for the growth stages. The best results were obtained for early growth stages (leaf development, early and late stem elongation). We observed a significant improvement in the estimation of CCC when the pixel-based retrieval approach was used. We argue that high-resolution UAV imagery is well suited for biochemical variable retrieval, as shadows and background soil can be precisely removed, leaving only green plant pixels for the analysis. Further research is needed to validate the transferability of the model using similar sensor settings to the maize canopies. Furthermore, a more detailed characterisation of the canopy structure could improve the retrieval results, specifically of LAI. In addition, 3D RTMs would enable such a canopy characterization and should be explored in future studies.

3.3 Crop Stress Detection

Scientific context

Environmental stressors pose a significant threat to the crop production [236]. These stressors can be broadly categorized into abiotic and biotic factors, with abiotic stressors including extreme temperatures, drought, flooding, salinity, and nutrient deficiencies, while biotic stressors encompass pests, diseases, and weed competition. Monitoring crops for possible stress is vital to avoid the losses caused by these stressors. Manual monitoring of large areas is time-consuming, additionally the farmers and breeders are not able to get a larger picture of the area under stress and identify the cause. UAV RS methods enable to monitor the fields at high frequency and cover areas up to 500 ha depending on the flight parameters, sensor and the location of the field.

Drought is posing a significant challenge for agricultural systems worldwide. Some plants have evolved mechanisms to combat water scarcity. One of such mechanisms is paraheliotropism also known as light-avoidance through leaf movement [163, 136]. While the leading factor in paraheliotropic leaf movement is excess

light, temperature and water availability also influence the process [170]. Paraheliotropism causes the leaves to align parallel to the incident light. This way plants avoid high leaf temperature and high evapotranspiration [65, 78]. Despite many observations, the significance of this adaptive mechanism remains poorly understood [228].

Leaf movement can be described by leaf orientation parameters, one of which is the average leaf inclination angle (ALIA). ALIA is the angle between the leaf normal and the zenith, influencing light interception, photosynthetic efficiency, canopy competition, and serving as an early indicator of plant stress [179, 228]. Despite its significance in plant physiology and crop production, ALIA has been relatively underexplored due to the labor-intensive and error-prone nature of in-situ measurements. As a result, many studies have favored indirect methods such as photographic [34, 153, 110, 241] and laser scanning approaches [237, 15], which allow for diurnal and near-instantaneous ALIA measurements in field conditions. Although these methods yield reliable results, they struggle with scalability due to the time-intensive procedures, especially as study areas increase. The challenge is compounded by rapid changes in leaf orientation over time, further complicating measurements in larger areas. A promising, though underutilized, alternative involves using radiative transfer models (RTMs) and optical data from airborne platforms. This approach offers faster and more efficient data acquisition, making it a viable option for broader applications compared to photographic and laser scanning methods.

While single optical sensors may be sufficient for monitoring crop status, integrating multi-sensor data from airborne or UAV platforms provides a more comprehensive understanding of plant responses to various biotic and abiotic stressors [162, 2, 149, 86]. For instance, combining multispectral (MS, discrete spectral bands) or hyperspectral (HS, continuous spectral coverage) sensors with thermal infrared (TIR) sensors offers a broad spectral range for detecting and quantifying early-stage crop stress. By measuring leaf or canopy temperature, rapid changes in plant traits like stomatal conductance can be detected within minutes to hours, providing an early, pre-visual indication of stress [92]. Additionally, incorporating VIS-NIR data allows for the analysis of stress responses linked to pigment levels, such as chlorophyll, carotenoids [90], and anthocyanins [89], which are crucial for photosynthesis and productivity. The combination of different spectral resolutions and sensor types enhances spectral coverage and provides complementary insights into plant stress responses.

The synergistic use of sensors across different spectral domains enhances the ability to monitor both early and long-term crop responses to external stressors that

impact growth and productivity [167]. For instance, integrating MS VIS-NIR sensors with a broadband SWIR sensor or an NIR+SWIR multi-camera array has proven effective for assessing leaf water status and nitrogen concentration in crops [122, 119]. This VIS-NIR+SWIR combination is particularly beneficial for detecting medium- to long-term stress responses. Moreover, the simultaneous collection of hyperspectral (HS) and thermal infrared (TIR) imagery, along with solar-induced fluorescence (SIF) data, offers valuable insights intothe mechanistic understanding of the link between SIF and plant stress [86, 38]. Additionally, data from RGB, MS, HS, and TIR sensors can be used to derive biophysical traits and aid in the quantification and interpretation of physiological changes reflected in SIF measurements. These physiological changes include photosynthetic efficiency, non-photochemichal quenching, stomatal conductance, changes in chlorophyll content etc. Integrating data from multiple sensors is essential for advancing our mechanistic understanding of plant responses to stress.

Publication 4 (Peer-reviewed, Journal, submitted)

Chakhvashvili, E., Zabawa L., Siegmann, B., KLingbeil, L., Bendig, J., Kuhlmann, H., & Rascher, U. (2024). Multispectral imaging and terrestrial laser scanning for the detection of drought-induced paraheliotropic leaf movement in soybean. International Journal of Applied Earth Observation and Geoinformation, 135, 104250.

In publicaiton 4 we describe methods how leaf angle can be measured using TLS and UAV and relate our measurements to the drought. We have established that two very distinct soybean varieties have different response to the drought, where chlorophyll-deficient variety (Minngold) shows less change in leaf angle during diurnal measurement compared to dark-leaf variety (Eiko).

Our environmental data confirmed meteorological drought in the study area and soybeans were expected to display a paraheliotropic response. We demonstrated for the first time that it is possible to conduct diurnal TLS measurements to reveal differences between the soybean varieties. In the mornings, both had similar leaf angles, but by the afternoon, Eiko's leaves became vertical, showing a classic paraheliotropic response, while Minngold's leaves remained unchanged. As the drought persisted, Eiko's response intensified, with leaves becoming vertical earlier in the day and, by August, even inverting to expose the abaxial side. This response, previously documented, has now been tracked using remote sensing methods.

Unlike Eiko, Minngold showed a weaker paraheliotropic response, with minimal variation in leaf angles throughout the day. This subdued reaction is linked to

a genetic mutation causing its upper leaves to be more yellow, reducing light absorption and evapotranspiration. This adaptation allows Minngold to conserve water more effectively.

Our findings suggest a strong relationship between the reflectance in the red edge (740 nm) and near-infrared (842 nm) spectral bands and the ALIA. However, this relationship is not consistent during morning and afternoon measurements, with the latter showing a stronger correlation. Moreover, the near-infrared band at 840 nm is influenced by LAI, complicating the decoupling of the effects of ALIA and LAI on top of canopy reflectance. The ratioing of the 740 and 842 nm bands to eliminate the effects of sun-target-sensor viewing geometries proved successful in combining morning and afternoon measurements and establishing correlation with ALIA. Additionally, we observed that LAI has no significant correlation with the 740/842 index. Inversion of PROSAIL had different outcomes for the constrained and non-constrained with the latter significantly underestimated, compared to the former. ALIA retrieval worked significantly better for Minngold than Eiko. Future research should explore whether this relationship is applicable to ALIA estimations in other crops than soybean.

Publication 5 (Peer-reviewed, Journal)

Chakhvashvili, E., Machwitz, M., Antala, M., Rozenstein, O., Prikaziuk, E., Schlerf, M., ... & Rascher, U. (2024). Crop stress detection from UAVs: best practices and lessons learned for exploiting sensor synergies. Precision Agriculture, 1-29.

Using multiple sensors comes with its challenges, which at first glance might be trivial but that will have a large impact on the time-sensitive measurement campaigns. The number of sensors is constantly increasing on the market. At the same time, these sensors are becoming smaller while UAVs are becoming more versatile. This allows for multiple sensors to be mounted on the UAV platforms. It is already a standard practice to fly high-resolution RGB cameras together with multispectral cameras.

Measuring with multiple sensors requires careful planning. In publication 5 we discuss steps that need to be taken into account when planning multiple sensor campaigns. These steps include UAV mission planning, the optimal time for data acquisition, calibration targets and ground control points, etc.

The first part of the manuscript focused on acquiring high-quality multi-sensor imagery, highlighting several key points: (i) Optimal timing for data collection is essential, as some sensors have specific timing requirements. (ii) Sensor char-

acteristics must be considered in mission planning. (iii) Calibration targets with varying properties are needed for sensors from different optical domains. (iv) It is highly recommended to use ground control points that are recognizable by all sensors to ensure accurate image co-registration. (v) Incorporating additional measurements, such as weather data, is advisable for atmospheric correction.

The second part of the guideline addressed data analysis, emphasizing the following points: (vi) Data fusion for synergistic use should occur at Level 1C (physical units). (vii) Data quality flags should filter out unstable or biased measurements. We presented simple methods, such as vegetation indices, to integrate information from various spectral domains, alongside more complex techniques like retrieving biophysical variables through radiative transfer model (RTM) inversion. This latter area requires further research, and it is anticipated that future studies will follow the recommendations by [29].

Chapter 4

Comparison of reflectance calibration workflows for a UAV-mounted multi-camera array system

This chapter is published as:

E. Chakhvashvili, B. Siegmann, J. Bendig and U. Rascher, "Comparison of Reflectance Calibration Workflows for a UAV-Mounted Multi-Camera Array System," 2021 IEEE International Geoscience and Remote Sensing Symposium IGARSS, Brussels, Belgium, 2021, pp. 8225-8228,
doi: 10.1109/IGARSS47720.2021.9555143.

E.C. acquired the image data, conducted the analysis, and drafted the manuscript. B.S. measured panels with ASD and contributed to the review process. J.B. and U.R. provided supervision and review feedback. The content of the text remains identical to the published work. However, the format has been adjusted to align with the requirements of the thesis.

Abstract

Well radiometrically calibrated UAV-derived reflectance maps are important when analysing time series of vegetation canopies. In this paper, we assessed the quality of reflectance calibration of a multispectral camera system, MicaSense Dual, using two different methods: a single-panel approach offered by the camera manufacturer and an empirical line method. The results show a significant discrepancy between the reference reflectance measurements, and the single-panel approach in the NIR and the red edge bands. This discrepancy is especially pronounced for dark targets. The empirical line correction method has proven to be more accurate, yet for shaded and densely vegetated areas it has led to negative reflectance values in the visible bands. Hence, we argue that users should be aware of the caveats of both reflectance calibration pipelines when working with time-series UAV data.

4.1 Introduction

Low-cost multi-camera arrays (MCAs), which are easily mounted on UAVs, are increasingly used for vegetation mapping. The main output from mapping missions with these cameras are reflectance orthomosaics. It is important to assess the quality of the reflectance products, especially when working with time-series analysis and radiative transfer models for canopy biophysical variable retrieval, like chlorophyll content and leaf area index (LAI). Camera manufacturers provide consumers with reflectance calibration workflows, which are often implemented in several photogrammetric software. These calibration procedures are usually based on capturing a single gray panel with a known reflectance factor before and after the flight campaign. It is assumed that the relationship between the measured reflectance and the radiance of the panel is linear. Nevertheless, the single panel approach is known to overestimate the reflectance of the NIR and red edge bands in some MCAs, especially for dark targets [74, 164]. Furthermore, as panels are imaged lose to the ground and not at the flight altitude, the atmospheric effects cannot be accounted for. The more robust way of calibration, which has been largely applied to satellite data, is the empirical line method (ELM), where at least two targets with contrasting and known reflectance factors are used to create a simple linear model which is subsequently applied to the radiance image data [186].

In this paper, we explored two calibration workflows for the MicaSense Dual camera [MicaSense Inc, USA] system mounted on an UAV: a single panel approach provided by the camera manufacturer and the ELM using several panels. Two flight campaigns were conducted over two crop breeding trials on the same day.

4.2 Material and Methods

4.2.1 Study area and materials

The study area was located at the agricultural research station Campus Klein-Altendorf in the western part of Germany (latitude 50°37′N, longitude 6°59′E, elevation 176 m). Two sets of calibration panels [Mankiewicz Gebr. & Co. (GmbH & Co. KG), Germany], referred to as set A and set B, were placed next to two experimental fields, denoted as BreedFACE (BF) and PhenoRob (PR). Each set was comprised of nine 30x30 cm panels with varying reflectance factors (Fig. 1). The reflectance profiles of the panels were nearly flat across the VIS-NIR range. The optical properties of the panels were close to that of Lambertian surfaces. A single gray calibration panel (52% reflectance over MicaSense Dual spectral region), provided by the camera manufacturer, was placed next to the departure point of the UAV. BF was a wheat experiment, while PR was covered by wheat, maize and sugar beet. The MicaSense Dual camera system, comprising of two cameras – the MicaSense RedEdge- MX and the RedEdge-MX Blue - was mounted on the DJI Matrice Pro 600 [SZ DJI Technology Co., Ltd, China] UAV platform. The camera captured images in 10 spectral bands (see Table 1).

Table 4.1: Centre wavelengths and bandwidths of the MicaSense Dual camera system

Band names	**Centre Wavelength [nm]**	**Bandwidth [nm]**
Blue444	444	28
Blue475	475	32
Green531	531	14
Green560	560	27
Red650	650	16
Red668	668	14
RE705	705	10
RE717	717	12
RE740	740	18
NIR840	842	57

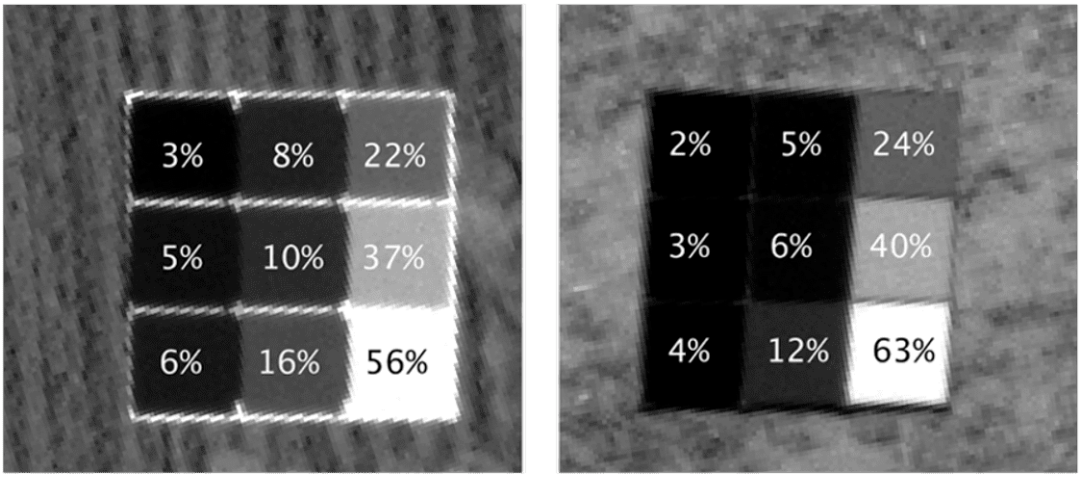

Figure 4.1: NIR images of panel set A (left) and panel set B (right) as seen from the flight altitude of 20 m; numbers on each panel represent average reflectance factors across the MicaSense wavelengths.

The flight campaigns took place on the June 23rd, 2020 under sunny conditions around solar noon (13:08 – 13:25 for PR and 13:55 – 14:09 for BF, UTC+1). The UAV was flying at 20 m above ground level in a survey pattern with 80% forward and 70% side overlap. Directly before and after the flights, images of the MicaSense calibration panel were taken from chest level (1m) without casting shadow on the panels. Images of panel sets A and B were captured during the flight survey. Additionally, reflectance measurements of the panel sets were collected timely close to the UAV image data acquisition using ASD FieldSpec4 spectroradiometer [Malvern Panalytical Ltd, UK]. From each panel, three measurements were recorded, averaged and spectrally resampled to match the spectral properties of the MicaSense cameras.

4.2.2 Photogrammetric processing

The datasets were processed in the photogrammetric software Agisoft Metashape [Agisoft LLC, Russia] using two approaches. For the ELM approach, before importing the images into the software, digital numbers were converted to radiance, using the radiometric calibration model (1) provided by the camera manufacturer [4]:

$$L = V(x,y) \cdot (\frac{a_1}{g} \cdot \frac{p - p_{BL}}{t_e + a_2 y - a_3 t_e y}) \tag{4.1}$$

where L is the radiance in $W/m^2/sr/nm$, V(x,y) is the vignette polynomial

function for pixel location (x,y), a1,m a2, a3 are the radiometric calibration coefficients, g is the sensor gain setting, p is the normalized raw pixel value (divided by 2N, where N is the number of bits in the image), x and y are pixel row and column numbers, respectively, $p_B L$ is the normalized black level value, and te is the image exposure time. Afterwards, the common Agisoft Metashape workflow was applied to align and georeference the images using ground control points distributed across the investigated fields. The generated orthomosaics were constructed with the mosaic blending mode enabled. For the single panel approach, the raw images were imported into Agisoft Metashape and the reflectance calibration workflow proposed by MicaSense and Agisoft was applied to the datasets [5]. The software employs the same reflectance calibration formula as described in [1]:

$$K = \frac{\rho_{\text{ref}}}{L_{\text{ref}}} \tag{4.2}$$

$$\rho = KL \tag{4.3}$$

where K is a calibration coefficient, ref is an average reflectance of the panel, Lref is the mean radiance of the panel and is a surface reflectance of the orthomosaic. The reconstruction settings remained identical to those used in the first approach. No sun sensor data was included in the workflow, as the clear sky condition remained throughout the flight. As a last step, the mosaics were exported for further processing.

4.2.3 Empirical line method

For the empirical line method, panel radiances of set A and B were extracted from the central part of each panel (96 pixels on average per panel) from the orthomosaic and the linear model was built based on the measured reflectance factors. Before the ELM application, it was observed that the images of spectral bands in the visible domain were saturated in the panels with high reflectivity (22%, 24%, 37%, 40%, 56%, 63%). For this reason, the saturated panels for each spectral band were removed from further analysis. This limitation has also been reported in another study using automatic exposure times on a different MCA [1]. To check the linearity of the model and validate the results, the panels were divided into calibration and validation sets. For calibration purposes, three panels were used, including the non-saturated brightest and the darkest panel.

4.3 Results

Results of the comparison between the two calibration workflows can be found in Table 2. Panel reflectance derived from MicaSense single-panel and ELM approaches plotted against reference measurements of the panel sets A and B from the field spectroradiometer can be seen in Figure 2. For single-panel approach, every non-saturated panel was used for validation. Results are plotted only for NIR and red edge bands.

Table 4.2: Comparison of calibration workflows against reference measurements. Values represent average RMSEs (%) of reflectance factors of the panels. A and B refer to the panel set names.

Bands	**MicaSense**		**Panel ELM**	
	BF (A)	**PR (B)**	**BF (A)**	**PR (B)**
Blue444	0.005	0.002	0.001	0.001
Blue475	0.007	0.004	0.001	0.001
Green531	0.002	0.004	0.002	0.001
Green560	0.002	0.006	0.001	0.001
Red650	0.002	0.006	0.002	0.002
Red668	0.003	0.008	0.002	0.002
RE705	0.005	0.011	0.002	0.003
RE717	0.006	0.012	0.002	0.002
RE740	0.007	0.018	0.002	0.001
NIR840	0.031	0.038	0.002	0.003

4.3.1 Single panel approach

The mean reflectance values were extracted from the central areas of the panel sets A and B to avoid adjacency effects. Standard deviations over the pixels were negligible. The single panel approach is overestimating the reflectance values over all wavelengths for both datasets. The overestimation is especially noticeable in the NIR and the red edge bands (Fig. 2), in both datasets for the darker targets with reflectance factors below 20%. The deviations from the 1:1 line are noticeably higher for the PR dataset than for the BF (Table 2).

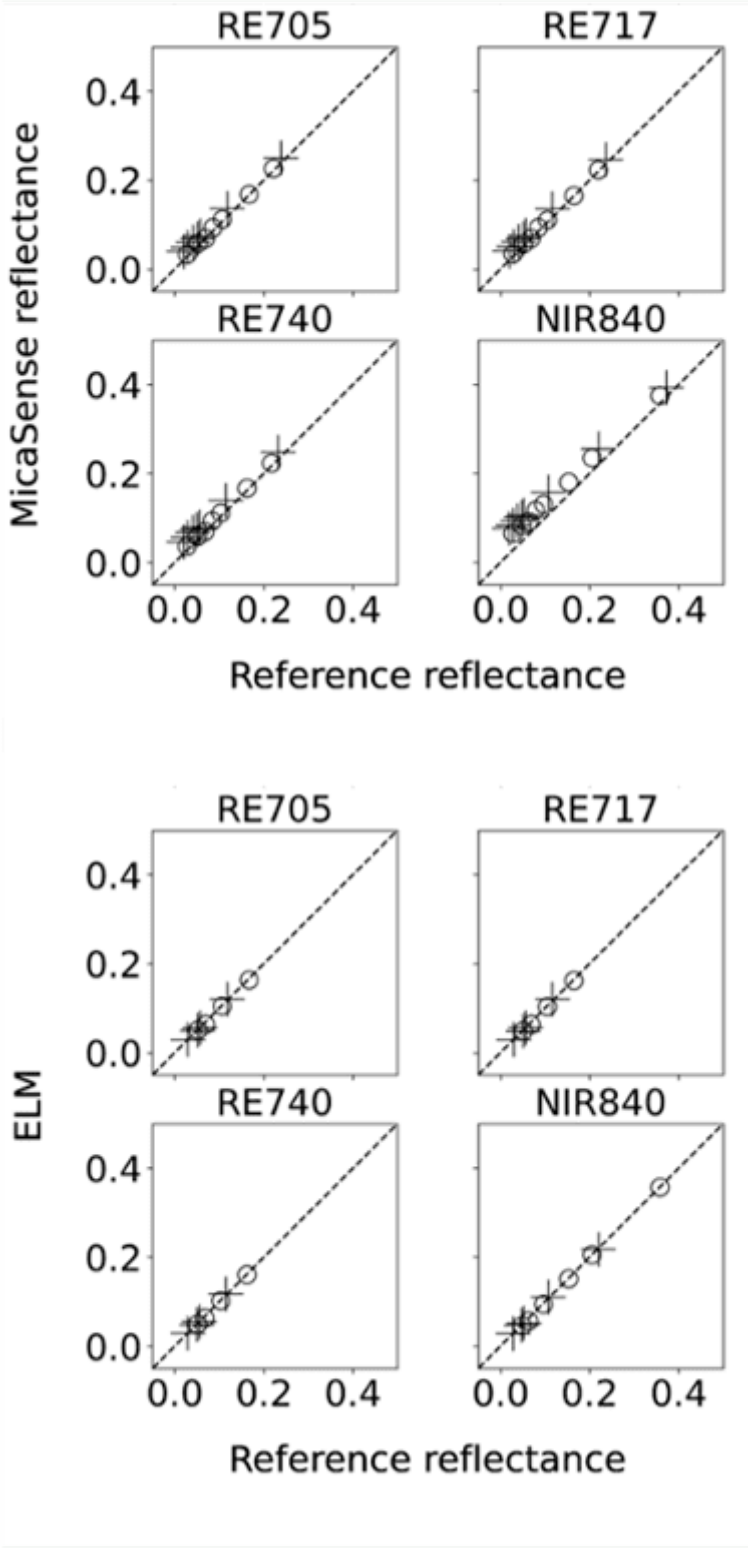

Figure 4.2: Comparison of panel reflectance as derived with MicaSense single-panel approach and the ASD measurements (upper plots) and with ELM approach (lower plots) for PR (crosses) and BF (circles) datasets. For the description of band names refer to table 1.

4.3.2 Empirical line method

The ELM approach yielded more precise calibration results compared to the single panel approach. The overestimation was not observed, including the dark targets (Table 2). It has to be noted that negative reflectance values were present in both datasets. These values were most pronounced in the blue and the red bands in the PR dataset with dense winter wheat and heavily shaded areas. Some negative reflectance values were also obtained for BF, but they were sparse, and mostly located near artificial surfaces.

4.4 Discussion and conclusion

We observed some errors with deriving surface reflectance using the single panel approach for the MicaSense Dual camera system. The errors were mostly pronounced in the NIR and the red edge bands, which is in accordance with findings reported in a previous study [6]. The highest inaccuracies were found for the dark panels with reflectance factors lower than 20% and were the lowest for the brighter panels with reflectance factors higher than 20%. It is not clear why the differences were generally higher for the PR than the BF dataset. Errors from the reference measurements can be ruled out, since panel set B was additionally measured several times during later flight campaigns and the measurements remained consistent. Negative reflectance values were already reported with other MCAs and several solutions were proposed [1,6]. The first one entails forcing the intercept of the empirical line method through zero. Another method proposes to shift the reflectance values in each band, by subtracting the maximum negative value recorded in the vegetated area. In both cases, the determined reflectance values are altered. This alteration might not have a significant effect on a single dataset when working on a regression or classification problem, but may cause issues for time-series analysis and radiative transfer modeling. One way to reduce the appearance of negative reflectance values, without compromising the accuracy of the calibration, would be to fly the UAV at higher altitudes and thereby avoid the acquisition of pixels only containing spectral information of shadows. In that case, panel dimensions need to be increased to allow extraction of sufficient number of pixels per panel. In conclusion, ELM delivers more accurate reflectance values than the single panel approach for the bands that are important in vegetation mapping. Unlike the single panel approach, it accounts for atmospheric effects that might become significant when flying at high altitudes. Nevertheless, users should be aware of the shortcomings of ELM described in this paper.

Chapter 5

LAI and leaf chlorophyll content retrieval under changing spatial scale using a UAV-mounted multispectral camera

This chapter is published as:

E. Chakhvashvili, J. Bendig, B. Siegmann, O. Muller, J. Verrelst and U. Rascher, "LAI and Leaf Chlorophyll Content Retrieval Under Changing Spatial Scale Using a UAV-Mounted Multispectral Camera," IGARSS 2022 - 2022 IEEE International Geoscience and Remote Sensing Symposium, Kuala Lumpur, Malaysia, 2022, pp. 7891-7894,
doi: 10.1109/IGARSS46834.2022.9883446

E.C. acquired the image data, conducted the analysis, and drafted the manuscript. B.S, O.M, J.V contributed to the review process. J.B and U.R. provided supervision and review feedback. The content of the text remains identical to the published work. However, the format has been adjusted to align with the requirements of the thesis.

Abstract

Recent advancements in unmanned aerial vehicle (UAV) technologies made it possible to monitor agricultural fields at higher spatial and temporal resolution than commonly possible by aerial and satellite surveys. Mapping crop variables such as leaf area index (LAI) and leaf chlorophyll content (LCC) from low-cost UAV-based multispectral cameras can deliver vital information about crop status to farmers and plant breeders. Retrieval of these variables using radiative transfer models (RTMs) has been widely studied in the satellite remote sensing community but is still not well explored in the UAV remote sensing community. This study aims to investigate the advantages of high spatial resolution UAV image data for retrieving LAI and LCC using RTM inversion. A breeding experiment consisting of soybean plots has shown that high-resolution imagery (0.015m) delivers better retrieval accuracy compared to coarser resampled image data. Particularly, biochemical parameters, such as LCC, benefit from high spatial resolution.

5.1 Introduction

Leaf area index (LAI) and leaf chlorophyll content (LCC) are two key variables that play a critical role in photosynthesis and plant functioning. They can be used as a proxy of nitrogen content, biomass, transpiration and photosynthetic capacity [12, 53]. Mapping these variables can help farmers to optimize their management and help breeders to select resilient varieties. Unmanned aerial vehicles (UAVs) enable mapping these variables at high temporal and spatial resolution. Among the variable retrieval approaches, radiative transfer models (RTMs), have been known to provide a robust and transferable solution to the retrieval problem. The majority of the vegetation RTMs have been tailored for satellite data, mapping the variables at global or regional scales. Meanwhile, UAV-based variable retrieval has shown promising results [172, 117]. However, it has not yet been explored how plant parameter retrieval benefits from the high-resolution UAV imagery. This study investigates the effect of changing spatial resolution on LAI and LCC retrieval in soybean using RTM inversion. High resolution orthomosaics were resampled to coarser spatial resolution to mimic the image data acquisition at higher altitudes and retrieval accuracies were assessed for image data with the different resolutions.

5.2 Materials and Methods

5.2.1 Study area and ground measurements

The study area is located at the agricultural research station Campus Klein-Altendorf, Germany (50°37'N, 6°59'E, 176m). Two varieties of soybean (Eiko and Minngold), were sown in 3x3 m plots in late May 2021. The plots were divided into destructive and non-destructive subplots of 1.5x3 m size. Eiko is a wild soybean variety, while Minngold is a chlorophyll mutant, characterised by extremely low chlorophyll content [39].

Two variables, LAI and LCC were measured on three different dates (July 1, July 7, August 4) during the vegetation period in 2021. The large measurement gap between 7th of July and 8th of August is attributed to a major flooding event in the region, which prevented the sampling of more reference data. LAI was measured non-destructively using SunScan canopy analyzer (Delta-T Devices Ltd, UK). The SunScan probe was connected to the irradiance sensor, which measures total incident PAR. After placing the probe under the canopy, a fraction of penetrating PAR through the plants is recorded by the probe and the LAI is calculated. Measurements were acquired by placing the probe ten times diagonally in each plot (five times in each 1.5x3 m subplot) and averaging the values. Additionally, plant samples were taken from the destructive subplots (three plants per subplot) and analysed in the leaf area meter (LI-3100C Area Meter, LI-COR Biosciences, Lincoln, USA) to validate the SunScan measurements (R^2=0.93).

Chlorophyll measurements were taken with a SPAD-meter (Konica Minolta Inc, Marunouchi, Japan). Six elementary sampling units (ESUs) were identified in each subplot (four near the edges and two in the middle as shown in Figure 5.1). In each ESU three plants were randomly selected and two upper leaves of each plant were measured three times by placing the measurement clip on the leaf. SPAD measurements were averaged per plot and the calibration formula derived from [141] was applied to convert SPAD values to LCC values.

5.2.2 Image data acquisition and processing

Image datasets were acquired a day before, or on the date of parameter sampling on the ground. We used the MicaSense Dual camera system (MicaSense Inc, USA), comprising of two cameras the MicaSense RedEdge-MX and the RedEdge-

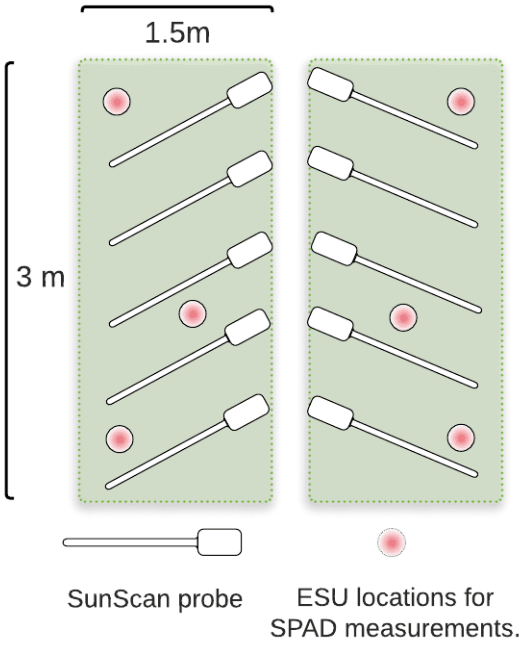

Figure 5.1: Schematic representation of a soybean plot consisting of two subplots with the different positions of LAI and LCC measurements. ESU stands for elementary sampling unit. Left subplot is non-destructive, right-destructive.

MX Blue. The camera system acquires images in ten spectral bands (centre wavelengths[nm]: 444, 475, 531, 560, 650, 668, 705, 717, 740, 842). A DJI Matrice PRO 600 UAV (SZ DJI Technology Co., LTd, China) served as sensor carrier platform. The UAV was flown at 20 m above ground level, which resulted in a ground sampling distance (GSD) of 0.014 m. Images were acquired under different illumination conditions (sunny and cloudy). A close to lambertian calibration panel set comprising of nine panels with varying reflectance factors, ranging from 3%-56%, were placed in the field during data acquisition. The reflectance factor of each panel was measured using an ASD Spectroradiometer (Malvern Panalytical Ltd, UK). The panels were used for calibrating radiance orthomosaics to reflectance.

Images were processed in the photogrammetric software Agisoft Metashape v.1.7.4 (Agisoft LLC, Russia, St. Petersburg). After the initial image alignment, image locations were optimized based on ground control points (n=20) that were evenly distributed in the field and which had been measured with a Trimble R4 real-time kinematic global navigation satellite system with an overall accuracy of 0.0115 m. Dense point clouds and DEMs were produced under low quality settings in Agisoft Metashape. Raw digital numbers (DN) were converted to radiance in the software by applying a radiometric calibration model, which accounts for lense vignetting, sensor gain and exposure time. For the detailed description of radiance

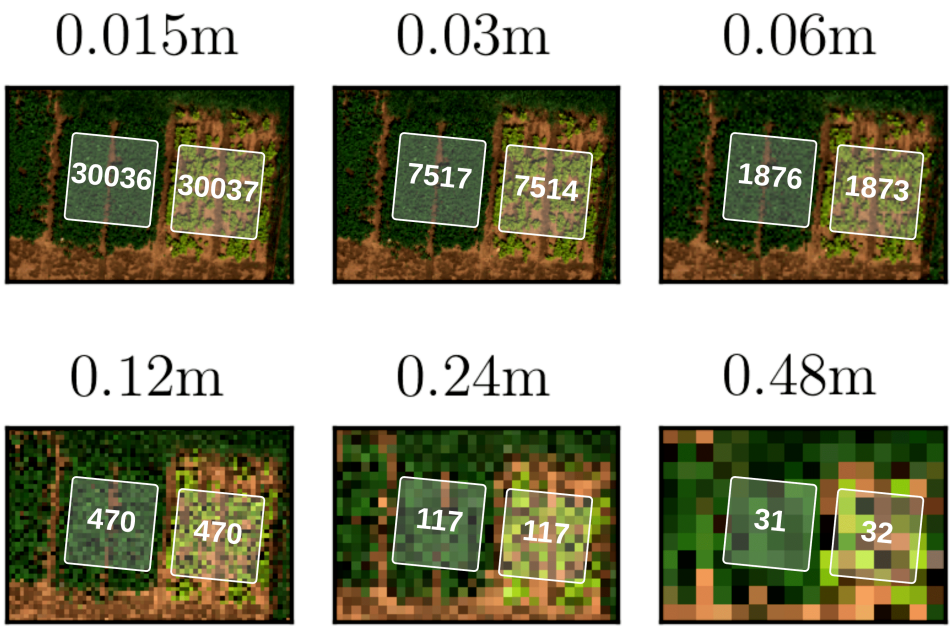

Figure 5.2: Depiction of resampled orthomosaics of soybean plots. The number above the plots shows the spatial resolution. The white areas show the buffer used for calculating mean spectra per plot and the number of pixels per area. The same process was applied to orthomosaics with removed soil pixels.

calibration refer to [43]. Orthomosaics were produced with the blending mode enabled and exported at 0.015 m spatial resolution. The empirical line method (ELM) for reflectance conversion and atmospheric correction was applied to the orthomosaic as described in [43]. We excluded saturated panels in each band from the ELM. After applying ELM, orthomosaics were resampled to lower spatial resolution by doubling the previous resolutions (Figure 5.2). The first three generated spatial resolutions are achievable with normal UAV operation (data acquisition below 100 m flight altitude), while the rest mimic image acquisitions with airborne sensors. Average spectra per plot were calculated using plot shapefiles with a negative buffer of 0.2 m to cancel out border effects and used as inputs for the RTM inversion.

Additionally, for the LCC retrieval soil was removed from every resampled orthomosaic by applying the Overall HUE index [67] thresholding to work with pure plant pixels. Values above 0 were considered as non-vegetated pixels and were removed.

5.2.3 PROSAIL inversion

For the retrieval of the LAI and LCC we used the PROSAIL model [115] in the ARTMO Toolbox [205]. The model was parameterised using the information acquired in the field as well as based on the information available in the literature (LAI range 0-6 m^2/m^2; LCC range 5-60 µg/cm^2). The model was run in forward mode to produce a look up table (LUT) containing 5000 simulations. A sampling constraint was applied to the variables (setting upper limits as observed in the field data) to avoid the ill-posed problem of the inversion. A LUT-based inversion scheme was then applied to the observed spectra. We used the root mean square error (RMSE) as cost function to reduce the error between simulated and measured reflectances and used the 2% mean of multiple best solutions. The retrieved variables then were compared to the reference measurements. The accuracy of the retrieval was assessed using RMSE and coefficient of determination (R^2).

5.3 Results

Results of the retrieval can be seen in the Figures 5.3 and 5.4. As shown in Figure 5.3, LAI retrieval accuracy decreased slightly with coarsening resolutions. It remained constant at ~ 0.2 m^2/m^2 for the first four studied resolutions and increased at > 0.24 m. A similar trend can be seen for LCC retrieval when using orthomosaics with soil (Panel B in Figure 5.3).

No changes were observed for the chlorophyll-deficient variety Minngold, whereas the wild variety Eiko showed a similar trend as observed for the LAI retrieval characterised by a decreasing accuracy at spatial resolutions > 0.24 m. As for the orthomosaics with removed soil (Panel C in Figure 5.3) we observed an overall decrease of accuracy for Minngold compared to Panel B, but no significant changes when comparing different resolutions. On the other hand, RMSEs for Eiko decreased from 3.51 to 2.10 at 0.15m resolution. Similar to Panel B, the accuracy decreased slightly for spatial resolution > 0.24 m .

5.4 Discussion and outlook

Generally, LAI retrieval worked well across all resolutions ($R^2 > 0.9$ and RMSEs below 0.3 m^2/m^2). Even at 0.48 m resolution (corresponding to 690 m flight altitude) sufficient number of plot pixels could be discerned to deliver satisfactory

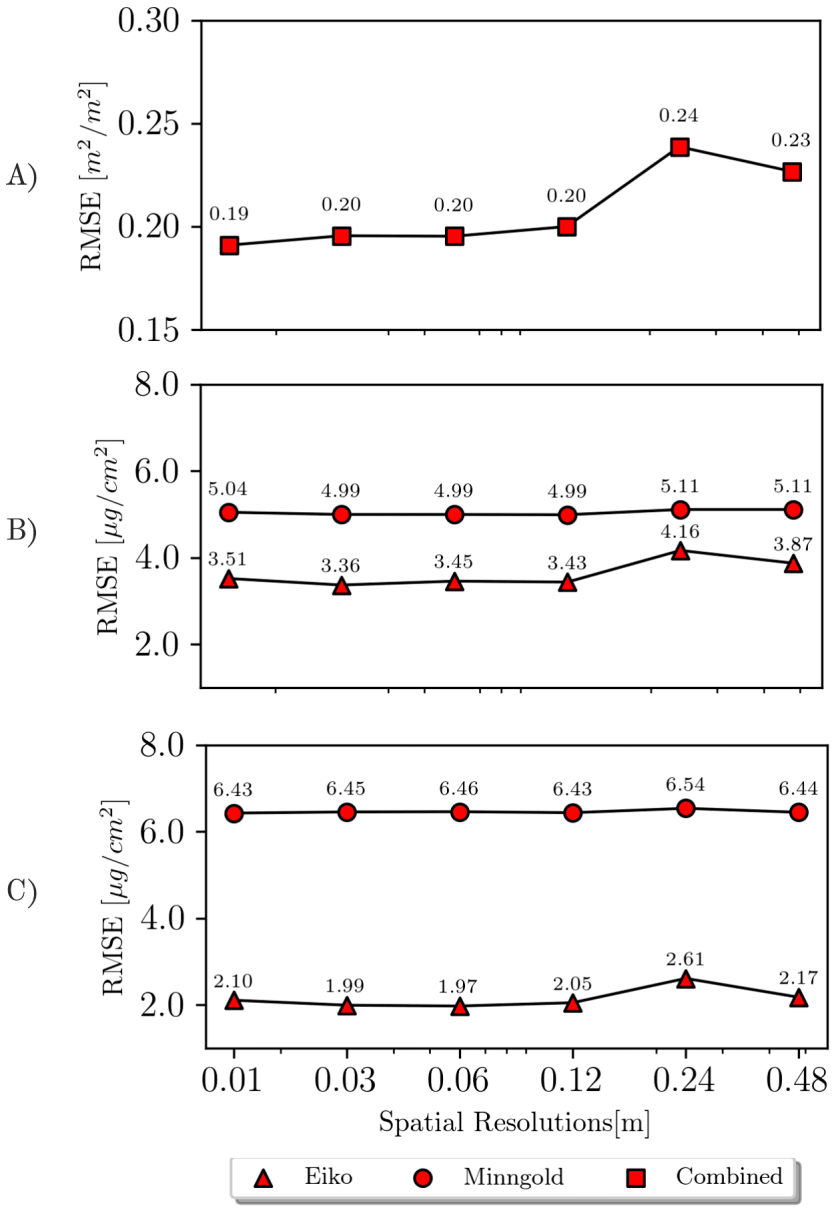

Figure 5.3: RMSE plots of LAI (A), LCC (B) and LCC with soil removed (C) for different spatial resolutions. For LCC a distinction between two varieties was made due significant difference observed after the retrieval.

results. As expected, LCC retrieval clearly benefits from high resolution image data due to the ability of high-resolution data to distinguish between different features such as shadows, soil, and plants, which is hardly possible in satellite or airborne images. The LCC overestimation observed in Minngold with removed soil could be attributed to the constraints of the PROSAIL model: Minngold is charaterised by two distinct canopy layers, low LCC in upper leaves and high LCC in lower leaves. This two layer canopy structure is not accounted for in PROSAIL, leading to overestimation. Better results for Minngold when using an

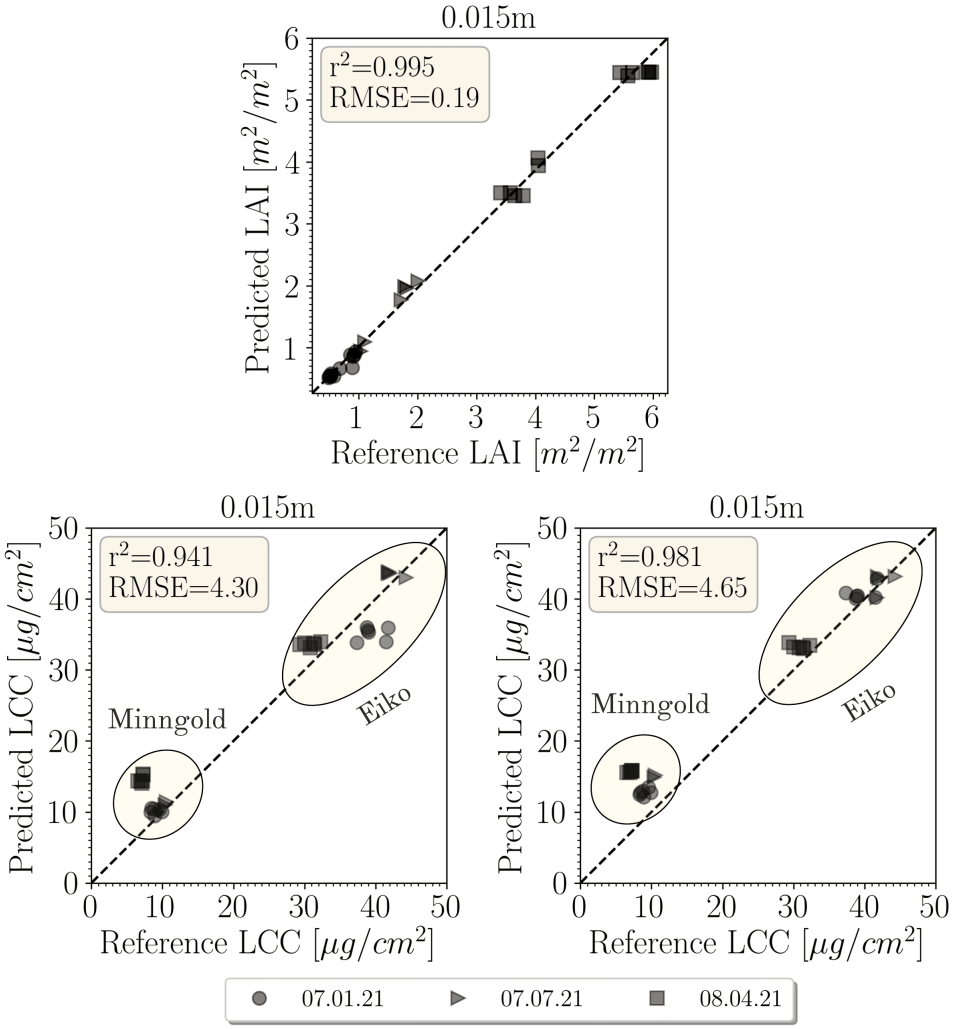

Figure 5.4: Scatter plots of variable retrieval at 0.015 m resolution. Accuracy metrics (R^2 and RMSE) were calculated using datasets from three dates. The upper panel shows LAI retrieval; the lower left panel shows LCC retrieval with orthomosaic containing soil pixels; lower right panel shows LCC retrieval results for orthomosaics with soil removed;. In LCC plots Minngold and Eiko clusters were marked to show differences between varieties.

unmasked orthomosaic can be attributed to the large contribution of soil signals that lower the LCC values.

In this study we have demonstrated that with decreasing spatial resolution the retrieval accuracy of both structural and biochemical parameters slightly decreases. The results for LAI retrieval are comparable with the findings of [191], where authors reported decrease of LAI accuracy with increasing resolution. Our study further demonstrates that soil removal is beneficial for estimating LCC with high precision. Even though soil removal was possible even for 0.48 m data, it is assumed that in more heterogeneous plots it may be more challenging and higher resolution data would deliver more precise results.

It needs to be noted that UAV operation in airspace is limited to a certain height and that some of the spatial resolutions tested here cannot be flown under current regulations. We demonstrated that the coarser resolution data that can be acquired from airborne sensors (0.48 m), would still deliver good retrieval results. In this project no additional atmospheric effects were applied to the resampled image data. It is assumed that correcting for atmospheric attenuation at higher altitudes might not deliver such good results as has been demonstrated in this study. For future research atmospheric simulations could be applied to the image data.

Chapter 6

Retrieval of Crop Variables from Proximal Multispectral UAV Image Data Using PROSAIL in Maize Canopy

This chapter is published as:

E. Chakhvashvili, B. Siegmann, O. Muller, J. Verrelst, J. Bendig, T. Kraska, U. Rascher, "Retrieval of Crop Variables from Proximal Multispectral UAV Image Data Using PROSAIL in Maize Canopy". Remote Sens. 2022, 14, 1247. https://doi.org/10.3390/rs14051247

E.C. acquired the image data, conducted the analysis, and drafted the manuscript. B.S, O.M, J.V, T.K contributed to the review process. J.B and U.R. provided supervision and review feedback. The content of the text remains identical to the published work. However, the format has been adjusted to align with the requirements of the thesis.

Abstract

Mapping crop variables at different growth stages is crucial to inform farmers and plant breeders about the crop status. For mapping purposes, inversion of canopy radiative transfer models (RTMs) is a viable alternative to parametric and non-parametric regression models, which often lack transferability in time and space. Due to the physical nature of RTMs, inversion outputs can be delivered in sound physical units that reflect the underlying processes in the canopy. In this study, we explored the capabilities of the coupled leaf–canopy RTM PROSAIL applied to high-spatial-resolution (0.015 m) multispectral unmanned aerial vehicle (UAV) data to retrieve the leaf chlorophyll content (LCC), leaf area index (LAI) and canopy chlorophyll content (CCC) of sweet and silage maize throughout one growing season. Two different retrieval methods were tested: (i) applying the RTM inversion scheme to mean reflectance data derived from single breeding plots (mean reflectance approach) and (ii) applying the same inversion scheme to an orthomosaic to separately retrieve the target variables for each pixel of the breeding plots (pixel-based approach). For LCC retrieval, soil and shaded pixels were removed by applying simple vegetation index thresholding. Retrieval of LCC from UAV data yielded promising results compared to ground measurements Sweet maize RMSE = $4.92\,\mu g\,cm^{-2}$, silage maize RMSE = $3.74\,\mu g\,cm^{-2}$ when using the mean reflectance approach. LAI retrieval was more challenging due to the blending of sunlit and shaded pixels present in the UAV data, but worked well at the early developmental stages (sweet maize RMSE = $0.70\,m^2\,m^{-2}$, silage RMSE = $0.61\,m^2\,m^{-2}$ across all dates). CCC retrieval significantly benefited from the pixel-based approach compared to the mean reflectance approach (RMSEs decreased from 45.6 to $33.1\,\mu g\,m^{-2}$). We argue that high-resolution UAV imagery is well suited for LCC retrieval, as shadows and background soil can be precisely removed, leaving only green plant pixels for the analysis. As for retrieving LAI, it proved to be challenging for two distinct varieties of maize that were characterized by contrasting canopy geometry.

6.1 Introduction

With the recent technological advancement of UAV platforms and diversification of sensor types, it became possible to retrieve and map crop biophysical variables from high-resolution imagery (<0.1 m) [178]. Biophysical and biochemical variable maps can support agricultural field management, by providing vital information on the plant status throughout the growing season [94]. Apart from supporting farmers in decision-making, spatial information on crop biophysical variables derived from UAV image data can assist the plant breeding community in the high-throughput phenotyping of large quantities of breeding plots [102, 220]. Leaf area index (LAI), which is linked to the absorption of photosynthetically active radiation, transpiration, energy exchange and other phytophysiological variables [12, 10], is one of the most widely explored structural state variables in the crop modeling community. Similar to LAI, leaf chlorophyll content (LCC) can also deliver crucial information on photosynthetic capacity, primary production and the nitrogen status [91, 47, 53]. For this reason, quantification of both variables is important to monitor the crop's status.

Various plant variable retrieval methods have been developed in the remote sensing community in the past few decades [207]. From these methods, parametric regression models have been used to establish an empirical relationship between the variable of interest and vegetation indices, such as for retrieving LAI [87, 130] and LCC [94]. Non-parametric models, e.g., machine learning algorithms, have also been explored to retrieve biophysical and -chemical variables [206, 182, 213]. Often, these methods are characterized by a lack of transferability in space and time and to different environmental conditions and sensors, which might limit their usability to the datasets they were calibrated for. Unlike these methods, vegetation radiative transfer models (RTMs), which describe the radiation interaction with the canopy based on physical laws, are not bound by the constraints of geographical location, time of data acquisition or the sensor configuration. Compared to parametric regression models, RTMs could make use of the whole spectrum, instead of exploiting subsets of the electromagnetic spectrum. This ability is crucial since plant biophysical variables are sensitive across spectral domains, not at specific wavelengths [88]. The inversion of RTMs allows us to derive a large variety of state variables from multi- and hyperspectral remote sensing image data. RTMs have been successfully applied to airborne and satellite data to retrieve plant variables [25, 214].

Multiple vegetation RTMs with varying complexity have been developed for specific purposes and are thus bound by conceptual and computational assump-

tions [139]. For example, 3D radiative transfer models enable us to calculate the radiation budget in a more complex 3D plant canopy, considering the vertical profile and shadows, but require a higher number of input variables to be taken into account [83]. Due to this fact and the demand for more computing power, until now, they have been mainly used for vegetation variable retrieval in complex canopies within a limited spatial extent [148, 116]. In contrast, the combination of the leaf RTM PROSPECT-D [75] and the canopy bidirectional reflectance model (4SAIL) [204], known as PROSAIL [115], requires only a few input variables. However, the assumptions imposed by the simplicity of the model limit its applicability to various scenarios and complex canopy types. Nevertheless, PROSAIL offers a well-balanced compromise between model complexity and required computational effort, and therefore is especially efficient when it comes to large images [26].

In order to retrieve plant variables, the RTM inversion scheme needs to be applied to the reflectance data. RTM inversion is inherently an ill-posed problem: similar simulated reflectance spectra can lead to a wide range of solutions [19]. To overcome the issue of ill-posedness, several inversion schemes have been proposed: numerical optimization (i), look-up table (LUT)-based inversion (ii) and hybrid approaches (iii). (i) Numerical optimization minimizes a cost function value between the measured and predicted reflectance spectrum in an iterative manner. This method requires significant computing power and is time-intensive if applied to a huge number of pixels. (ii) In contrast, the LUT-approach uses a high number of simulations to produce several hundred or thousand reflectance spectra from numerous combinations of input variables. The subsequent inversion is based on finding the best match between a simulated and measured reflectance spectrum by applying a cost function, with the aim to minimize the summed error between a simulated and observed reflectance spectrum. The approach requires a moderate amount of time to build up the LUT, but the subsequent error minimization is very fast [221]. (iii) Hybrid approaches combine the fast computation power of machine learning and generalization level of RTMs [207]. In this approach, RTM simulations are used as training data, leaving ground measurements only for validation.

Ill-posedness can be further alleviated by constraining the variables during the LUT generation. Variables can be constrained based on a priori knowledge about a certain variable and its value range observed in the field [19, 57]. Another way to reduce ill-posedness is exploring different cost functions [207, 56], the application of multiple best solutions instead of a single best solution [17, 126] and adding artificial noise to include uncertainties during the measurements [56, 128].

The applicability of PROSAIL to UAV data has been explored in various studies for various crops. The most widely retrieved variables are green fraction (GF), LAI, LCC and canopy chlorophyll content (CCC) [172, 202, 117, 3, 63, 191]. In the majority of these studies, UAVs were either flown at high altitudes to produce coarse-resolution imagery that mimics airborne or satellite data [172, 202, 63], or the resolution of the final orthomosaic was artificially reduced [172]. This reduction was done to meet the assumption of a turbid medium model such as PROSAIL. While reducing the spatial resolution might be sensible for structural variable retrieval, it has an adverse effect on the estimation of biochemical variables: image data become affected by mixed pixels, meaning that it is no longer possible to separate shaded and soil pixels from vegetation (leaves). This blending effect in turn influences the proper estimation of leaf variables per plot. Images of higher spatial resolution allow the separation of only vegetated pixels from the scene to better estimate the leaf variables. Additionally, in the majority of the above-mentioned studies, hyperspectral sensors were employed. While these sensors deliver spectrally contiguous data, their applicability in breeding and precision agriculture is currently limited due to their high cost and complex data post-processing. Multispectral sensors, on the other hand, are much cheaper and provide information of important spectral regions, which proved to be sufficient to retrieve crop biophysical variables of comparable quality [202]. A common method of retrieving vegetation variables at plot level is averaging the measured spectra per plot and applying the inversion scheme to it. While this method works well for coarse-resolution imagery and for structural variables, we assume that leaf biochemical variables could be better estimated by applying the inversion scheme to the reflectance maps and then averaging the variables per plot. In this way, valuable information on each canopy feature can be obtained.

Therefore, the objective of this study is to explore the potential of PROSAIL LUT inversion for estimating LAI, LCC and CCC from spatial high-resolution multispectral imagery. The specific questions that we aim to answer are:

1. How well can LAI, LCC and CCC be retrieved from high-resolution UAV multispectral image data for complex canopies such as maize?
2. Which inversion scheme, mean reflectance (applying the scheme to a single spectrum averaged per plot) or pixel-based approach (applying the scheme to every pixel and then averaging), leads to more accurate results?
3. How does the retrieval accuracy vary within the growing season for different growth stages?

For this purpose, we have acquired a time-series of image data over a maize canopy

throughout the growing season in 2020. Two types of maize (sweet and silage), which have contrasting structural and functional canopy traits, were sampled during the vegetation period. We have compared estimated variables to non-destructive ground measurements of LAI and LCC conducted shortly before or after UAV data acquisitions.

6.2 Materials and Methods

6.2.1 Study Area

The study area is located at the agricultural research station Campus Klein-Altendorf in the western part of Germany (50°37′ N, 6°59′ E, altitude 176 m) (Figure 6.1). The average annual precipitation is 603 mm and the long-term average annual temperature is 9.4 °C. Two cultivars of silage (*Zea mays*) and seven cultivars of sweet maize (*Zea mays convar. saccharata var. rugosa*) were sown in a field experiment. The total area of the maize trial was 0.12 ha. Silage maize was represented by two varieties, Sunshinos and Stacey, and a mixture of these varieties. Sweet maize was represented by seven varieties: Caramelo, Khan, Mirza, Sweet Nugget, Tatonka, Sweet Nugget and MS Vega. A total of 84 plots, each with the size of 3 × 3 m, were divided into non-destructive and destructive subplots, each 1.5 × 3 m in size. Moreover, 23% of the total plots had two maize rows. The varieties Sweet Nugget and MS Vega were sown in 1 row per subplot. The other sweet maize varieties, except for Tatonka, were sown either in two or one rows. The middle plots of the silage maize part of the trial were a mixture of two silage maize varieties.

6.2.2 Aerial Campaigns

A DJI Matrice Pro 600 (SZ DJI Technology Co., Ltd., Shenzhen, China) served as a sensor carrier platform. The MicaSense Dual camera system, consisting of two multichannel cameras—the MicaSense RedEdge-MX and the RedEdge-MX Blue (AgEagle Sensor Systems Inc., Wichita, KS, US)—was mounted on a Ronin MX gimbal attached to the UAV. The cameras capture images synchronously in ten spectral bands and store them as separate image files (Table 6.1). Each camera has a field of view (FOV) of 47.2° and focal length of 5.4 mm. The images were geotagged with the help of a global navigation satellite system (GNSS) receiver mounted on the UAV. A downwelling light sensor (DLS) provided by the camera

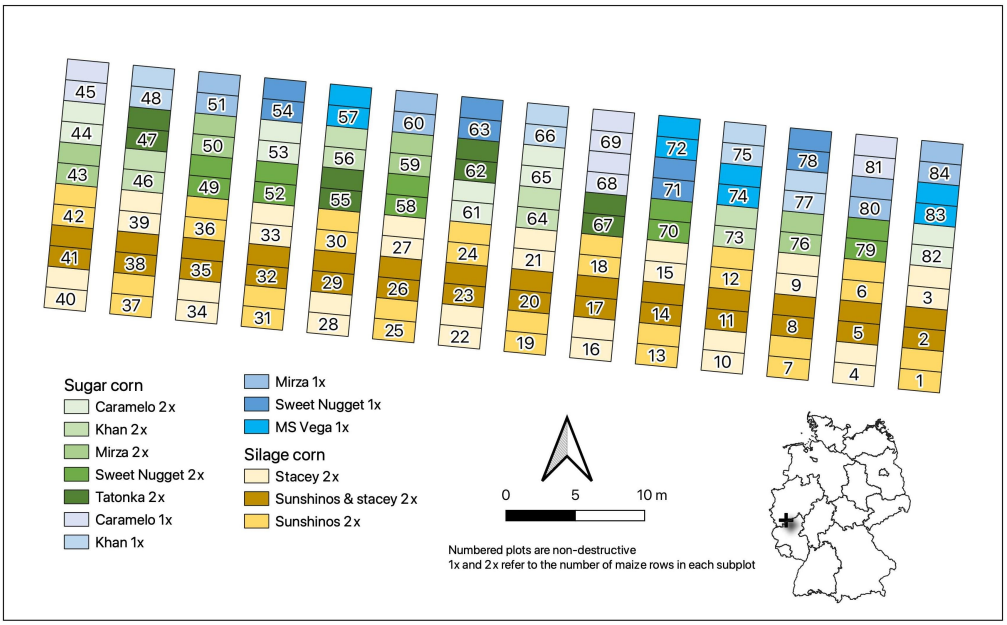

Figure 6.1: Map of the maize trial in PhenoRob Central Experiment, at agricultural research station of campus Klein-Altendorf. Two-row sweet maize plots are depicted in green, one-row sweet maize plots are depicted in blue, and silage maize plots are shown in yellow gradient colors. Inset map shows the location of the experimental field within Germany.

manufacturer was installed at the top of the UAV. The DLS measures irradiance for each band and saves this information in the image metadata. The UAV acquired image data at 20 m above ground level, which resulted in 1.39 cm ground sampling distance (GSD). The flight altitude was set as low as possible to ensure high spatial resolution, but high enough to guarantee proper scene reconstruction with a sufficient number of matching features in image pairs. The UAV was flown at a speed of 3 m/s, resulting in a forward overlap of 80% and sidelap of 70%. Setting these parameters to be high is crucial for achieving good geometry and successful scene reconstruction. Flights were conducted around solar noon on days with stable illumination conditions (Table 6.2). A set of nine near-Lambertian panels (Mankiewicz Gebr. & Co. (GmbH & Co. KG), Hamburg, Germany) with varying reflectance factors and a flat spectral response across the VNIR spectral range, ranging from dark (2%) to bright (63%), was placed within the experiment on bare soil before each flight. The panels were recorded from the same height as the experimental plots (20 m). During post-processing, the panels were used to convert the radiance orthomosaic of the study area to top-of-canopy reflectance [43]. Panel reflectances were measured in the field on 23 June 2020 under sunny conditions using an ASD FieldSpec 4 spectroradiometer (Malvern Panalytical, Malvern, UK). The collected spectral measurements were resampled to match the spectral bandwidths of the MicaSense sensor. In total, eight flight campaigns were carried out throughout the growth season of maize,

which lasted from early June until the harvest in late September (Table 6.2). The measurement dates covered principal growth stages of maize (BBCH scale), which are important from an agronomic perspective for fertilizer application, irrigation and disease control: leaf development, stem elongation, inflorescence, flowering fruit development and ripening.

Table 6.1: Centre wavelengths and bandwidths of the MicaSense Dual camera system.

Band Names	**Centre Wavelength [nm]**	**Bandwidth [nm]**
Blue444	444	28
Blue475	475	32
Green531	531	14
Green560	560	27
Red650	650	16
Red668	668	14
RE705	705	10
RE717	717	12
RE740	740	18
NIR840	842	57

Table 6.2: Details about flight campaigns in 2021. The scale of the Biologische Bundesanstalt, Bundessortenamt und CHemische Industrie (BBCH scale) was used to identify crop growth stages. SZA stands for solar zenith angle and was calculated for each date at 13:00 local time.

Date	**Flight Time (CEST)**	**SZA**	**BBCH**	**Weather Conditions**
23 June	13:08–13:25	27.81°	13–34	sunny
14 July	13:03–13:21	29.52°	39–55	partially sunny, few clouds
21 July	13:21–13:38	30.73°	-	sunny
30 July	13:20–13:37	32.71°	53–65	sunny, few clouds
6 August	13:19–13:40	34.55°	65–68	sunny, few clouds
19 August	13:35–13:53	38.55°	68–71	sunny, few clouds
27 August	13:17–13:33	41.33°	71–73	sunny, few clouds
14 September	13:27–13:40	48.14°	83–87	sunny, few clouds

To assess the illumination conditions during the flights, we mapped the irradiance measurements collected by the DLS. A seamline file was exported from Agisoft MetaShape (v. 1.6.5 photogrammetric software, Agisoft LLC, St. Petersburg, Russia), containing the information for the image footprint that was used to create an orthomosaic. Seamlines corresponded to the borders between parts of images that were used for orthophoto generation. The mosaic blending mode was chosen to minimize optical disruption, i.e., to generate a smooth orthomosaic

without any texture differences between blended images. The DLS measurements were assigned to each respective footprint. Due to rapidly changing illumination conditions, the dataset recorded on 14 July was removed from further processing.

6.2.3 Image Processing

Raw MicaSense images were converted to radiance using the equation provided by the camera manufacturer [169],

$$L = V(x, y) * \frac{a_1}{g} * \frac{p - p_{BL}}{t_e + a_2 y - a_3 t_e y} \tag{6.1}$$

where L is the radiance in W/m^2/sr/nm, *V(x, y)* is the vignette polynomial function for pixel location *x, y*), a_1, a_2, a_3 are the radiometric calibration coefficients, g is the sensor gain setting, p is the normalized raw pixel value (divided by 2N, where N is the number of bits in the image), x and y are the pixel row and column numbers, respectively, p_{BL} is the normalized black level value, and t_e is the image exposure time in ms. The MicaSense python library [146] was used to convert raw images to radiance.

Radiance images were stitched in Agisoft Metashape. They were georectified using 15 ground control points (GCPs) distributed in the field. GCPs were measured with a real-time kinematic GNSS (Trimble R4 GNSS system) with a horizontal accuracy of 8 mm and vertical accuracy of 15 mm. Orthomosaics were generated with mosaic blending mode enabled and exported with the highest resolution shared between all flight campaigns (0.015 m). To correct spectral data for atmospheric attenuation with the empirical line method (ELM) [186], mean radiance values were extracted from the central parts of the panels located within the orthomosaic. Panels with a reflectance factor of >22% were saturated in the visible spectral bands and thus were not considered in the ELM. The same bright panels were not saturated in red-edge and NIR regions and were used in ELM. A simple linear regression was calculated based on the mean radiance values of the panels in the orthomosaic and the measured and resampled reflectance spectra of the panels collected with the ASD spectroradiometer. The resulting linear equations determined for each spectral band were applied to the orthomosaic to convert the radiance values of the image pixels to reflectance, which were used as the basis for the RTM inversion.

For the retrieval of leaf chlorophyll content, shaded and soil pixels were removed from the orthomosaics using a threshold of 0 based on the Hue index [67] in the R package FIELDimageR [143]. Soil removal was problematic for the dataset

acquired on 14 September, since a considerable number of leaves in sweet maize were brown and had a spectral reflectance similar to soil. Thus, soil removal with the index thresholding approach also removed brown leaves from the scene. To avoid this, a crop surface model approach [84] was explored. We subtracted the digital terrain model (DTM) produced from the image dataset acquired before sowing from the digital surface model (DSM) based on the dataset recorded on 14 September to create a crop height model. We removed all pixels with values close to zero from the scene by employing manual thresholding and applied the resulting mask to the orthomosaic.

6.2.4 Field Measurements

Field measurements were conducted before and/or after each aerial campaign. On every measurement date, 18 plots were sampled (seven silage and eleven sweet maize plots). From 30 July onward, more plots (Table 6.3) were measured. LAI was sampled non-destructively using the SunScan plant canopy analyzer (Delta-T devices Ltd., Burwell, United Kingdom). The SunScan system consists of a probe, a sunshine sensor and a personal digital assistant (PDA). The probe has 64 PAR sensors placed on a 1-m-long probe. During data acquisition, the measurements of all sensors are transferred to the PDA. A sunshine sensor, transmitting information on direct and diffuse light to the probe via radiolink [199], was placed between the plots at a height of 1.5 m to avoid shading. The probe was used to collect measurements at six different positions in a non-destructive subplot. According to the SunScan user instructions for each reading, the probe was diagonally placed on the crop rows [199]. The ellipsoidal leaf angle distribution parameter (ELADP) value was set to 1.37, based on the average value for maize taken from the SunScan user manual [40]. Measurements were performed in the period three hours before to three hours after solar noon, as recommended by the manufacturer. LAI readings were averaged for each subplot.

Chlorophyll measurements were collected with a SPAD-502 Chlorophyll Meter (Konica Minolta, Tokyo, Japan). In each subplot, five plants were randomly selected to measure the five upper leaves. Each leaf was measured three times by placing the SPAD at the base, middle and the tip of the leaf. All SPAD readings were averaged per plot. The calibration equation that was used to convert SPAD readings into chlorophyll content ($\mu g\,cm^{-2}$) has been adopted from Haboudane [94]:

$$LCC = 9.1411e^{0.0318*SPAD} \tag{6.2}$$

Table 6.3: Statistics of leaf area index (LAI) and leaf chlorophyll content (LCC) field measurements collected for silage and sweet maize at CKA throughout the growing season; n—number of plots; Stdev—standard deviation, CV—coefficient of variation.

Variable	Maize Type	Stat	23.06	21.07	30.07	6.08	19.08	27.08	14.09
LCC [µg/cm^2]	**Sweet**	**n**	11	11	11	11	6	20	13
		Min	39.0	46.9	41.8	34.2	30.3	31.6	19.0
		Max	53.1	54.3	53.2	54.7	53.5	53.4	42.6
		Mean	47.6	50.4	45.9	43.4	43.2	43.1	30.7
		Stdev	5.1	2.2	3.5	6.8	6.6	6.2	6.5
		CV	0.11	0.04	0.08	0.16	0.15	0.15	0.21
	Silage	**n**	7	6	7	-	7	6	6
		Min	30.6	48.9	46.1	35.5	41.9	40.8	35.3
		Max	44.2	56.9	56.5	56.8	57.9	61.4	53.6
		Mean	38.1	52.8	52.2	46.0	50.2	50.4	42.6
		Stdev	6.0	3.0	3.6	7.8	5.8	5.6	5.4
		CV	0.16	0.06	0.07	0.17	0.12	0.11	0.13
LAI [m^2/m^2]	**Sweet**	**n**	6	8	9	8	14	7	-
		Min	0.5	1.5	2.1	1.9	1.4	1.6	1.4
		Max	1.6	3.7	5.0	5.5	5.1	3.2	3.9
		Mean	0.9	2.9	3.5	3.5	2.9	2.6	2.9
		Stdev	0.3	0.8	0.8	1.0	0.8	0.5	0.6
		CV	0.37	0.27	0.22	0.30	0.28	0.19	0.22
	Silage	**n**	7	7	15	27	6	4	-
		Min	0.5	2.0	1.9	1.6	2.1	2.8	1.6
		Max	0.7	3.3	4.6	5.3	5.6	5.2	5.2
		Mean	0.5	2.5	3.5	3.9	4.1	3.9	3.6
		Stdev	0.1	0.5	0.9	0.9	1.2	0.9	1.3
		CV	0.18	0.21	0.24	0.24	0.30	0.23	0.35

CCC is the product of LAI and LCC:

$$CCC = LCC * LAI \tag{6.3}$$

6.2.5 LUT-Based PROSAIL Inversion

Variable retrieval was conducted in the ARTMO toolbox (Automated Radiative Transfer Models Operator) [205]. The ARTMO toolbox is a software package written in MatLab that provides various tools for running different RTMs in forward or inverse mode, both at leaf and canopy scale. We used PROSAIL [115], a coupled RTM model consisting of the leaf model PROSPECT-5 [75] and the canopy model 4SAIL [203].

For the retrieval of LAI, LCC and CCC, PROSAIL model inversion was conducted using a LUT-based approach. To parameterize the model, we used the variable ranges observed in the field during each measurement date (Table 6.3) or took values from the literature. Separate LUTs were constructed for each date to constrain the model and reduce the effect of ill-posedness [19].

Leaf structure index N was set to a value range of 1.2–1.8, as has been reviewed in the literature for maize [26]. Brown pigment content was set to zero for the datasets acquired at early crop development. For datasets from 19 August onward, the range of 0–0.5 with uniform distribution was used, as the leaf browning was observed in the majority of the sweet maize plots. The range of dry matter content was set to 0.004–0.0075 (g/cm^2), according to a literature review [26]. Since silage and sweet maize had visually different leaf inclination angles, the leaf angle variable was set to a range of 20–70. Silage maize varieties had predominantly erectophile/spherical leaves, while sweet maize leaves had predominantly planophile/spherical leaves. Soil reflectance information was extracted from pure soil pixels from the radiometrically calibrated orthomosaics. From every orthomosaic, several areas with visually differentiable soil characteristics (compressed, ploughed) were extracted using the mean reflectance of different regions of interest. Soil spectra were extracted for dry and wet soil separately. For LCC retrieval, the soil reflectance was of low importance in this study, as the high-resolution image data allowed us to easily differentiate soil from plant pixels and remove them when necessary. The hot spot parameter was set to the range given in the literature of 0–0.2 [26]. Fixed sun zenith angles were used as input for different dates. Observer zenith angle (OZA) was fixed to 0°, as the images were acquired from the nadir position. We did not calculate the OZA [172] for every pixel as it was beyond the scope of this study. However, the reader should keep in mind

that in the generation of orthomosaics, not only the nadir part of the images was used but, to some degree, the peripheral parts as well.

Table 6.4: PROSAIL variables used in the construction of individual LUTs. LAI and LCC ranges were adjusted for each LUT separately.

Variable	Description	Range	Distribution
PROSPECT-5			
N	Leaf structure index	1.2–1.8 [26]	Uniform
C_{ab}/LCC [µg/cm^2]	Leaf chlorophyll content	0–70	Gaussian
C_{cx} [µg/cm^2]	Leaf carotenoid content	Default value	-
C_{bp} [unitless]	Brown pigments	0–0.5	Fixed/Uniform
C_m [g/cm^2]	Dry matter content	0.004–0.0075 [26]	Uniform
C_w [g/cm^2]	Leaf water content	Default	-
4SAIL			
LAI [m^2/m^2]	Leaf area index	0–7	Uniform
ALIA [°]	Average leaf inclination angle	20–70 [26]	Step of 1
Hot	Hot spot parameter	0.01–0.5 [26]	Uniform
ρ_{soil} [%]	Soil reflectance	Extracted from image	-
SZA [°]	Sun zenith angle	Different for each date	-
OZA [°]	Observer zenith angle	0	-
rAA [°]	Relative azimuth angle	0	-

To produce LUTs, PROSAIL was first run in forward mode separately for each date. We used either Gaussian or uniform distributions for the variables (Table 7.2). Multiple studies have successfully used Gaussian distributions for chlorophyll content retrieval [27]. It has been demonstrated that applying sampling constraints to the LUT generation based on a priori information may increase the retrieval accuracy [19]. Combination of these variables resulted in LUTs having hundreds of thousands of entries. We used the Latin hypercube sampling (LHS) [176] method implemented in ARTMO to select only a subset of 10,000 entries for each LUT.

Gaussian noise of 2% was added to the LUTs to account for variable measurement uncertainties. We used the mean (5%) of the multiple best solutions to find the best match between simulations and measurements to reduce the effect of ill-posedness. Two different approaches were applied to retrieve the variables: (1) the inversion scheme was applied to mean reflectance spectra calculated for each plot (mean reflectance approach) to retrieve the variables; (2) the inversion scheme was applied to orthomsoaics with reduced spatial resolution (GSD = 0.09 m) to retrieve LAI and CCC, with the aim to speed up the mapping procedure. It was also applied to the orthomosaics with the original spatial resolution to map LCC. Afterwards, mean LCC values for each plot were determined and compared

to the ground measurements (Figure 6.2).

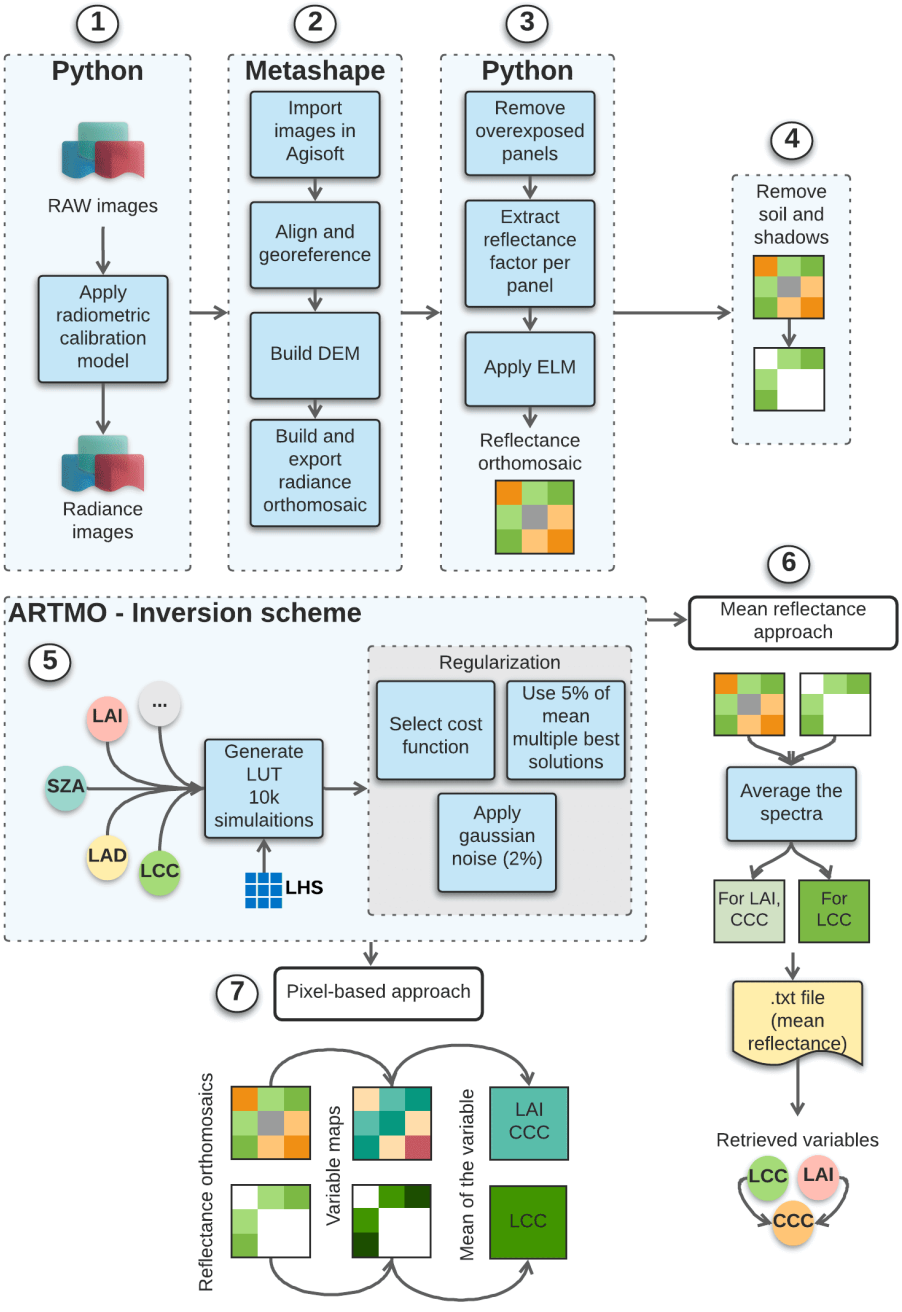

Figure 6.2: General workflow for the retrieval of LAI and chlorophyll content using different software packages: (1) conversion of raw images to radiance, (2) scene reconstruction in photogrammetric software, (3) application of ELM, (4) soil/shadow removal for pigment retrieval and (5) LUT construction and inversion, (6–7) application of inversion scheme using two different approaches. LHS—Latin hypercube sampling.

6.2.6 Statistical Analysis

To study the accuracy of the plant trait retrieval, several metrics were employed: root-mean-square error (RMSE), relative RMSE (rRMSE) and the coefficient of determination (r^2):

$$RMSE = \sqrt{\frac{1}{n}\sum_{i=1}^{n}\Big(d_i - f_i\Big)^2} \tag{6.4}$$

$$rRMSE = 100 * \frac{RMSE}{\langle d \rangle} \tag{6.5}$$

where d_i are observations, f_i are the estimates and $\langle d \rangle$ is the statistical mean.

6.3 Results

6.3.1 Variable Retrieval

A visual overview of the retrieval results for all dates can be found in Figure 6.3. Results of the LAI, LCC and CCC retrieval using the mean reflectance approach and pixel-based approach can be found in Figures 6.4 and 6.5, respectively. For LCC retrieval, mean reflectance values were calculated on pure green, sunlit pixels. For LAI and CCC retrieval, mean reflectances of soil, shadows and plant pixels were included. In the following sections, each variable will be analyzed by comparing the two above-mentioned approaches.

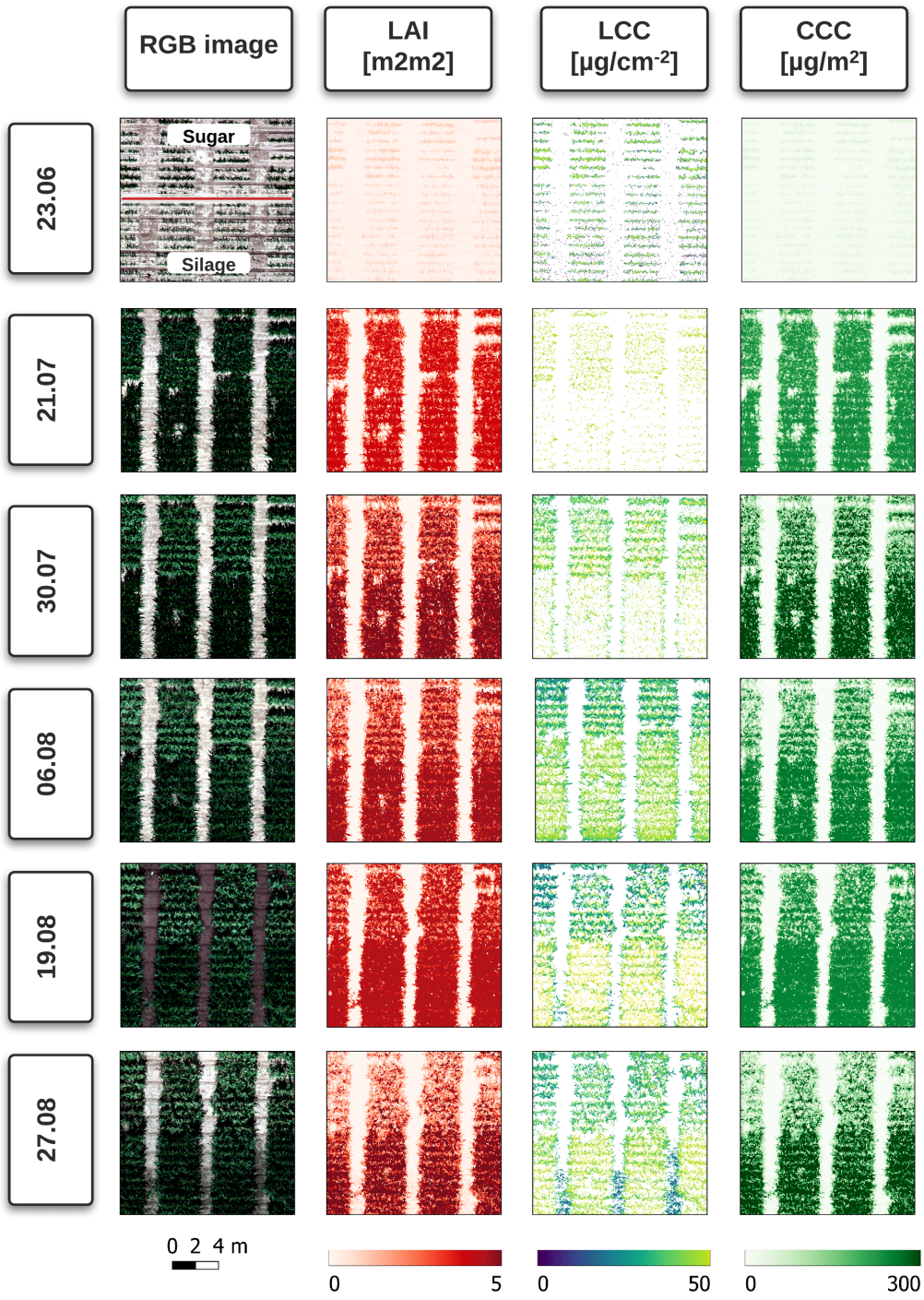

Figure 6.3: Maps of LAI, LCC and CCC on acquisition dates. RGB orthomosaics are depicted at 0.015 m spatial resolution. The first RGB map (23.06.) displays the separation between the two maize types. For fast processing, LAI and CCC maps were created using 0.09 m resolution orthomosaics. LCC maps are displayed at original resolution of 0.015 m.

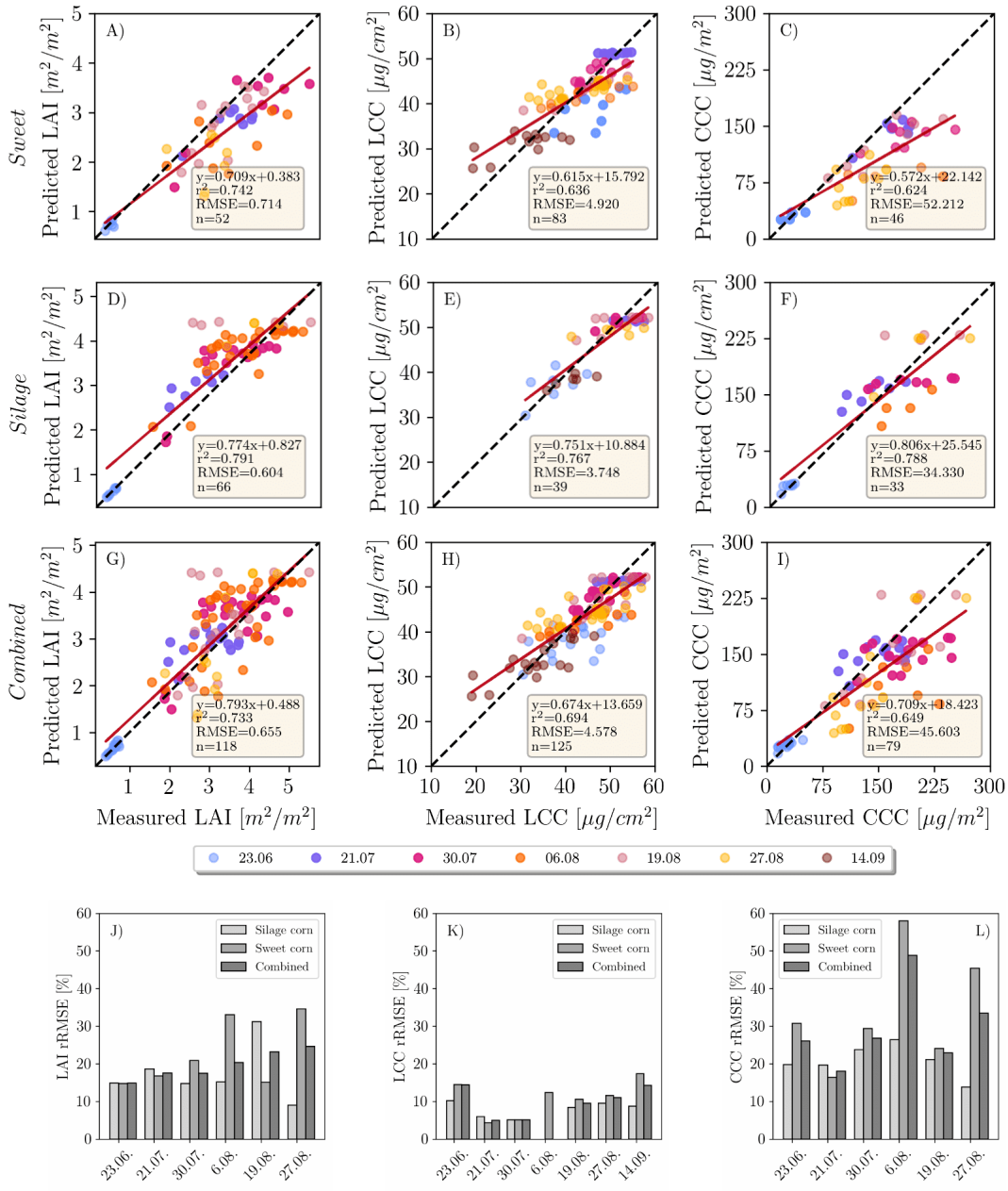

Figure 6.4: Comparison of predicted mean LAI, LCC and CCC values per subplot to the reference measurements throughout the growing season. The first row represents the inversion results for the mean reflectance approach applied to the sweet maize plots (A-C), second row—silage maize plots (D-F) and third row—both maize types (G-I). rRMSE plots for each date and variable are displayed in the lowermost row (J-L).

6.3.1.1 LAI

The accuracy of the LAI retrieval for silage maize is higher (RMSE = 0.604 m^2/m^2) compared to sweet maize (RMSE = 0.714 m^2/m^2) when looking at the

pooled data of the mean reflectance approach (Panels A and D in Figure 6.4). There is a general trend of overestimation for the silage maize and underestimation for the sweet maize. When looking at separate dates (Figure 6.4J), the retrieval accuracies were higher in earlier plant growth stages (23.06., 21.07., 30.7.) compared to late stages. This is well depicted in Figure 6.6. Among these dates, the highest prediction accuracy could be achieved on 23.06., which corresponds to the growth stage of early stem elongation (rRMSE = 14.9%, Figure 6.4J), followed by late stem elongation (21.07., rRMSE = 17.6%) and start of heading (30.07., rRMSE = 17.5%). Retrieval accuracy decreased for sweet maize on 06.08. (flowering, rRMSE = 30%), while it remained stable for silage maize (rRMSE = 15%). The reason for this substantial decrease in the retrieval accuracy for the sweet maize might be attributed to the pollination, which covered plant leaves with a thin layer of yellow pollen, affecting the reflectance signal. On 19.08. (end of flowering, start of fruit development), we observed the opposite trends: low retrieval accuracy for silage maize (rRMSE = 31%) and high accuracy for sweet maize (rRMSE = 15.1%). This was unexpected, since, for the following measurement date (27.08.—fruit development), the trend again reversed (silage maize, rRMSE = 9%; sweet maize, rRMSE = 34%). One of the explanations for this shift might be the illumination conditions on 19.08. (cloudy) compared to other dates, when it was predominantly sunny. The underestimation of LAI in sweet maize might be attributed to the SunScan measurements, during which a fixed ELADP value was used. As mentioned before, sweet and silage maize had different LADs (leaf angle distribution). We used average ELADP for both maize types, as suggested in the manual. Thus, differences in LAD were not taken into account. Furthermore, LAD slightly changes over the plant growth period and this change was not reflected in the selected ELADP value.

In the pixel-based approach (Figure 6.5G), the total accuracy decreased only slightly (RMSE = 0.65 m^2/m^2) compared to the mean reflectance approach. Accuracy slightly increased for sweet maize (average rRMSE = 22%) and decreased for silage maize (average rRMSE = 20%) (Figure 6.5J). The highest rRMSE was determined for the silage maize dataset recorded on 23.06. (rRMSE = 36%), while sweet maize rRMSE also increased (23%) compared to the mean reflectance approach. In both cases, the models were overestimating.

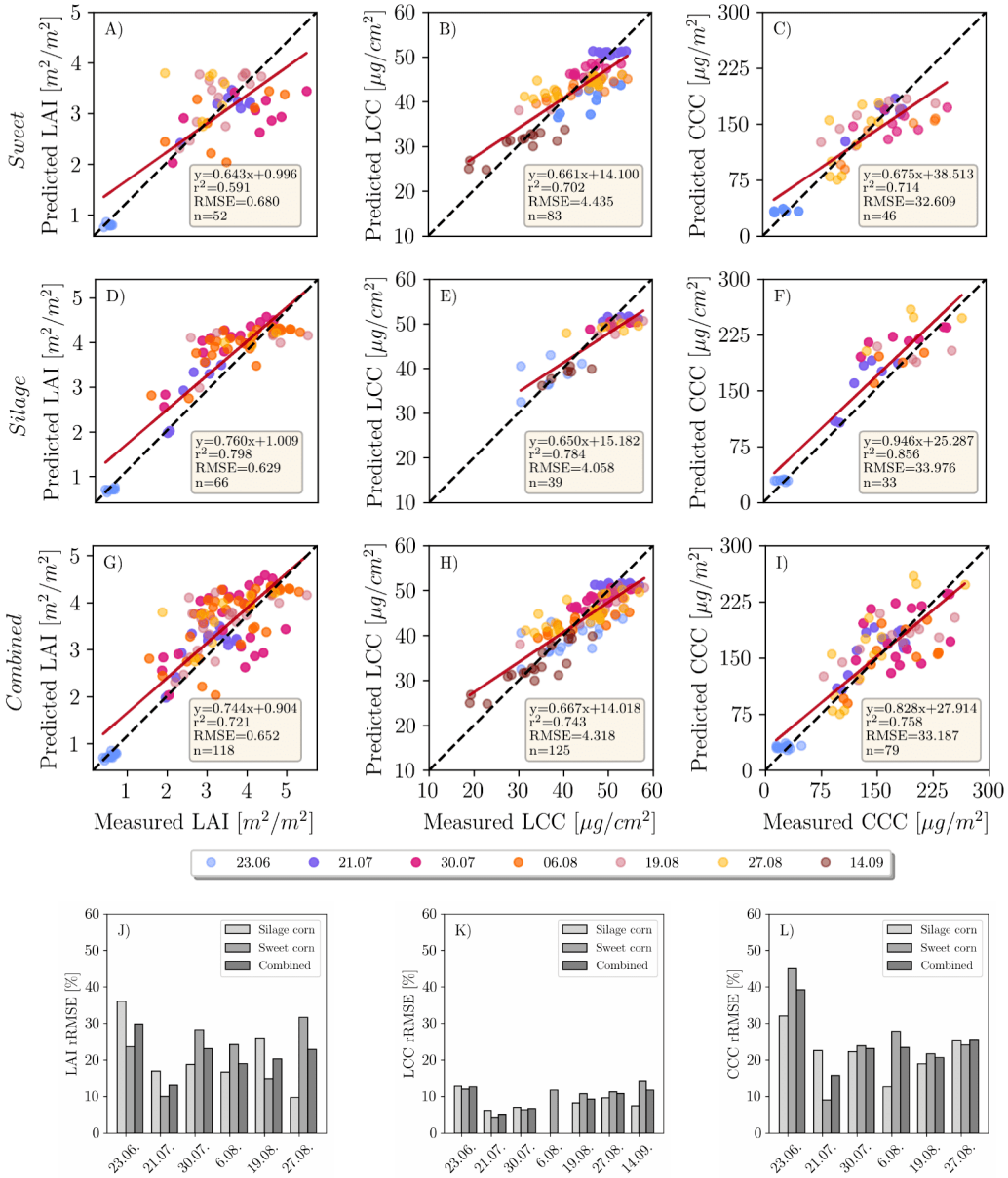

Figure 6.5: Comparison of predicted mean LAI, LCC and CCC values per subplot to the reference measurements throughout the growing season. The first row represents the inversion results for the pixel-based approach applied to the sweet maize plots (A-C), second row—silage maize plots (D-F) and third row—both maize types (G-I). rRMSE plots for each date and variable are displayed in the lowermost row (J-L).

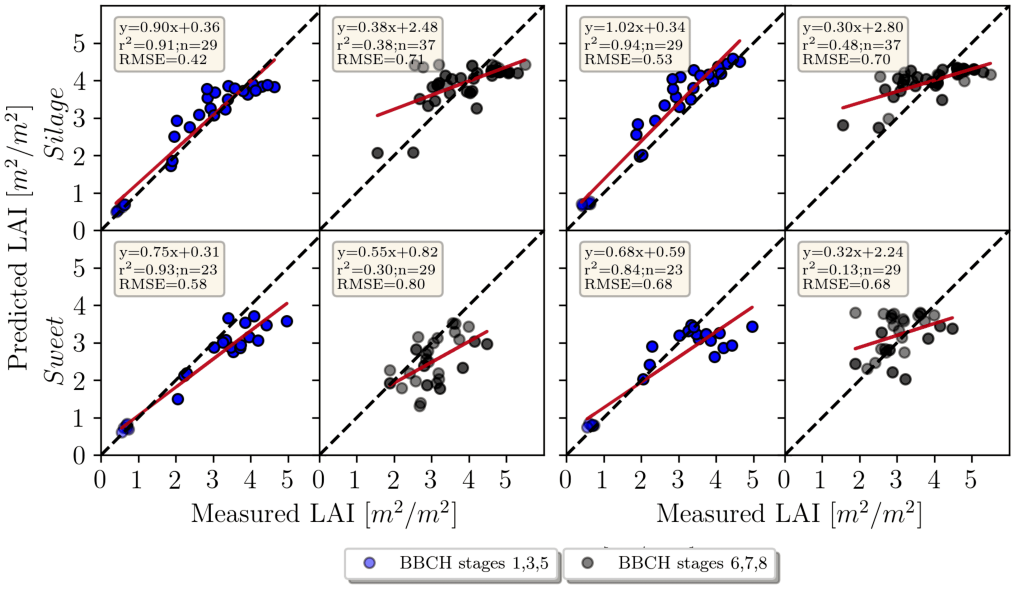

Figure 6.6: LAI retrieval using two approaches (**left** mean reflectance, **right** pixel-based) for early and late growth stages. BBCH principal growth stages 1, 3 and 5 correspond to leaf development, stem elongation and the start of inflorescence. Stages 6, 7 and 8 correspond to flowering, fruit development and ripening.

6.3.1.2 LCC

Compared to LAI, LCC retrieval produced more reliable results when using the mean reflectance approach. RMSE for silage maize (RMSE = 3.74 µg/cm^2) was lower than for sweet maize (RMSE = 4.88 µg/cm^2) (Panels B and E in Figure 6.4). It has to be noted that the numbers of samples taken in sweet maize plots were double the size compared to silage maize. Additionally, sweet maize in general was characterized by a larger variation in chlorophyll content at later growth stages, while LCC in silage maize within single dates showed little variation, except for 06.08., when the pollination was observed (Table 6.3). The coefficient of determination for pooled data is also higher for silage maize (r^2 = 0.76) than for sweet maize (r^2 = 0.63; Figure 6.4H). As for the single dates, the highest rRMSEs were recorded on 23.06. (early stem elongation, rRMSE = 14.5%) and 14.09. (start of senescence, rRMSE = 17.4%) for sweet maize (Figure 6.4K). The lowest rRMSEs were recorded for the datasets where LCC ground measurements had small Stdev (Table 6.3). The lowest chlorophyll content for sweet maize was retrieved for the dataset acquired on 14.09., when all sweet maize varieties were approaching senescence (Figure 6.4H). On the same date, the upper leaves of silage maize were still green, but decreased chlorophyll values were observed compared to 27.08. (Table 6.3). A general trend of overestimation is observed for

low chlorophyll content, while higher LCC is characterized by underestimation (Figure 6.4H).

When looking at the pixel-based approach, the total estimation accuracy increased slightly (RMSE = 4.318 µg/cm^2), driven by the accuracy increase in sweet maize (Figure 6.5H). Here, again, we observe overestimation with low LCC values and underestimation with high values Figure 6.5H). For silage maize, accuracy slightly decreased on 23.06. (rRMSE = 12%) and increased on 14.09. (rRMSE = 7.4%; Figure 6.5K).

6.3.1.3 CCC

CCC retrieval is largely influenced by the LAI when looking at the mean reflectance approach (Figures 6.4I and 6.5I). The observed underestimation of LAI for sweet maize also caused an underestimation in the CCC (RMSE = 52.21 µg/m^2, Figure 6.4C). When looking at single dates, the highest rRMSE (58%) was produced for the 06.08. (flowering) followed by 27.08. sweet maize datasets (rRMSE = 45.4%; Figure 6.4L). For silage maize, the achieved results were better (rRMSE across all dates ≈ 20%; Figure 6.4L). The retrieval accuracy drastically changed when applying the pixel-based approach (Figure 6.5I). A distinct decrease in RMSE from 52.21 to 33.18 µg/m^2 (Figure 6.5C) could be observed for sweet maize. The main reason for the improvement was the distinctly reduced underestimation of predicted sweet maize LAI values (Figure 6.5I).

6.4 Discussion

In this study, the advantages of high-resolution imagery for maize crop variable retrieval using the PROSAIL model were demonstrated. The retrieval of LCC benefited from using a high spatial resolution to differentiate between distinct features in the scene, such as soil, shadow and plant pixels. For LAI, retrieval appeared to be challenging for the maize canopy. A clear discrepancy in LAI retrieval accuracy between different growing stages could be observed. We achieved an RMSE of 0.65 m^2/m^2 for the combined maize dataset retrieving LAI using the PROSAIL model (Figure 6.4G), which is comparable with the results observed for maize in satellite-based studies [25, 95, 214]. Comparison of our results to other UAV-based studies is challenging due the low number of studies focusing on high-resolution UAV-based variable retrieval with PROSAIL. Su et al. [189] reported an RMSE of 0.33 m^2/m^2 for a maize experiment with different sowing

densities and across the entire growth period (which relates to our study) using a four-band multispectral camera. Our experiment, however, did not include different sowing densities, which tend to create significant contrasts in LAI. These contrasts are largely driven by the exposed soil, which differs by area based on the sowing density. In another study [63], the authors achieved an RMSE of 0.58 m^2/m^2 using hyperspectral UAV data of maize with a spatial resolution of 0.7 m. It has to be noted that the number of samples they used was very limited (four samples in total), and thus the comparison across growing stages cannot be made.

One of the reasons for the different LAI prediction accuracies achieved for sweet and for silage maize (RMSE = 0.714 and 0.628 m^2/m^2, respectively) might be the particular choice of the ELADP value used for leaf angle distribution during the SunScan measurements. In both maize types, a fixed value was used; however, the LAD visually differed between the two maize types. Therefore, the observed overestimation of LAI in the case of silage, and underestimation in the case of sweet maize, could be attributed to the fixed ELADP value chosen for the ground measurements. Additionally, the SunScan measurement results varied strongly depending on the probe placement in the canopy during data acquisition, which had a significant effect on the LAI estimation. Neighboring silage maize plots might also cast shadows on the sugar maize plots, distorting the measurements in the latter.

The discrepancy in LAI estimation at early (stem elongation) and late growth stages (flowering, etc.) is another point that requires attention. Better estimation results for early stages can be attributed to the smaller number of leaves compared to later growth stages, when leaf clumping is more pronounced, especially for nadir imagery, where row effects are clearly discernible [69, 104]. It is known that PROSAIL simulations have limited applicability in row crops such as maize [13], which are characterized by large gaps between the rows and rather open canopies. Similar to [104], the underestimation observed specifically in sugar maize (Figure 6.4A) could be attributed to the absence of leaf clumping correction in the PROSAIL model. While these canopy characteristics were partially considered when conducting ground measurements, they cannot be parameterized in PROSAIL. PROSAIL assumes a homogeneous and closed canopy, the condition partially met by the satellite and airborne images but not by the high-resolution UAV images. For better estimation of LAI in maize, RTMs that account for leaf clumping and shading can be explored. Moreover, 3D radiative transfer models such as DART [83] consider the complex canopy structure and thus leaf clumping. However, for practical purposes, 3D RTMs have some disadvantages, such as their high computational demand and the larger number of

parameters needed for model parameterization, which limits their application for agricultural practices.

Regarding the comparison of the pixel-based and mean reflectance approaches, we did not see significant improvements when using the pixel-based approach for LAI estimation. The latter generally overestimates the LAI values for both maize types compared to the mean reflectance approach (Figure 6.5). In the case of silage maize in the early growth stages, the measured RMSE for the mean reflectance approach was lower than for the pixel-based approach, yet underestimation was observed for high LAI values. This is not the case for the pixel-based approach, which is characterized by overestimation at all growth stages, resulting in a slope value of 1.02, as contrasted to a slope of 0.90 for the mean reflectance approach (Figure 6.6). The general overestimation of the pixel-based approach can be attributed to the usage of every pixel in the inversion. The shaded pixels, which cover larger areas in silage maize plots than the sunlit leaf pixels, result in higher LAI values compared to the sunlit green pixels (Figure 6.3). This in turn results in overestimation of LAI. The overestimation is apparent with the mean reflectance approach for the silage maize, where the shaded pixels distinctly contribute to the overall reflected radiation. The sugar maize is mostly characterized by a denser canopy, with shaded pixels only between the rows (see RGB images in Figure 6.3) and overall smaller areas covered by shaded pixels as compared to silage maize. The amont of LAI underestimation observed in sugar maize is in agreement with the findings of [104, 114].

Although there is evidently a substantial benefit in using the very high-resolution imagery for LAI retrieval in breeding plots, for agricultural applications, it is not so beneficial. High-resolution imagery has proven advantageous for better discrimination between the pure plant pixels and the soil/shadows for biochemical parameter retrieval. We achieved high accuracy in LCC estimation by removing soil/shadows from the scene, when using the mean reflectance approach (combined RMSE 4.6 µg/cm^2). Additionally, LCC retrieval benefited from the pixel-based approach (combined RMSE from 4.6 to 4.3 µg/cm^2; combined r^2 from 0.69 to 0.75). The results deliver better estimates than satellite-based studies (RMSE 8–10 µg/cm^2) [114, 58, 104]. LCC estimation worked better for sweet than for silage maize. A possible explanation could be the low fractional cover in silage compared to sweet maize during the early growth stages—for example, on 23.06.—which led to limited vegetation pixels retrieved from the scene.

Furthermore, the in situ, non-destructive measurements may contribute to uncertainties in LCC retrieval. SPAD calibration equations are species- and variety-specific [42, 171], but a fixed equation adopted from the literature was used in

this study. Retrieval accuracy could be improved by deriving separate calibration equations per maize type, converting SPAD measurements to chlorophyll content in physical units. The constant overestimation of low LCC and underestimation of high LCC values by both approaches (Figures 6.4H and 6.5H) for each date may be attributed to the use of a calibration equation that does not reflect the actual relationship between SPAD values and real chlorophyll content.

We used all available spectral bands provided by the MicaSense Dual camera system for the LCC estimation. It is known that chlorophyll retrieval is mostly sensitive in the visible spectral range [27]. One of the ways to increase the LCC retrieval accuracy would be to apply a spectral constraint to the model. This would entail removing the spectral bands that are not sensitive to chlorophyll content from the reflectance data. As demonstrated previously [27], the removal of red-edge bands, characterized by the largest error between simulated and measured reflectance in maize, enabled higher retrieval accuracy.

Being a product of LAI and LCC, CCC retrieval accuracy depends on the retrieval of the two state variables. We found significant improvements in CCC retrieval when using the pixel-based approach (RMSEs reduced from 45.6 to 33.1 µg/cm^2, and r^2 from 0.64 to 0.75). This increase in accuracy is driven by the better estimation of LCC when applying the pixel-based approach.

Although the pixel-based approach delivers better results for LCC and CCC retrieval, the computing time of applying a LUT-based inversion scheme to each pixel is not practical. Compared to numerical optimization, the LUT-based approach is not as computationally intensive when the inversion scheme is applied to single plots, but it becomes inefficient when mapping the high-resolution orthomosaics of large areas. In this regard, hybrid approaches, which employ the power of machine learning combined with simulated spectra produced by an RTM, can distinctly speed up the process [28, 207].

We demonstrated that high spatial resolution is beneficial for pigment retrieval, as well as LAI retrieval for small breeding plots, but we did not explore the impact of artificially reducing the spatial resolution on the final results. For application in large farming fields, UAVs need to be flown at much higher altitudes, producing orthomosaics with lower resolution. Thus, the effects of different spatial resolutions on the retrieval accuracy has to be better understood and studied in the future. Furthermore, a better understanding of the impact of LAD in both maize types is required. In this regard, plant architecture reconstructed from terrestrial laser scanners (TLS) [15] could potentially deliver information on leaf inclination angles that can be used to better parameterize the model and explore

their impact on the parameterization.

6.5 Conclusions

In this study, we investigated the potential of the inversion of the radiative transfer model PROSAIL to retrieve LAI, LCC and CCC of sweet and silage maize, using spatial high-resolution UAV data acquired throughout one growing season. Two different retrieval approaches were investigated: (1) the mean reflectance approach—applying the inversion scheme to the mean reflectance spectrum per plot; (2) the pixel-based approach—applying the inversion scheme to all pixels of an orthomosaic and then calculating the variable mean for each plot. The performance of both approaches was evaluated based on the goodness of fit parameters RMSE and rRMSE by comparing the estimated variables to ground-truth measurements collected in the field.

Compared to spatially lower-resolution satellite and airborne imagery, high-resolution UAV images allowed the separation of soil, shaded and sunlit pixels. Thus, it was possible to retrieve the leaf chlorophyll content (LCC) by applying the inversion scheme only to green sunlit pixels. The LCC retrieval yielded promising results in comparison to ground measurements when using both retrieval approaches and led to higher accuracies compared to satellite or airborne studies. The measurement uncertainties associated with LCC retrieval could be further reduced by acquiring destructive chlorophyll measurements for a more accurate SPAD to LCC conversion equation. Furthermore, the impact of constraining the spectral range used for the retrieval of the different parameters should be further investigated. The retrieval of the structural variable leaf area index (LAI) was more challenging due to the mixing of sunlit and shaded pixels present in the UAV data. Further difficulties arose from plants grown in rows and having a complex canopy structure with varying leaf angles. The best results were obtained for early growth stages (leaf development, early and late stem elongation). We observed a significant improvement in the estimation of canopy chlorophyll content (CCC) when the pixel-based retrieval approach was used. We argue that high-resolution UAV imagery is well suited for biochemical variable retrieval, as shadows and background soil can be precisely removed, leaving only green plant pixels for the analysis. Compared to empirical approaches, vegetation RTMs offer a more robust, transferable solution to the retrieval problem and deliver results in real physical units. Further research is needed to validate the transferability of the model using similar sensor settings to the maize canopies. Furthermore, a more detailed characterisation of the canopy structure could improve the retrieval re-

sults, specifically of LAI. In addition, 3D RTMs would enable such a canopy characterization and should be explored in future studies.

Chapter 7

Multispectral imaging and terrestrial laser scanning for the detection of drought-induced paraheliotropic leaf movement in soybean

This chapter is published as :

E. Chakhvashvili, L. Stausberg, J. Bendig, L. Klingbeil, B. Siegmann, O. Muller, H. Kuhlmann, U. Rascher, "Multispectral imaging and terrestrial laser scanning for the detection of drought-induced paraheliotropic leaf movement in soybean", International Journal of Applied Earth Observation and Geoinformation, 2024, 135, p.104250.
https://doi.org/10.1016/j.jag.2024.104250

E.C. and L.S share the contribution. E.C acquired the image data, conducted the analysis, and drafted the manuscript. L.S acquired laser scanning data, conducted the analysis and drafted the manuscript. B.S and O.M contributed to the review process. J.B, L.K, H.K and U.R. provided supervision and review feedback. The content of the text remains identical to the published work. However, the format has been adjusted to align with the requirements of the thesis.

Abstract

Plant foliage is known to respond rapidly to environmental stressors by adjusting leaf orientation at different timescales. One of the most fascinating mechanisms is paraheliotropism, also known as light avoidance through leaf movement. The leaf orientation (zenith and azimuth angles) is a parameter often overlooked in the plant and remote sensing community due to its challenging measurement procedures under field conditions. In this study, we investigate the synergistic potential of uncrewed aerial vehicle (UAV)-based multispectral imaging, terrestrial laser scanning (TLS) and radiative transfer model (RTM) inversion to identify the paraheliotropic response of two distinct soybean varieties: Minngold, a chlorophyll-deficient mutant, and Eiko, a wild variety. We examined their responses to water stress during the boreal summer drought in 2022 in western Germany by measuring average leaf inclination angle (ALIA) and canopy reflectance. Measurements were taken in the morning and at midday to track leaf movement. Our observations show significant differences between the paraheliotropic response of both varieties. Eiko's terminal and lateral leaves became vertically erect in the midday ($54 \rightarrow 63°$), while Minngold's ALIA remained largely unchanged ($52 \rightarrow 57°$). Apart from the vertical leaf movement, we also observed leaf inversion (exposing the abaxial side of the leaf) in Eiko under extreme water scarcity. The red edge band at 740 nm showed the strongest correlation with ALIA ($r^2 = 0.52 - 0.76$), as predicted by sensitivity analysis of the PROSAIL radiative transfer model (RTM). The ratio of the far red edge to near infrared (RE740/NIR842) vegetation index compensated for varying light levels during morning and afternoon measurements, exhibiting strong correlations with ALIA when considering only sun-lit leaf spectra ($r^2 = 0.72$). In contrast, the correlation of leaf area index (LAI) with RE740/NIR842 was low ($r^2 = 0.35$). The retrieval of ALIA with PROSAIL varied based on ALIA constraints and the spectra used for retrieval (full spectrum or the combination of bands 742 and 842), resulting in a root mean square error (RMSE) of 7.7-12.9°. PROSAIL faced challenges in simulating the spectra of plots with very low LAI due to the soil background. The exclusion of these plots from the analysis resulted in RMSEs of 3.7-13.0°, depending on ALIA constraints. This study made the first attempt to observe different paraheliotropic responses of two soybean varieties with UAV-based multispectral imaging. Proximal sensing opens up the possibilities to observe early stress indicators such as paraheliotropism, at much higher spatial and temporal resolution than ever before.

7.1 Introduction

Monitoring crop biophysical parameters has gained increased importance due to the challenges arising from extreme climatic and biotic events [48]. Water, heat and light stress are the leading causes of crop yield reduction [71]. Plants have evolved various adaptations to cope with these stressors, including chloroplast movement [98], changes in chlorophyll concentration [154], non-photochemichal quenching (NPQ) [152] and paraheliotropism also known as light-avoidance through leaf movement [163, 136]. While the leading factor in paraheliotropic leaf movement is excess light, temperature and water availability also influence the process [170]. Paraheliotropism involves turgor pressure changes at the base of lamina [156], which causes the leaves to align parallel to the incident light. This way plants avoid high leaf temperature, high evapotranspiration [65, 78], and excess light during drought (photoinhibition) [136]. Despite many observations, the significance of this adaptive mechanism remains poorly understood [65, 145, 228].

Paraheliotropism is commonly seen in legumes such as soybean [145, 160, 173, 124]. Soybean accounted for approximately 29% of oilseed production in 2022 [73]. Its production increased nearly 13-fold from 1961 to 2017, owing to its significance as a vital source of protein for both humans and animals [133]. Given its widespread importance, monitoring the health status of soybean in the face of adverse environmental events, such as drought, is important. An early indicator of water scarcity in soybeans is the paraheliotropism [145]. Typical leaf movement patterns involve erecting leaves vertically during midday as well as leaf inversion (exposing the abaxial side) in the presence of extreme drought.

Leaf movement can be characterised by leaf orientation parameters, one of which is the average leaf inclination angle (ALIA). ALIA is described as an angle between leaf normal and the zenith. It influences light interception, photosynthesis efficiency, competition in plant canopies and acts as an early stress indicator [179, 228], making it an essential parameter in plant physiology and crop production. Despite its importance, ALIA has been relatively overlooked due to the challenges associated with in-situ measurements being laborious and error-prone. Many studies opt for indirect retrieval methods instead of in-situ ones, which include photographic [34, 153, 110, 241] and laser scanning approaches, [237, 15] allowing diurnal and almost instantaneous measurements of ALIA under field conditions. While these systems deliver good results, they face limitations in scalability due to their labor-intensive measurement procedures. The efficiency of these systems diminishes as the study area expands. The challenge arises from

the rapid changes in leaf orientation parameters over time, making the measurement process more difficult for larger areas. An alternative, yet under-explored, approach to measure ALIA involves radiative transfer models (RTMs) using optical data acquired from airborne platforms. This method holds considerable potential for wider application as data acquisition is faster and easier compared to the photographic or laser scanning methods.

Together with leaf area index (LAI), ALIA is an important parameter for radiation transfer within the canopy and significantly contributes to the signal detected by optical sensors. While a substantial research attention has been given to LAI as a proxy for physiological processes [11] retrieval of ALIA using RTMs has been understudied [26]. RTMs simulate absorption, transmittance and reflectance of single leaves or plant canopies. Due to their physical nature, RTMs can be universally applied, which eliminates the need to calibrate the model to specific sensor, crop or geographical location. The most widely used RTM, PROSAIL, which is a coupled leaf- (PROSPECT) [113] canopy (SAIL) [203] model, employs ALIA as one of the main structural input parameters. In the electromagnetic spectrum, ALIA is most sensitive in the far red edge and near-infrared (NIR) regions and shares this sensitivity with LAI [115, 241]. Since these two parameters have a similar effect on the reflectance spectrum of vegetation, a constraint, specifically a priori knowledge of the parameter should be introduced [112]. To obtain this knowledge, field-based ALIA measurements are integral.

RTMs have primarily been applied to satellite data, which often lacks the necessary spatial and temporal resolution to be effective in high-throughput field phenotyping applications. In contrast, uncrewed aerial vehicles (UAVs) deliver both the required spatial and temporal resolution.

Miniaturisation of optical imaging sensors and rapid developments in UAV technology opened up ways for retrieving crop parameters at centimeter-level spatial scales [32, 233, 224]. UAVs are versatile in terms of sensor payloads, flight altitude and direction, and angle of image acquisition, which in turn enables exploring parameter retrieval using various flight configurations. Additionally, UAV images allow the user to discriminate between different canopy constituents (soil, shaded leaves, sun-lit leaves) and study them separately. UAVs have been used to retrieve structural and biochemical crop parameters using parametric [32, 123], machine learning [62] and physical models [202, 44]. While there is a considerable research on the retrieval of LAI from UAV-based multispectral or hyperspectral imaging, only a few studies have explored ALIA retrieval [240], particularly in the context of paraheliotropic response of the plants.

The objective of this study is to explore paraheliotropic response of two soybean varieties by quantifying ALIA through terrestrial laser scanning, multispectral imaging and RTM inversion. For this purpose we have employed TLS and very high-resolution multispectral UAV image data in combination with the radiative transfer model PROSAIL. Both measurements were conducted at three time points throughout the vegetation period close to each other. To follow the diurnal leaf movement, morning and afternoon measurements were taken on two occasions. PROSAIL was parameterised using field-collected data and ALIA was retrieved using the lookup-table (LUT)-based inversion approach.

7.2 Materials and methods

7.2.1 Study area

The study area is located at the agricultural research station Campus Klein-Altendorf, in the federal state of North-Rhine Westphalia, west of the city of Bonn (50°37′N, 6°59′E, altitude 176 m) in Germany. The annual average precipitation is 603 mm, while the long-term average annual temperature is 9.4° C. Soil can be classified as luvisol. A soybean experiment, consisting of two varieties (Eiko and Minngold) was sown in two densities (30 and 60 $seeds/m^2$) in 1.5x3 m plots (Fig. 7.1). Minngold (University of Minnesota) is a chlorophyll-deficient mutant characterised by lower chlorophyll content in the upper leaves compared to the lower leaves ([39]). Several studies have assessed the photosynthetic performance of this mutant [177, 85]. Meanwhile, Eiko (Asgrow, USA) is a commercial soybean cultivar. Sowing happened on the 4th of May, herbicide treatment on the 5th of May and fungicide treatment on the 2nd of June.

7.2.2 UAV data collection

A DJI Matrice PRO 600 (SZ DJI Technology Co., Ltd., Schenzhen, China) served as a sensor carrier platform for image data acquisition. The Micasense dual camera system, consisting of two multi-camera arrays, MicaSense RedEdge-MX and the RedEdge-MX Blue (AgEagle Sensor Systems Inc., Wichita, KS, USA), was mounted on a Ronin MX gimbal attached to the UAV. The images are captured synchronously for each band as separate files. Each camera has a field of view (FOV) of 47.2° and focal length of 5.4 mm. The images were geotagged through the camera's global navigation satellite system (GNSS) receiver. Images were

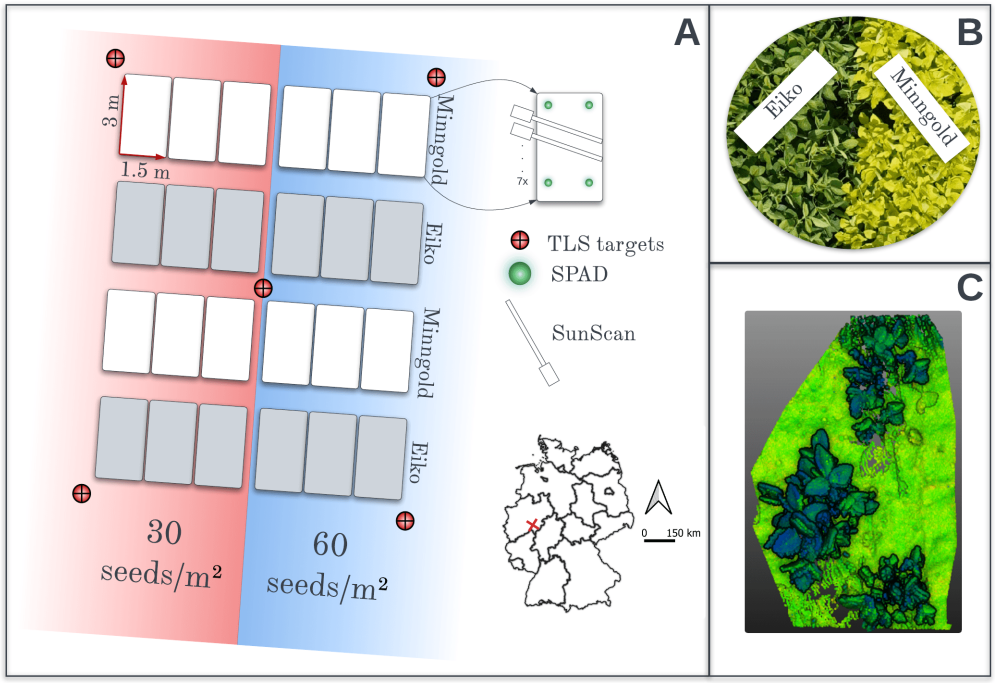

Figure 7.1: Experimental design of soybean density experiment and measurement locations (A); RGB image of two soybean varieties taken from UAV (B); 3D point cloud of soybean plot (C).

acquired at 20 m above ground level, which resulted in 1.39 cm ground sampling distance (GSD). The flight altitude was set as low as possible to ensure high spatial resolution, but high enough to guarantee proper scene reconstruction with a sufficient number of matching features in image sets. The UAV was flown at a speed of 3 m/s, resulting in a forward overlap of 80% and sidelap of 70%. For more details on flight and camera setup see [43]. Afternoon flights were conducted between 12:00-13:00h local time on days with stable illumination conditions. Morning flights were conducted at 8:00 - 9:00h (Table 7.1). A set of nine near-lambertian panels (Mankiewicz Gebr. & Co. GmbH & Co. KG, Hamburg, Germany) with varying reflectance factors and a flat spectral response across the VNIR spectral range, ranging from dark (2%) to bright (63%), was placed within the experiment on bare soil during each flight. A large enough gap was left between the panels to avoid adjacency effects of the panels. The panels were recorded from the same height as the experimental plots (20 m). Panel reflectances were measured in the field on 23 June 2020 under sunny conditions using an ASD FieldSpec 4 spectroradiometer (Malvern Panalytical, Malvern, UK). The collected spectral measurements were resampled to match the spectral bandwidths of the MicaSense sensor.

Table 7.1: Flight times during summer season of 2022. SZA - solar zenith angle; DAS - days after sowing.

Date	Time of the day	Flight time	SZA	DAS	Illumination conditions
June 14	Afternoon	12:37 - 12:56	29	42	Sunny
July 13	Morning	9:00 - 9:20	60	71	Sunny
	Afternoon	14:00 - 14:20	29		Sunny
August 10	Morning	8:30 - 8:40	70	98	Sunny
	Afternoon	13:05 - 13:15	35		Sunny

7.2.3 Image processing

Image data was processed in Agisoft Metashape Professional (Agisoft LLc, St. Petersburg, Russia). Images were stitched and georeferenced using ground control points that were evenly distributed in the field. At sensor radiance orthomosaics were generated by applying the Micasense radiometric calibration model using a python script within Metashape and exported for reflectance calibration as described in [43]. Saturated reflectance panels were removed from the empirical line correction. Reflectance was compared to airborne imaging spectroscopy data acquired with the HyPlant sensor [183] conducted in summer 2022. To remove soil pixels from the UAV orthomosaics, we calculated the Excess Green (ExG) index [223] and used manual thresholding to separate soil from plant pixels. A manual threshold was used on the blue band to remove shaded pixels.

7.2.4 Reference measurements

For the parametrisation of the PROSAIL model, LAI and SPAD measurements were taken directly before or after the overflights. LAI measurements were also important for discerning the impact of ALIA from LAI on canopy reflectance. LAI was sampled non-destructively using a SunScan canopy analysis system (Delta-T Devices, UK). Destructive samples of both varieties were taken in selected plots in 2021 and 2022 after the overflights to validate SunScan measurements and calibrate the Ellipsoidal Leaf Angle Distribution Parameter (ELADP) value for LAI calculation. Four plants were randomly selected in each plot and leaf area was measured with a leaf area meter (LI-3100C Area Meter, LI-COR Biosciences, Lincoln, USA). Prior to derivation of LAI from destructive samples, the number of plants per plot was manually counted. For the non-destructive measurements, the SunScan rod was placed diagonally to the crop rows into the canopy seven times in each plot (see Figure 7.1) and the result was averaged. The largest uncertainties were found in plots with heterogeneous distribution of soybean plants, which resulted in individual plants growing at different speeds. Hence, the sam-

pling with four plants in these plots was not sufficient. Compared to these plots, homogeneous plots showed higher accuracy between SunScan LAI and destructive sampling. For SPAD measurements, two plants were randomly selected in each plot. Measurement procedure differed for Minngold and Eiko. For Eiko three upper leaves were measured, each leaf four times. For Minngold the three upper and three lower leaves were measured, each leaf four times to account for variability in chlorophyll content in Minngold canopy layers.

7.2.5 TLS measurements

Terrestrial laser scanning (TLS) measurements were taken prior to the UAV flights at two different times on the same day. For data acquisition, four Leica tilt-and-turn targets were positioned at the four corners of the field and one in the middle (Fig. 7.1). Scans were conducted with a Leica ScanStation P50 (Leica Geosystems, Heerbrugg, Switzerland) with a spatial resolution of 6.3 mm at 10 m distance to the scanner. In order to scan the entire field at a sufficiently high resolution, the TLS was placed at 15 different positions in and around the field. These different scans were spatially registered to each other by a target-based registration using the software *Leica Cyclone*. The result is a 3D point cloud, which contains x, y and z components. The whole measurement with the 15 positions took 3 h.

7.2.6 ALIA estimation

To estimate ALIA values from TLS measurements, a surface representation of the plants in each plot was produced. A fully automated pipeline was employed, which takes a 3D point cloud as input and generates a meshed surface (TIN) as output, implemented in Open3D [238]. As the data was acquired under real-world conditions noise and outliers had to be removed. A statistical approach was used that removes points that are farther away from their neighbours compared to the average point distance of the entire point cloud. In empirical experiments it was shown that five neighbours and a standard deviation of 1.0 are suitable parameters. To reduce the computation time, the point cloud is uniformly sub-sampled which reduced the point number P to P/k. The down-sampling parameter k was determined directly from the data set by choosing a point density of 40 points per $1\,\mathrm{cm}^2$. The surface was reconstructed using the Ball-Pivoting algorithm [31] to create a triangular mesh from the point cloud. In this algorithm, a virtual ball with a certain radius ρ is randomly placed onto the point cloud. The radius is

automatically generated depending on the average point distance. To ensure that all points are connected with triangles, this process is repeated three times with a scaling factor of 10, which has been shown to be appropriate for plants. As a last step, the remaining holes in the meshed surface are detected, extracted, and filled with a flat surface. Holes are detected due to the fact that they are surrounded by boundary edges (edges that only belong to a triangle). It should be noted that all edges of the sheet are also defined as boundary edges in this step. To correct only the holes within the surface, the threshold value of the boundary edges e is set to $e \leq 30$. All holes with a lower number of boundary edges than e are filled with flat triangles, resulting in an almost completely closed surface model.

After generating the meshed surface of joined triangles, this representation was used to calculate the $ALIA$ values for each experimental plot. First the normal vectors $\vec{n} = (n_x, n_y, n_z)$ of the triangles were calculated and aligned in one direction. Afterwards, the different components of the normal vectors were used to determine the distribution of the leaf inclination angles θ (see Figure 7.2) using $\theta = \arccos(n_z)$. The median value of the resulting distribution than is calculated to get the $ALIA$ value as $ALIA = \overline{\theta}$.

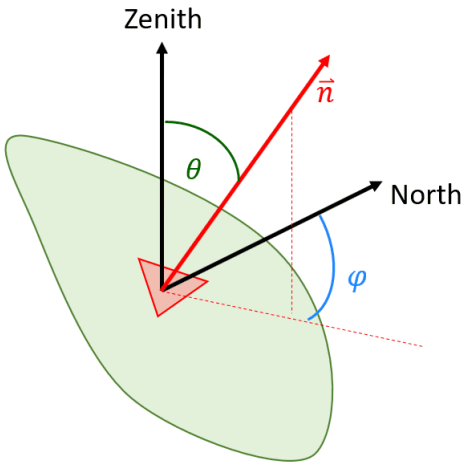

Figure 7.2: Leaf orientation parameters: θ is zenith angle; φ is azimuth angle; $\overrightarrow{n}$ is a normal on the surface of the leaf.

7.2.7 Environmental data collection

Environmental data (precipitation, temperature and soil water content) were collected at the study site. A weather station (Wilmers Messtechnik GmbH, Hamburg, Germany) was located 200 m away from the experimental setup and was logging temperature, precipitation and other parameters every 10 minutes.

SoilNet [35] sensors that measure soil water content (SWC) and several other parameters were installed within the same field in a wheat subexperiment at three different depths (10, 20 and 50 cm). The sensor was logging SWC at 15 min intervals.

7.2.8 PROSAIL parametrisation and inversion

PROSAIL parametrisation was done partly based on the reference measurements (Table 7.2) and partly using the parameter ranges available in the literature ([26]). The leaf optical depth (N-parameter) was calculated using PROSPECT-PRO [76] and the leaf optical measurements (leaf reflectance and transmittance measured with a field spectrometer) acquired during the SoyFlex campaign in 2016 (SoyFlex 2016). N-parameter was sampled using uniform distribution. A range of leaf chlorophyll content (LCC) with Gaussian distribution (mean 30 [μg/cm^2], standard deviation 5) was used to construct the look-up table (LUT). LAI was fixed to avoid confounding effects on ALIA. Two ALIA scenarios were simulated: a) no constrain of ALIA, b) ALIA constrained to the values that were observed (+- 5 added to upper and lower limits) in the field. Soil reflectance was extracted from the bare soil areas in the multispectral UAV orthomosaics distributed over the whole field to account for variations in soil conditions (compact, plowed). Solar zenith angles were calculated for each date and time. A global sensitvity analysis was performed to confirm the sensitivity of ALIA and LAI in the red edge and NIR bands of the multispectral sensor.

Table 7.2: PROSAIL variable ranges used in the construction of individual LUTs. LAI and LCC ranges were adjusted for each LUT separately.

Variable	Description	Range	Distribution
PROSPECT-5			
N	Leaf structure index	1.2–1.8	Uniform
C_{ab}/LCC [µg/cm^2]	Leaf chlorophyll content	0–70	Gaussian
C_{cx} [µg/cm^2]	Leaf carotenoid content	-	-
C_{bp} [unitless]	Brown pigments	0–0.5	Fixed/Uniform
C_m [g/cm^2]	Dry matter content	0.004–0.0075	Uniform
C_w [g/cm^2]	Leaf water content	-	-
4SAIL			
LAI [m^2/m^2]	Leaf area index	3	Fixed
ALIA [°]	Average leaf inclination angle	0–90 / 35–70	Step of 1
Hot	Hot spot parameter	0.01–0.5	Uniform
ρ_{soil} [%]	Soil reflectance	Extracted from image	-
SZA [°]	Sun zenith angle	Different for each date	-
OZA [°]	Observer zenith angle	0	-
rAA [°]	Relative azimuth angle	0	-

The Look-Up-Table (LUT) inversion scheme was used to retrieve ALIA. For this

purpose, 10.000 simulations were selected out of every possible combination, using latin hypercube sampling. The full spectrum was used for the model inversion with 2% of Gaussian noise added to the spectra. To find the best match between simulated and measured reflectance we used simple RMSE (root-mean square error) as a cost function.

7.3 Results

7.3.1 Hydrometeorological conditions at the study site

The Figure 7.3 displays environmental data, including weekly temperature and precipitation measurements, as well as continuous SWC measurements at three different depths. The summer of 2022 exhibited exceptionally dry conditions, as evident from the climate diagram. There was little to no precipitation in the months of June (26.9 mm), July (4.2 mm) and August (0.6 mm). For reference, the long term average precipitation (1961-1990) recorded at DWD station (Deutscher Wetterdienst), located 30 km northeast from the study site at Cologne-Bonn Airport for the months June, July and August are 86, 84 and 77 mm, respectively [59]. The mean daily temperatures during June, July, and August (18° C, 19° C, and 20° C, respectively) exceed the corresponding long-term averages of 16° C, 18° C, and 18° C [59]. Due to an extended period of drought, the soil water content (SWC) in the soil profile, extending to a depth of 50 cm, remained exceptionally low throughout the entire summer. Specifically, in the 10 cm layer, the SWC percentages were 12%, 12%, and 10% for the months of June, July, and August, respectively. In the 20 cm layer, the corresponding values were 16%, 14%, and 14%, while in the 50 cm layer, they were 22%, 19%, and 19%. In comparison, the average nFK% (plant available water) at Cologne-Bonn Airport station is 75%, 70% and 67% for the respective months.

7.3.2 ALIA measurement results

The results of TLS measurements can be found in Figure 7.4 represented as distribution plots with median values marked with vertical lines. Minngold and Eiko exhibited different diurnal patterns of leaf movement during every measurement. On the 14th of June a strong difference between ALIA of Minngold (51°) and Eiko (60°) was observed in the afternoon. The plants were still very small (BBCH stages (Biologische Bundesanstalt, Bundessortenamt und CHemische Industrie)

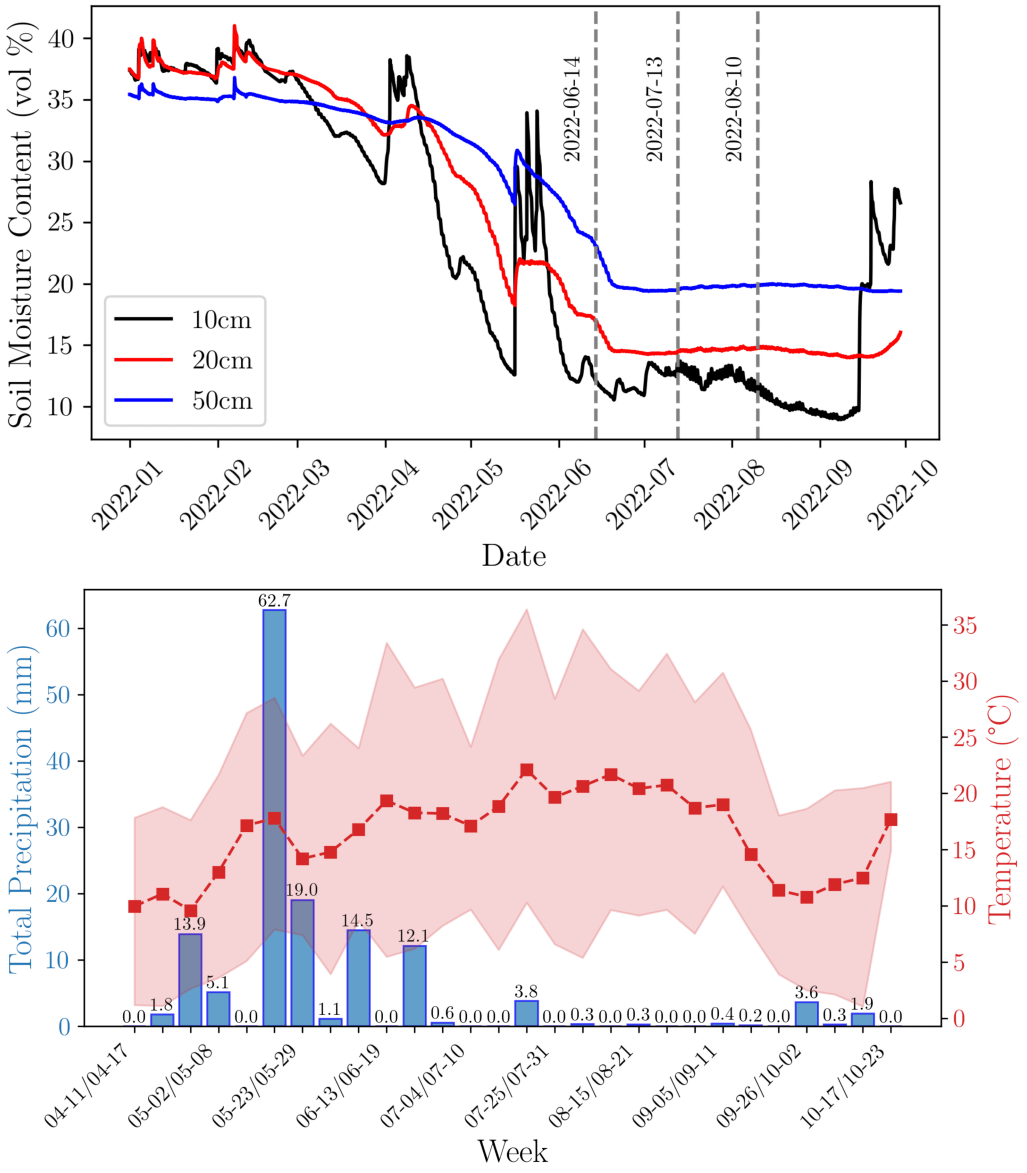

Figure 7.3: Soil water content (upper plot) during January-October timespan and climate diagram (April-October) of the CKA study site in 2022.

22-26) as can be seen on the RGB images.

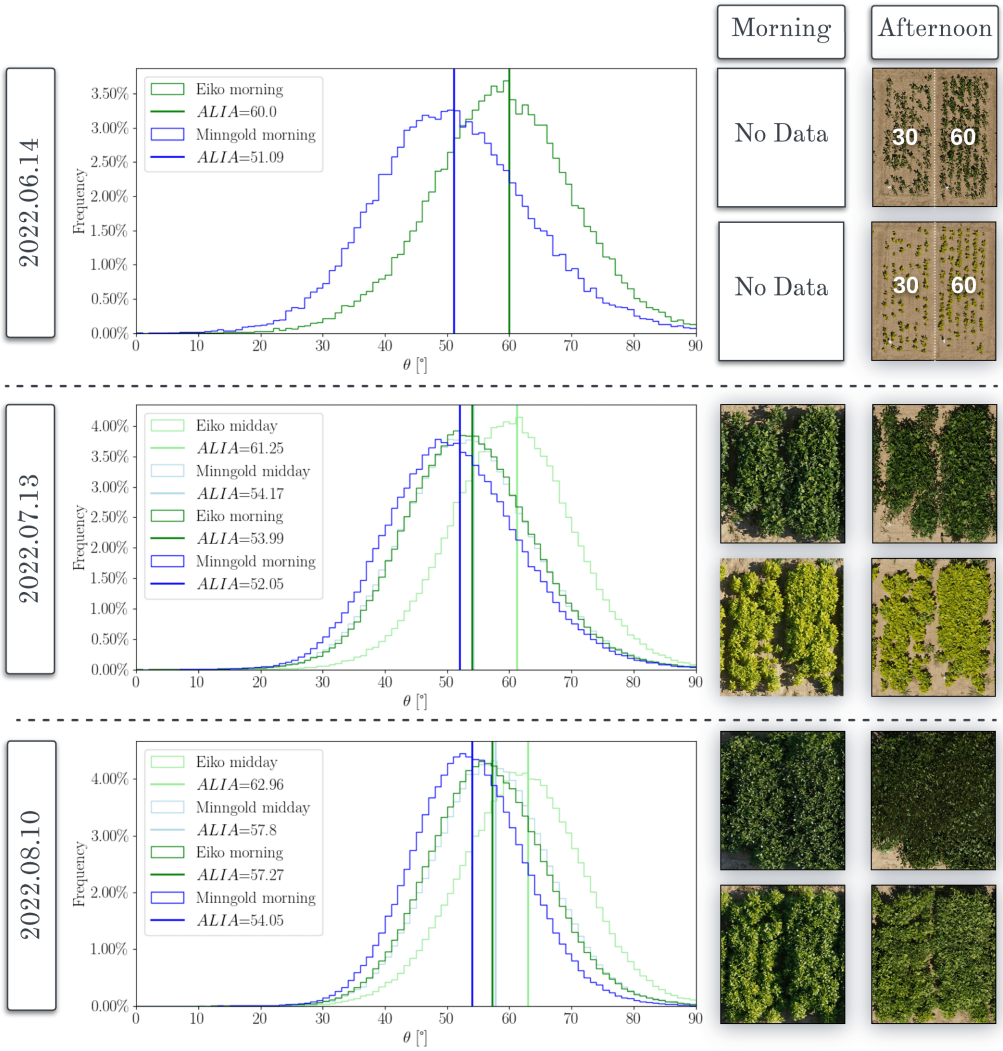

Figure 7.4: (L)ALIA distributions of Minngold and Eiko varieties derived from TLS measurements acquired on 15th June, 13th July and 10th August in the morning and afternoon; (R) Example RGB images of soybean plots recorded during the morning and afternoon overflights at the respective days. The left subplots within each image had 30 kernels per square meter, the right subplot - 60.

On the 13th of July both varieties show similar ALIAs in the morning: 52° - Minngold and 54° Eiko. This trend changed in the afternoon measurement: Eiko's ALIA increased to 61°, while Minngold's remained stable at 54°. On the 10th of August, ALIA values of Eiko were higher (57°) compared to previous measurements, but increased further towards the afternoon (63°). In comparison, Minngold's leaf angle increased only slightly.

7.3.3 Relationship between ALIA and spectral bands

The results of global sensitivity analysis (7.5) confirm the impact of ALIA on red edge and NIR regions (740-842nm, light blue). ALIA shares this sensitivity with LAI (purple). Simulated reflectance of two spectral bands (742 and 842nm) with changing sun zenith angle (morning and afternoon) displays that the canopy reflectance is not affected by the SZA.

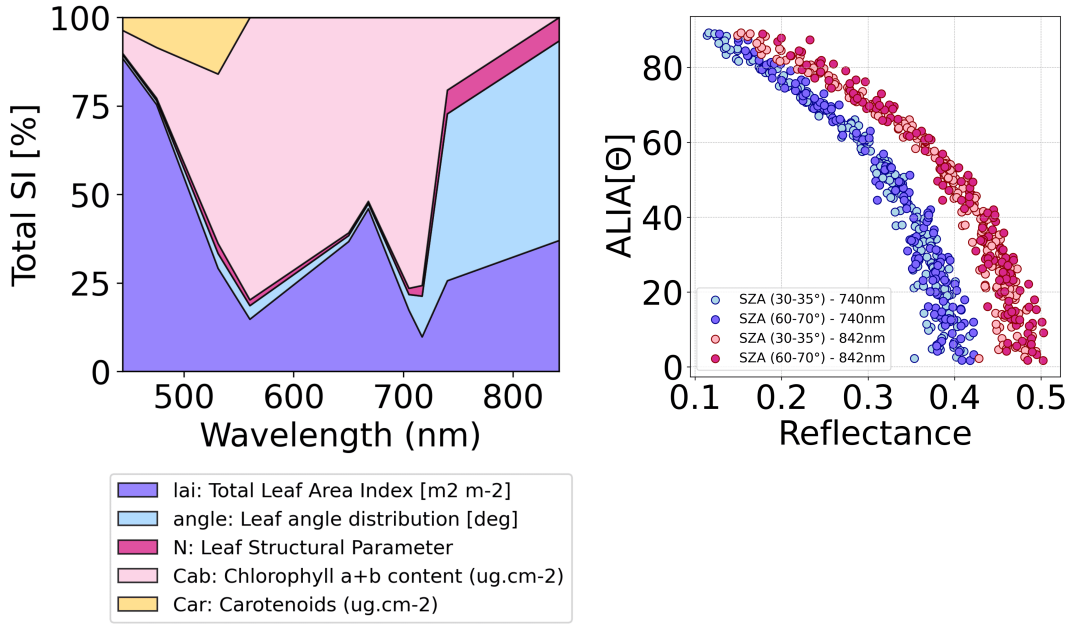

Figure 7.5: Left plot: Results of the global sensitivity analysis (GSA) applied to reflectance spectra simulated with PROSAIL having the spectral resolution of the MicaSense Dual camera system. SI stands for Sobol Index. The sobol index helps to identify the importance of input variables, in this case crop parameters, on the model output. Right plot: PROSAIL simulated reflectance representative for morning (SZA 60-70°) and afternoon data acquisitions (SZA 30-35°) of the MicaSense dual red-edge (740nm) and NIR (842nm) spectral bands. SZA: sun zenith angle.

To illustrate the relationship between ALIA and the visible/near-infrared bands of the multispectral camera, reflectance of each spectral band with soil and shaded pixels removed was compared to the median morning and afternoon TLS-derived ALIA measurements for both varieties (see Figure 7.6). Morning measurements showed no correlation in the spectral bands that are expected to be sensitive to ALIA, specifically at 740 nm ($r^2 = 0$) and 842 nm ($r^2 = 0.2$). Minngold exhibits a generally higher correlation in the green (531 and 560 nm), red (650 and 668 nm) and red edge bands (705 and 717 nm) compared to Eiko.

The afternoon measurements show strong correlation in visible and red edge

bands. For Minngold, the r^2 values range from 0.51 to 0.88, while for Eiko, they are between 0.47 and 0.74. Correlations are still higher for Minngold than Eiko. Compared to morning measurements correlations are much higher for both varieties, especially at 560 nm. Correlations are low for the bands located at 740 and 842 nm. For Minngold r^2 are 0 and 0.36, and for Eiko r^2 0.35 and 0.16 calculated for the bands at 740 and 842 nm, respectively.

To see the effect of plots with low LAI on the relationship with bands 740 and 842 nm, the June measurement was removed (Figure 7.7). The correlation between band 740 ($r^2 = 0.5-0.7$) and ALIA improved significantly for the afternoon when removing June measurement, but did not change for the morning measurement and band 842. In order to differentiate the effects of LAI on spectral signature compared to ALIA, LAI was plotted against 740 and 842nm bands. We observed higher correlations between LAI and the two bands ($r^2 = 0.4-0.7$) in the morning compared to ALIA and no correlation in the afternoon.

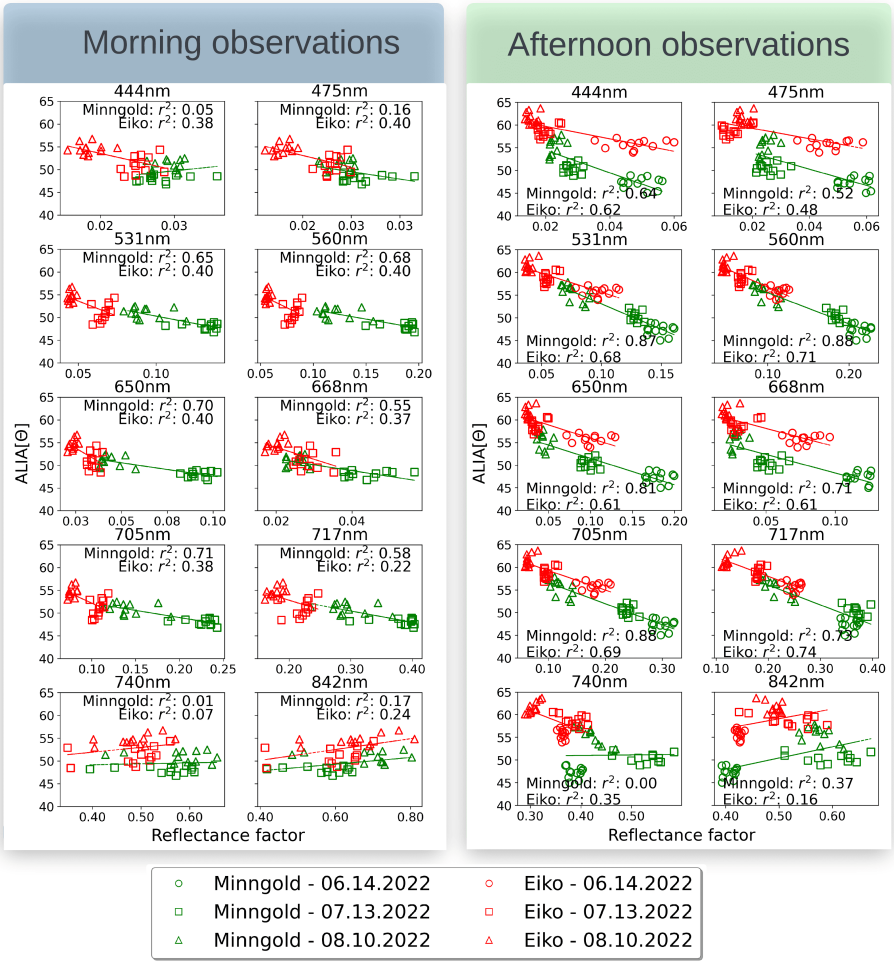

Figure 7.6: Relationship between LIDAR-based ALIA and spectral bands from the UAV image data of Eiko and Minngold recorded during the morning and afternoon data acquisitions.

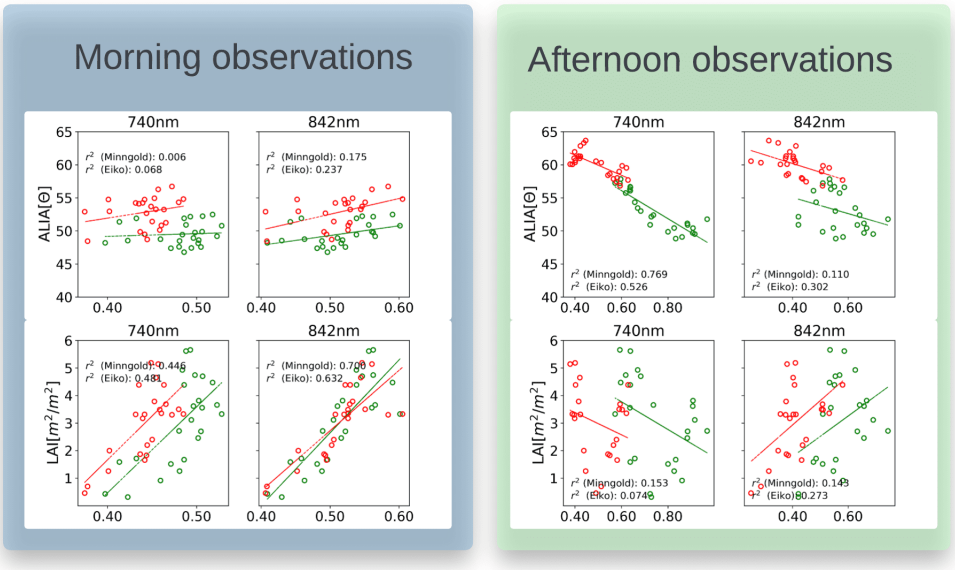

Figure 7.7: (l) Correlations between ALIA, LAI and bands 740 and 842 nm with the June measurements removed during the morning ; (r) correlations between ALIA, LAI and bands 740 and 842nm during the afternoon with June measurements removed. The legend for color coding can be found in Figure 6

Since the anticipated correlations of ALIA with the reflectance data at 740 nm and 842 nm were not observed, we explored the ratio of the two bands. The results are depicted in Figure 7.8. We examined the relationships using different image processing approaches: a) averaging spectra per plot using every pixel (soil, plants, and shade), b) averaging spectra without soil pixels (but including shade), and c) averaging spectra without soil and shade (pure plant pixels). The highest correlation was found for approach c) using pure plant pixels, with an r^2 value of 0.72. The relation between LAI and the RE/NIR ratio was also tested to rule out the influence of LAI on the ALIA RE/NIR ratio relationship. The lower row in Figure 7.8 shows the low correlations ($r^2 = 3.55 - 0.44$) determined for the three approaches.

7.3.4 ALIA retrieved using PROSAIL

The results of ALIA retrieved with PROSAIL using the full spectrum are depicted in the Figure 7.9. In Panel b) and d) in Figure 8 the measurements recorded on the first data acquisition day (16 June) were removed from the analysis as uncertainties associated with PROSAIL simulations of very low LAI canopies was high. ALIA for the non-constrained case are significantly underestimated (Figure 7.9 a, b; RMSE 13°), compared to the constrained case (Figure 7.9 c, d;

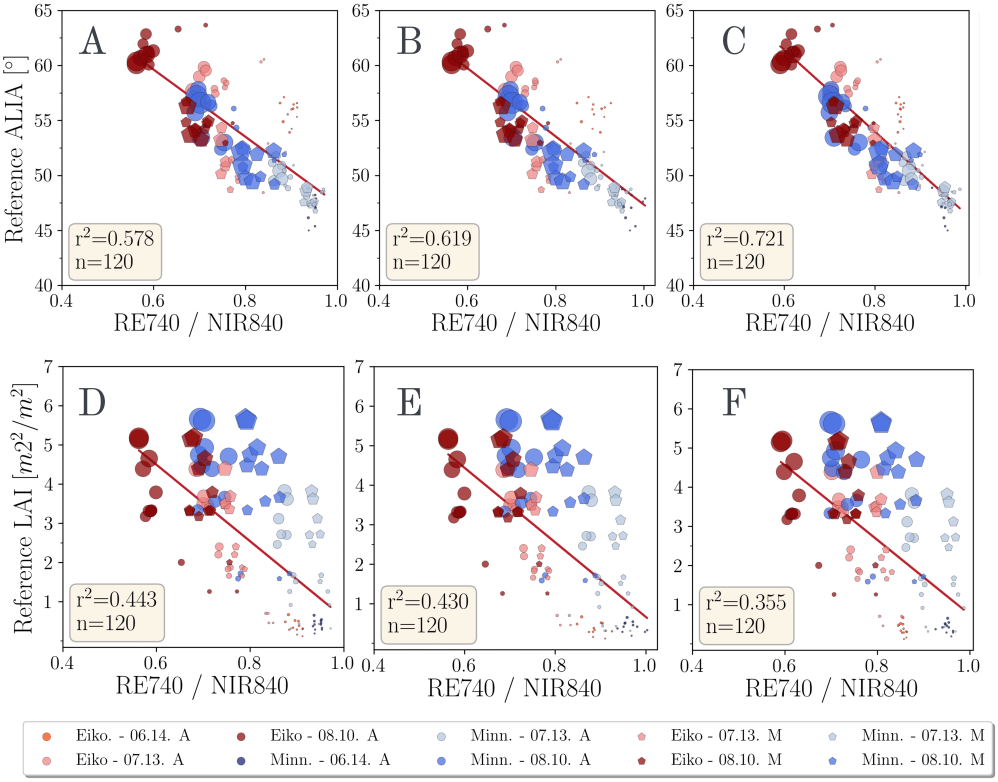

Figure 7.8: Scatter plots showing the relationship of ALIA (A-C) and LAI with the Red Edge (740 nm) - near infrared (840 nm) ratio (D-F) using the three different image processing approaches. (A and D)) soil and shaded pixels included in the image data (B and E)) soil pixel removed but shaded pixels included in the image data; (C and F)) soil and shaded pixels removed from the image data.

RMSE 7.7 and 3.8 degrees, respectively). ALIA estimation based on PROSAIL worked significantly better for Minngold than Eiko. The PROSAIL simulation for Eiko having high ALIA does not match well the ALIA reference measurements.

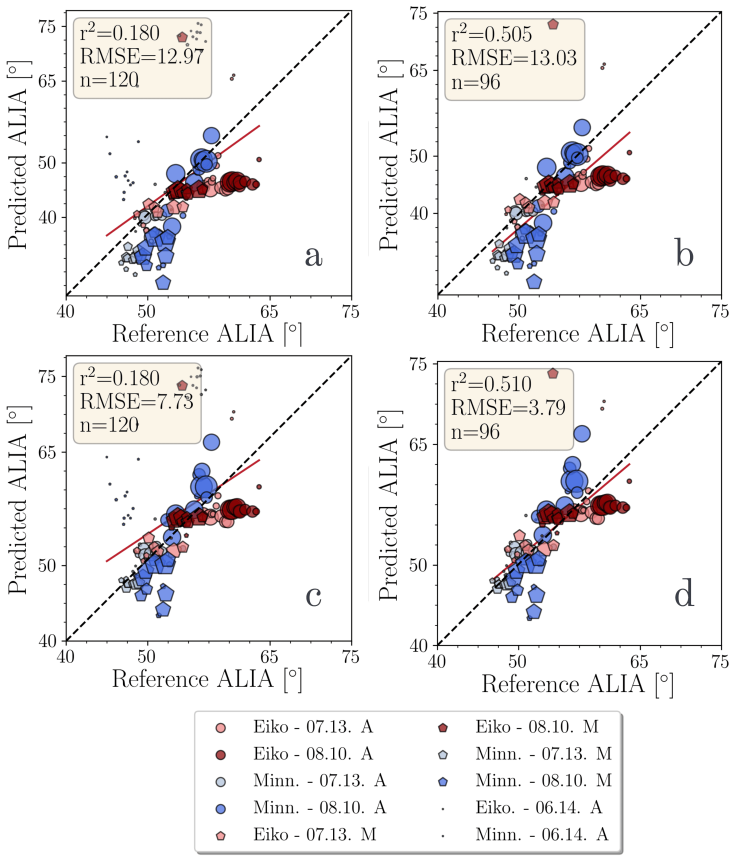

Figure 7.9: Retrieval of ALIA using different approaches: (a) ALIA not constrained, data from 06.14 included; (b) ALIA constrained and 06.14 measurements removed; (c) ALIA's lower limit constrained and 06.14 data included; (d) ALIA's lower limit constrained and 06.14 data removed. Only the sunlit spectra were used for validation. Retrieval is based on the full spectrum; A stand for afternoon and M for morning measurements

Results depicting only selected bands (740 and 842nm) and June measurements removed without constraining the model is displayed on Figure 7.10. Compared to the full spectrum method the RMSE here is lower (6.68°), but r^2 is higher (0.64). There is a significant underestimation of the Minngold July measurement.

7.4 Discussion

This study presents the first attempt to observe paraheliotropic leaf movement using TLS and optical remote sensing approaches. We characterised leaf move-

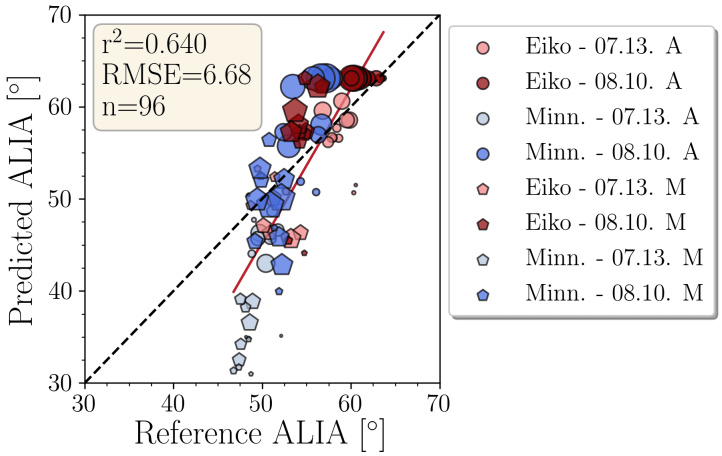

Figure 7.10: ALIA retrieved using only bands 740 and 842 nm without constraining ALIA to the observed values.

ment throughout the dry boreal summer months and evaluated the relationship between the canopy reflectance and the leaf movement.

7.4.1 Paraheliotropic response of soybean varieties

Environmental variables collected at the study site strongly indicate drought during the boreal summer (Figure 7.3). The area experienced an abnormal summer precipitation deficit of 215 mm and high temperature anomalies (>1.5° C). Data from the German Drought Monitor [239] also confirm extreme drought throughout most parts of Germany by the end of August (reference period 1951-2015). According to the analysis conducted by [196], the self-calibrated Palmer Drought Severity Index (PDSI) in large parts of Europe dropped below -3, including Germany. For reference, a value that is -3 or below is classified as drought.

Leguminous plants are known to exhibit paraheliotropism when exposed to water scarcity and high temperatures ([145, 124]). As the local environmental data indicate drought conditions in the study area, soybeans were expected to show the paraheliotropic response. The results of diurnal TLS measurements reveal an interesting discrepancy in the paraheliotropic response of Eiko and Minngold. In the mornings (8:00 - 9:00 AM local time), Eiko and Minngold had similar leaf angles (Figure 7.4). In the afternoon the leaves of Eiko became vertical, while Minngold's remained almost unchanged. Eiko's response is a classical example of paraheliotropism, which has been documented in several other studies [145, 160, 124], but has not been tracked before using remote sensing methods. As the drought persisted throughout the entire boreal summer, we observed the gradual

impact of water scarcity on Eiko. Our measurements revealed that the paraheliotropic response in June and July was characterized by terminal and lateral leaves becoming vertical in the afternoon. By August, when SWC was at its lowest, Eiko's leaves were already vertical in the morning. In the afternoon, we observed the inversion of the leaves, exposing the abaxial side. This phenomenon has been documented and various explanations have been proposed by [124]. The higher reflectance of the abaxial side, attributed to reflective trichomes, allows plants to reduce the thermo-radiative load, thereby lowering temperature and evapotranspiration rates and minimizing the inhibition of photosystem II. Additionally, the abaxial surface exhibits higher conductance under water stress compared to the adaxial side, which, in the case of leaf inversion, helps the plant to conserve more water.

In contrast to Eiko, Minngold exhibited a less pronounced paraheliotropic response. In fact, diurnal morning and afternoon measurements throughout the boreal summer showed minimal variation (range 51-58°). This subdued response in Minngold can be attributed to an additional defense mechanism against high light intensity and water scarcity. The genetic mutation causing the upper leaves to appear more yellow allows Minngold to reduce evapotranspiration rates by receiving a lower thermo-radiative load compared to the dark-leaved Eiko. Less chlorophyll content leads to decreased absorption of photosynthetically active radiation (APAR), thus more light is transmitted and reflected. Consequently, the paraheliotropic response in the upper leaves of Minngold is less evident. Previous studies have proposed that chlorophyll-deficient mutants, characterized by a higher surface albedo, could lead to significant water savings and help mitigate the effects of future heatwaves [61, 230, 177], further highlighting the importance of breeding climate-resilient crop varieties.

Together with photosynthetic activity, variations in leaf temperature, and changes in the xanthophyll cycle, leaf movement serves as an important early stress indicator [29, 228]. Unlike leaf-level measurements of photosynthetic activity, which are often labor-intensive, possess limited spatial coverage, or lack sufficient resolution, tracking leaf movement using proximal multispectral imaging can be promising to be used in breeding applications to identify varieties better adapted to higher temperatures and lower water availability. This characteristic makes ALIA particularly compelling as one of the parameters to investigate early stress responses in various crops.

7.4.2 Effect of changing ALIA on the spectral reflectance of different soybean varieties

The red-edge and NIR part of the spectrum are most sensitive to changes in ALIA, as evident from the sensitivity analysis of the PROSAIL model [112](Figure 7.5). This sensitivity is shared with LAI, particularly in the NIR, creating challenges in disentangling the magnitude of the effects these two variables have on canopy reflectance. For example, the spectral signature of a sparse planophile canopy (horizontal leaves) is similar to a dense erectophile canopy (vertical). [241] have demonstrated a negative correlation between canopy reflectance at 748 nm and ALIA across various crops, by using a hyperspectral image dataset acquired at a single time point.

In our results (Figure 7.6), the interaction between ALIA and the single spectral bands differed with the time of the measurement. The high correlation coefficient observed for Minngold in both morning and afternoon, specifically in the visible range, can be attributed to variations in leaf chlorophyll content (LCC) throughout the summer. This variation was manifested by the increase of LCC of the upper and lower leaves in the canopy from July to August. In contrast, Eiko showed minimal changes in LCC during the same period. This leads us to infer that the correlation across most visible bands is driven by variations in LCC rather than by ALIA. This explanation does not hold true in the blue bands (444 and 475 nm), where a lower r^2 was observed for Minngold compared to Eiko. A possible reason for this discrepancy could be the significant reflectance of the blue light by the Minngold canopy, attributed to its transparent upper leaves and high light penetration rates, in contrast to Eiko.

The afternoon measurements reveal distinct trends in the correlation patterns between ALIA and the single spectral bands. In this context, both Eiko and Minngold exhibit high correlations in the visible range up to the red edge (740 nm) driven possibly by the variation in LCC rather than ALIA. Both varieties show lower correlations in the blue bands, albeit higher than those observed during the morning measurements. This discrepancy can be attributed to variations in photosynthetically active radiation (PAR) intensity between morning and afternoon, with the latter period providing higher PAR (stronger signal and lower signal to noise ratio) for plant canopies to redistribute energy (absorb, transmit, or reflect). The varying correlations observed between 650 and 668 nm and ALIA for both varieties can be explained by differences in LCC between two varieties and light penetration, rather than disparities in ALIA.

At first glance in the Figure 7.6, the low r^2 at 740 nm and 842 nm in the afternoon appears inconsistent with the literature. However, these instances involve outliers, specifically plots with very low LAI values measured in June. When these extremely low LAI plots were removed from the analysis, the r^2 increased significantly for both varieties (Figure 7.7). These results align with the findings of [241], where the authors established a similar negative relationship between ALIA and the far red edge band (748 nm). The reflected light from the low LAI plots do not provide sufficient information on canopy architecture as reflectance is mostly from soil and only a small number of plant pixels are left after removing the soil background. The strong correlation does not extend to the NIR band, where a more substantial spread is observed. However, when combining data from both varieties, a general negative trend becomes apparent (Figure 7.7).

The results for LAI and RE-NIR bands show an opposite trend when low LAI plots are removed. Here, a positive and strong correlation for both bands is observed in the morning, with no correlation in the afternoon. This suggests that we observe the effect of LAI in the spectral data during the morning measurement and the combined effect of changing ALIA and LAI during the afternoon.

Since no similar trend in relationship was found in the morning and afternoon between ALIA and the spectral bands at 740 nm and 842 nm, respectively, in comparison to the visible bands, it is suggested that the relationship is influenced by environmental factors, in this case difference in light intensity. Vegetation indices, compared to individual spectral bands, exhibit more pronounced sensitivity to vegetation parameters. This is due to the normalisation of spectral bands as part of a vegetation index, which enhances the data and removes environmental effects [101]. These effects, including different sun-target-sensor geometries, have been demonstrated by multiple studies to be mitigated with the help of ratioing [129, 211]. Since the main difference between morning and afternoon measurements was the difference in sun-target-sensor geometry, using the RE and NIR bands ratio, which is sensitive to ALIA (Figure 7.8), seemed reasonable.

Using the RE-NIR band ratio also helped in identifying whether changes in canopy reflectance were driven by ALIA or LAI. Figure 7.9 shows that variability of RE/NIR cannot be explained by variability in LAI. The RE/NIR ratio remains constant during one measurement (either morning or afternoon) while the LAI changes.

7.4.3 ALIA retrieval

A limited number of studies have explored the retrieval of ALIA using imaging spectroscopy data, making the comparison of results rather challenging. [241, 238] used a hyperspectral imaging sensor to retrieve ALIA of various crops (faba beans, narrow-leafed lupin, turnip rape, oat, barley and wheat) in combination with PROSAIL modelling. The authors used a single band (748 nm) to retrieve ALIA (range 18-62°) with a reasonable accuracy (root mean squared error = 11.4°).

In our study we used ten wider spectral bands across the visible-near infrared range to explore the capacity of PROSAIL to retrieve ALIA , while fixing the LAI to 3. One noticeable aspect of the retrieval was the difficulty in simulating the reflectance of plots with low LAI values, particularly in the June data. As illustrated in the Figure 7.4 plants were still relatively small and surrounded by large soil areas. Our assumption here is that after soil removal, little vegetation spectra were left which led to noisy data in the early growth stage. As can be seen in Figure 7.9 after the removal of the first June date, the outliers that remained were mostly plots with extremely low LAI values from the remaining two days, suggesting that our initial assumption was correct. Since we found correlations of ALIA with the spectral bands at 740 and 842 nm, it is also reasonable to assume that these two bands are sufficient for ALIA retrieval (Figure 7.10). In the future different PROSAIL simulation configurations and retrieval algorithms should be explored to optimize ALIA retrieval. For example, hybrid approaches that combine RTMs with machine learning, can provide estimation uncertainties and provide parameter importance.

There was a discrepancy between the retrieval of ALIA of both soybean varieties. Eiko's ALIA retrieved from August 10 data exhibits almost no variation in predictions between morning and afternoon. This observation can be explained by the leaf inversion that was recorded on that day. The abaxial sides of the leaves have higher albedo and hence different spectral properties than the adaxial side of the leaf. Since the percentage of inversed leaves were much higher in the afternoon measurement, it had significant impact on the spectral signature (high reflectance over the entire visible-near infrared spectrum) of the whole canopy. This in turn made it difficult to simulate reflectance using PROSAIL, as it does not account for leaf inversion and assumes uniform distribution of plant pigments.

7.5 Conclusion

With this study, we present the first attempt at a novel approach to observe the drought-induced paraheliotropic response of two distinct soybean varieties, using multispectral imaging and terrestrial laser scanning. The extremely dry summer in the study area in 2022 unveiled differences in response mechanisms between the chlorophyll-deficient mutant Minngold and the wild variety Eiko. We observed an increase in the leaf angle (with leaves becoming vertical) of Eiko from morning to afternoon and leaf inversion when extremely dry conditions occurred. Meanwhile, Minngold did not exhibit pronounced signs of paraheliotropism. This observation can be attributed to its low chlorophyll content, allowing it to avoid photoinhibition. In the face of future extreme drought events predicted by climate models, it becomes increasingly important to study the defense mechanisms of crop varieties for breeding purposes.

Our findings suggest a strong relationship between the reflectance in the red edge (740 nm) and near-infrared (842 nm) spectral bands and the ALIA. However, this relationship is not consistent during morning and afternoon measurements, with the latter showing a stronger correlation. Moreover, the near-infrared band at 840 nm is influenced by LAI, complicating the decoupling of the effects of ALIA and LAI on top of canopy reflectance. The ratioing of the 740 and 842 nm bands to eliminate the effects of sun-target-sensor viewing geometries proved successful in combining morning and afternoon measurements and establishing correlation with ALIA. Additionally, we observed that LAI has no significant correlation with the 740/842 index. Future research should explore whether this relationship is applicable to ALIA estimations in other crops than soybean. Even though a simple parametric model using a ratio index was sufficient to retrieve ALIA, further research is needed if the same correlations are valid for other crops and sensors. In this regard, RTMs like PROSAIL offer a transferable solution to the retrieval problem and should not be underestimated.

We successfully retrieved ALIA using PROSAIL with reasonable accuracy. For very low Leaf Area Index (LAI) values, ALIA could not be reliably retrieved. In future studies, it is recommended to only consider plots with LAI values higher than 1. Constraining ALIA to observed values resulted in higher prediction accuracy (RMSE 3.7°) compared to an unconstrained model (RMSE 13.0°). The parametrization of PROSAIL significantly influenced the retrieval process. While we explored both constrained and unconstrained ALIA simulations with fixed LAI, future studies should delve into the impact of other parameters, especially those related to leaf chlorophyll content and other leaf pigments. Our findings

indicate that Look-Up Table (LUT)-based inversion is sufficient for ALIA retrieval. However, hybrid methods incorporating machine learning approaches could enhance retrieval accuracies and reduce the computing time of the inversion pipeline.

Chapter 8

Crop stress detection from UAVs: Best practices and lessons learned for exploiting sensor synergies

This chapter is published as:

E. Chakhvashvili, M. Machwitz, M. Antala, O. Rozenstein, E. Prikaziuk, M. Schlerf, P. Naethe, Q. Wan, J. Komárek, T. Kloucek, S. Wieneke, B. Siegmann, S. Kefauver, M. Kycko, H. Balde, V. Sobejano Paz, J. A. Jimenez-Berni, H. Buddenbaum, L. Hänchen, N. Wang, A. Weinman, A. Rastogi, N. Malachy, M.L. Buchaillot, J. Bendig, U Rascher, "Crop stress detection from UAVs: best practices and lessons learned for exploiting sensor synergies", Precision Agriculture, 2024, 25, pp. 2614–2642,
https://doi.org/10.1007/s11119-024-10168-3

This publication is a collaborative work of members of working group 3 of SENSECO cost action. E.C. led the publication. Other co-authors contributed to their expertise area. The content of the text remains identical to the published work, except for appndices, which can be found online. However, the format has been adjusted to align with the requirements of the thesis.

Abstract

Detecting and monitoring crop stress is crucial for ensuring sufficient and sustainable crop production. Recent advancements in unoccupied aerial vehicle (UAV) technology provide a promising approach to map key crop traits indicative of stress. While using single optical sensors mounted on UAVs could be sufficient to monitor crop status in a general sense, implementing multiple sensors that cover various spectral optical domains allow for a more precise characterization of the interactions between crops and biotic or abiotic stressors. Given the novelty of synergistic sensor technology for crop stress detection, standardized procedures outlining their optimal use are currently lacking. This paper provides practical information on how to combine different UAV-mounted optical sensors and discuss the proven scientific practices for image data acquisition and post-processing in the context of crop stress monitoring. The first part covers aspects that lead to the acquisition of high quality image data (radiometric calibration targets, ground control points) suitable to detect the type of crop stress or related traits (timing, pixel size). The second part deals with data pre-processing (georectification, atmosphere correction) and the use of radiative transfer models for crop trait retrieval and their integration with crop growth models. The last part explores the best practices and lessons learnt that can help scientists and practitioners in making informed decisions regarding sensor selection, mission planning and the challenges associated with multiple sensor data processing.

8.1 Introduction

Climate change is expected to increase crop abiotic (heat, drought, etc.) and biotic (pests, diseases, etc.) stresses, putting crop productivity at risk [71, 33]. Therefore, detecting and identifying crop stress prior to irreversible damage is essential to support management decisions and minimize stress impacts on crop growth and yield. While well-planned studies and experiments are essential for detecting and identifying crop stress, these endeavors are not exempt from technical challenges.

Optical remote sensing (RS) is an established method to detect the impact of different stressors on agricultural crops [29]. Several optical sensors based on imaging spectroscopy, fluorescence spectroscopy, and thermal imaging have been developed and are being used in unoccupied aerial vehicles (UAVs), and airborne science campaigns [4, 16, 144]. Over the past decade, combinations of differ-

ent spectral domains have been used in agriculture to estimate plant traits, and productivity [221, 55]. These spectral domains include the visible (VIS; 400-700 nm), near-infrared (NIR; 700-1300 nm), which are also used for sun-induced fluorescence (SIF) retrieval, shortwave infrared (SWIR; 1300-2500 nm) and thermal-infrared (TIR; 8-14 μm).

The spectral signature of vegetation in the optical region is primarily determined by the plant's biochemical and structural properties, related to plant vegetative growth and canopy development [114]. Consequently, various plant traits are often estimated based on empirical relations with different spectral bands [125], or they are retrieved with radiative transfer models (RTMs). Another promising approach for monitoring vegetation dynamics is to combine RTMs with plant physiological models [200, 82, 227, 161]. The assimilation of multi-sensor data from complementary spectral domains into crop models has the potential to facilitate decision-making by identifying specific stressors and even predicting stress before it occurs [29].

While using single optical sensors may suffice to monitor crop status, integrating multi-sensor data acquired from airborne/UAV platforms is more powerful for understanding plant responses to different biotic or abiotic stressors [162, 2, 149, 86]. For example, the combination of multispectral (MS, discrete spectral bands of a predetermined wavelength range) or hyperspectral (HS, continuous spectral coverage across a spectral domain) with TIR sensors provides broad spectral coverage for detecting and quantifying crop stress at an early stage of development. By measuring the leaf or canopy temperature, changes in plant traits such as stomatal conductance can be observed in minutes to hours, providing an early (and pre-visual) indication of the plant responses to stress [92] (Figure 8.1). Additionally, the incorporation of VIS-NIR information enables the analysis of stress responses related to pigment contents, such as chlorophylls, carotenoids [90] and anthocyanins [89] that are critical for photosynthesis and net primary productivity. In this context, the combination of different spectral resolutions and sensor types may complement the combination of spectral domains for increased spectral coverage.

The synergistic use of sensors from different spectral domains also improves the capacity for the observation of early to long-term crop responses to external stressors that affect growth and productivity [167] (Figure 8.1). The integrated use of MS VIS-NIR together with a broadband SWIR sensor or NIR+SWIR multi-camera array was shown as an efficient way to obtain information about crops' leaf water status or nitrogen concentration [122, 119]. The VIS-NIR+SWIR synergy is particularly useful for medium-term but also long-term stress response detection

(Figure 8.1.). The simultaneous collection of HS and TIR images in synergy with SIF data provides valuable insights into the response of SIF to crop stress [86, 38]. Additionally, RGB, MS, HS, and TIR image data can be used to derive biophysical traits and to assist in the quantification and interpretation of plant physiological changes reflected in SIF measurements.[24, 226, 232, 184, 219].

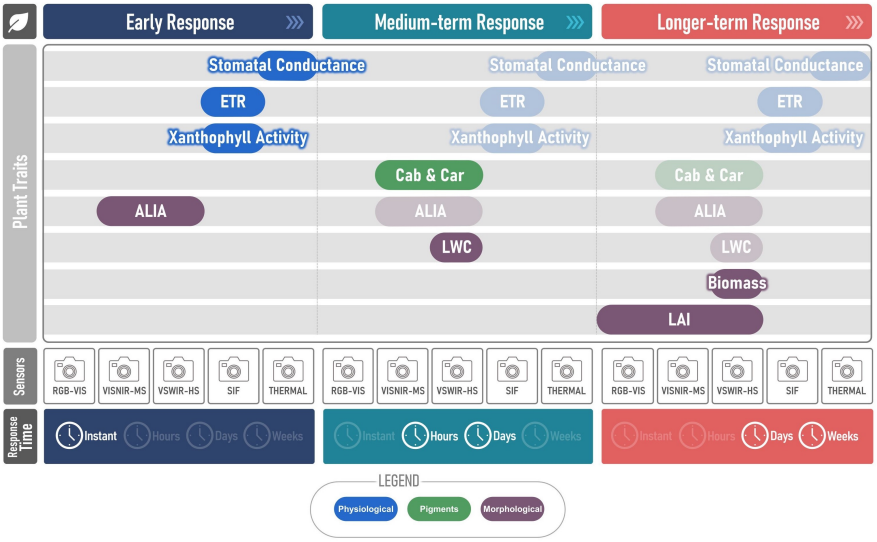

Figure 8.1: Optical sensor synergies for stress detection: different sensor combinations are useful to estimate different plant traits according to the period of time after plants started experiencing stress. Faded colors are used when the plant trait could still be measured but is less relevant than it was earlier. ETR = electron transport rate; ALIA = average leaf inclination angle; Cab = leaf chlorophyll a and b content; Car = leaf carotenoids content; LWC = leaf water content; LAI = leaf area index; RGB = red, green, blue; VIS = visible; NIR = near infrared; MS = multispectral; HS = hyperspectral; SWIR = shortwave infrared; SIF = sun-induced fluorescence.

Currently, few studies are available that make synergistic use of UAV-mounted sensors covering different spectral domains from which guidelines or best practice protocols can be derived. One exception is the use of MS or HS in combination with TIR for assessing crop water status and estimating crop evapotranspiration (ET). This approach, with a history in airborne science research [20], has been successfully adapted to UAV VIS-NIR and TIR sensors [155, 22]. By leveraging the higher spatial resolution of UAV sensors, researchers have improved ET calculations by extracting separate surface temperatures for soil and crops, enhancing accuracy. In another example, [231] employed high-resolution (40 cm) HS and TIR images, combined with radiative transfer model, to detect traits related to *Xylella fastidiosa* (XF) in olive trees, achieving over 80 percent accuracy in detection. Although the method section of the above-mentioned studies describe various aspects, including leaf physiological measurements, image data

collection and processing, RTM inversion methods, statistical analysis, detailed protocols and guidelines for combining multiple sensors from different spectral domains are scarce. Therefore, an integrated guideline is deemed beneficial for less experienced researchers to conduct similar experiments.

The guidelines that we present here are based on the collective expertise of a diverse group of remote sensing specialists, represented in the working group (WG3) of the [51]. They are a result of years of experience and professional collaboration within our group. Our aim is to enhance the synergistic use of sensors by offering recommendations and advice in situations where single-sensor protocols prove to be insufficient. In addition to best practice recommendations, we have gathered bad practice examples from our group's experiences (see Section 8.4), to help users avoid repeating them. However, guidelines, by their nature, are suggestive, not compulsory; they are intended to help practitioners follow some rules while allowing for flexibility and common sense in different scenarios.

The following outlines the structure of the paper: Data acquisition (Section 8.2) data analysis (Section 8.3), and Lessons learnt / Bad Examples (Section 8.4). In Section 8.4 we discuss lessons learned from selected examples that illustrate the loss of data or deterioration in data quality that could occur if certain preparations, installations, or rules have not been followed.

8.2 Pre-considerations on synergistic sensor use

Acquiring image data using multiple sensors poses unique challenges that would otherwise be approached differently when using only a single optical sensor. Without adequate preparation, users may face difficulties that cannot be easily resolved on-site, jeopardising the field campaign or research project. This chapter reviews pre-considerations for data acquisition with multiple sensors and briefly reviews important aspects of the process. These recommendations are summarized in Figure 8.2 and Table 8.1.

8.2.1 Mission planning

Mission planning for any airborne science campaign depends on various factors such as atmospheric conditions, illumination conditions, and optimal time of day,

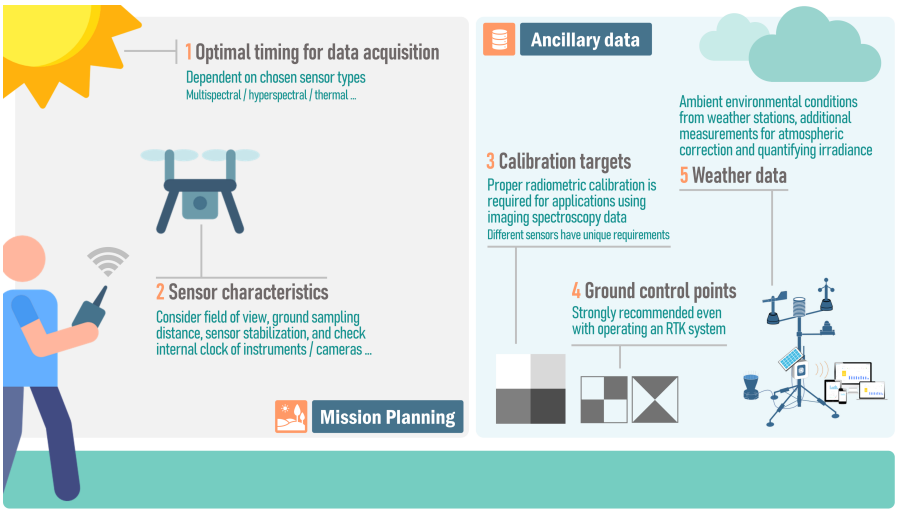

Figure 8.2: Overview of attention points during the data acquisition process for UAV-campaigns with multiple sensors. The items are described in more detail in the main text.

considering detailed sensor properties, targeted spatial resolution, and associated ground components of the field campaign. The initial factor to consider for any UAV or airborne campaign should involve conducting a comprehensive assessment of atmospheric conditions. While the suitability of flight conditions is of paramount importance, it is noteworthy that several factors affecting flight - such as wind, rain, clouds, humidity, and air temperature - can also significantly influence crop conditions during the time of measurement. Oftentimes, acceptable conditions for UAV flight will not be adequate for image data acquisition, but weather circumstances for flight and data capture should both be conceptualized as a range from optimal to adequate. Suboptimal conditions may require additional calibration measures, whereas some risks are not worth it for gathering unsalvageable data. Furthermore, when acquiring images via aerial platforms using multiple sensors, mission planning becomes crucial, and an accurate consideration of the diversity of sensor specifications is necessary. While recent reviews have addressed this issue [197], current mission planning applications do not support multi-sensor campaigns. Most UAV manufacturers include flight planning applications that consider only the basic camera characteristics like field of view, resolution, and pixel size. However, other aspects like sensor stabilisation and illumination conditions require extra attention or may need additional considerations in windy conditions. This section will briefly review the mission planning aspects that need to be taken into account when conducting multiple sensor campaigns. Finally, it is strongly recommended to conduct a test flight of all sensors and sensor combinations before conducting experimental flights in order to test for aeronautical stability, flight times, and to address any unexpected issues.

Table 8.1: Considerations for data acquisition; GCP - ground control point

Sensors	**Calibration targets**	**GCPs**	**Illumination conditions**	**Weather station data**
VIS-NIR	Gray-gradient	black and white	Stable (fully cloudy may be acceptable for RGB or broadband)	Not mandatory
SWIR	Gray-gradient	black and white	Direct sunlight	Recommended (water vapor)
TIR	Thermal calibration plates (warm/dry and cold/wet target - like a basin, dry and wet leaves, fabric)	Thermal high contrast	Direct sunlight, no wind	Highly recommended
SIF	Active/passive reference targets	Black and white or high contrast	Direct sunlight	Highly recommended

- **Optimal timing for data acquisition (#1 in Fig. 8.2).** Selecting the best time to perform data acquisition with UAV flights depends on the nature of the trait of interest, as well as the technical demands of optical sensors. For MS, HS, SIF, or TIR sensors, it is generally recommended to fly under clear sky conditions and around solar noon to minimize the effects of bidirectional reflectance distribution function (BRDF) and changes in irradiance (or temperatures). Not only are BRDF effects less at times closer to solar noon, but the sun angles are also changing slower, resulting in reduced changes in light conditions between the start and the end of flights. As crops often experience diurnal cycles of temperatures, it is important to consider the exact time of day for the level of stress (Figure 8.4). However, image data acquisition that targets structural traits [23] (i.e., 3D point clouds built using structure-from-motion (SfM) workflows) or texture-based object identification [77] (i.e, counting yield or crop components/organs) might be collected with overcast sky conditions to avoid shadows. Additionally, for dynamic traits like photosynthetic parameters such as stomatal conductance or SIF, repetitive sampling on the same day may be required to determine diurnal patterns [184]. Since some sensors, such as TIR, are influenced by shadow, image acquisition needs to consider shadowing, which is changing during the day and season. For the TIR signal wind might have higher priority than clear sky. For all sensors, it is important to be aware that solar azimuth and elevation change during the season, and protocols need to be adapted accordingly. The timing of image acquisition can be crucial for measuring certain phenomena. For instance, in crop water stress detection using TIR data, the typical recommendation is to acquire TIR data in the early afternoon around solar noon (Fig. 8.3).

  In case not all sensors fit on one platform, the sensors need to be flown separately, which thus requires defining an acceptable time gap between flights, and prioritization between optimal flight times. In those cases, the

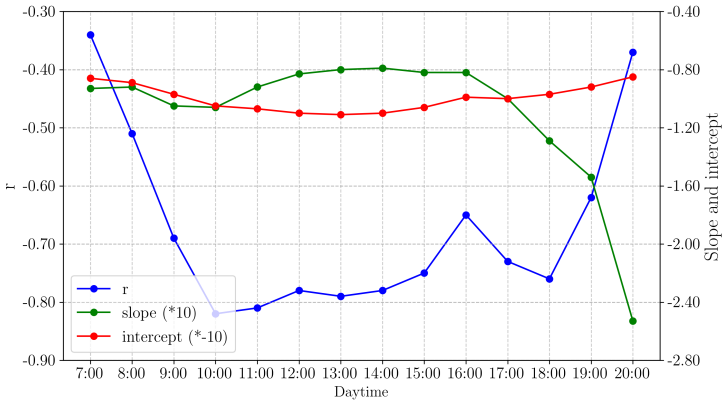

Figure 8.3: Daytime change of Pearson correlation coefficient (r) and slope and intercept of the linear model between Crop Water Stress Index and soil moisture in Hamerstorf, Germany (Lat: 52.91°, Long: 10.46°). Data stems from ground measurements of canopy temperature and soil moisture over an experimental potato field in 2019 during periods of water stress. Periods of water stress were the following days: DOY 158-160, 181-185, 208-210, 224-225 (in total 13 days), n=39 for the statistical measures. In the early to mid-afternoon (12-15 hours) the correlation is strongest and the linear model parameters reach relatively stable values which indicates a robust relation between the thermal infrared measurements and soil water availability. This illustrates the typical recommendation to acquire TIR measurements in the early afternoon for crop stress applications. Details on the computation of CWSI can be found in [66]. (Figure generated using data from the project "Sensor-based irrigation management in potatoes" funded by the program "European Innovation Partnership Productivity and Sustainability in Agriculture", as described in [66])

order of flights is vital as certain sensors favor specific environmental conditions. For example photosynthesis-related traits that can be obtained from SIF sensors are time-critical and could change in a matter of minutes, which is also true for TIR information with respect to crop evapotranspiration estimations. In contrast, plant pigment content or biomass are not as time-critical as flux-related traits but critical with respect to stable/clear sky illumination conditions. In general, flux-related traits such as photosynthesis rates derived from SIF or evapotranspiration from TIR are highly variable in time and should be prioritized over collecting data on plant pigments and/or biomass. Nonetheless, the latter are dependent on stable illumination conditions (i.e. clear-sky) but with respect to the phenological stage and stress intensity, these flights could also be postponed for a few days.

- **Ground sampling distance (GSD; #2 in Fig. 8.2).** GSD is a function of flight altitude, focal length, sensor resolution, and pixel size. This means that GSD will differ from sensor to sensor as well as between flights. In some cases, adjustments in focal length can offset minor differences in sen-

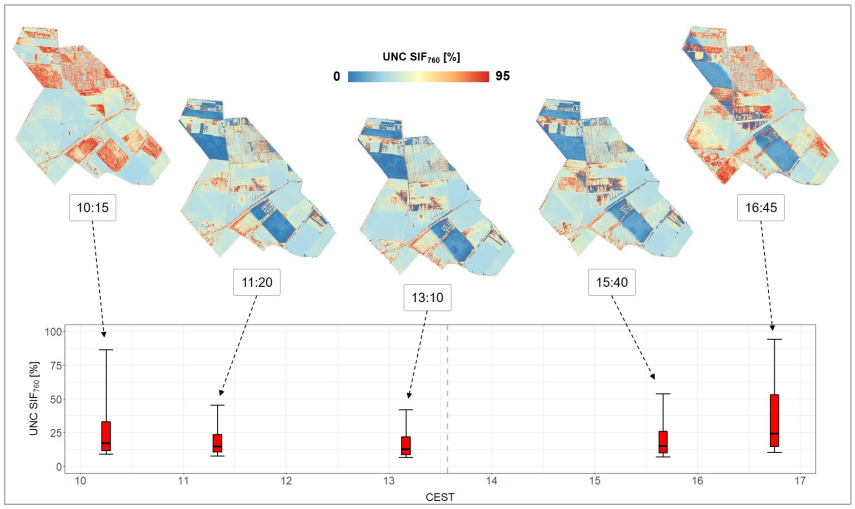

Figure 8.4: Relative uncertainties associated with diurnal measurements of SIF at 760 nm in June 2019 HyPlant campaign. The study area (Lat: 50.6°, Long: 6.9°) covered summer and winter varieties of wheat and barley, as well as sugar beet and winter rapeseed. The relative uncertainty is a combination of the uncertainty of the SIF retrieval, as well as the uncertainties associated with data pre-processing and the sensor measurement itself. For detailed description of uncertainty calculation please refer to FLEXSense 2019 report [168].

sor resolution, but for other cases, the differences in sensor resolution will be too large and require separate flights. Therefore, if the user is targeting a specific GSD when performing multiple-sensor campaigns, they should consider all the above-mentioned attributes for GSD calculation, most importantly, flight altitude. Users need to be aware that HS, MS, and TIR sensors generally have different spatial resolutions (Fig. 8.5) as well as flight acquisition requirements, so if there is interest in acquiring plant-level information at a specific spatial resolution, flight altitude must be adjusted according to the sensor with the lowest resolution. This consideration may lead to long flight times, which can be limited by UAV battery capacity. If multiple flights are planned, the number of available batteries and charging opportunities (including cables and multi-plugs) in the field have to be taken into account in the flight planning as well. Varying terrain elevation of the study area has an effect on GSD. If these variations are large e.g more than 10m, the flight altitude needs to be adjusted accordingly. In these scenarios the terrain following option in the flight planning software should be used to ensure consistent GSD.

- **Image overlap and flight patterns.** The choice of image overlap depends on many factors including but not limited to: type of the targeted crop traits (morphological, physiological or biochemichal), complexity of the terrain (homogeneous or heterogeneous), UAV battery capacity, type of the sensor and sensor resolution, data storage capacity etc. [68]. When

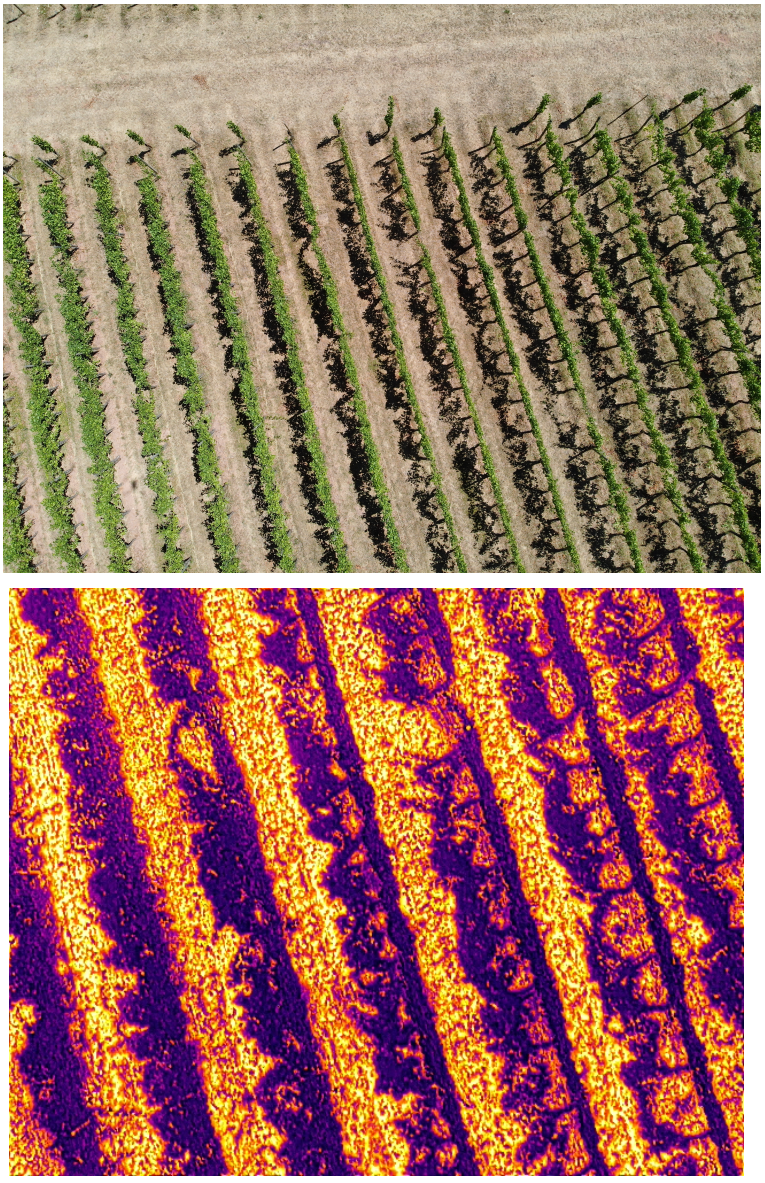

Figure 8.5: An example of the different fields of view between data of a MS (a) and TIR (b) sensor acquired during the same UAV flight over viticulture.

flying frame (camera array) imaging sensors over homogeneous agricultural fields characterised by a low number of discerning features, a high lateral (between flight lines) and longitudinal (along a flight line) overlap of >70% ensures the correct stitching of the images in the mosaicking process. Besides, it is important to optimize the placement of the different sensors on the UAV to ensure a high degree of overlap between images. During a multi-sensor mission, image overlap has to be computed for the sensor with the narrowest field of view. This will ensure that they capture images of the same area. Planning flight patterns with sufficient overlap so that every section of the ground is imaged close enough to nadir direction will ensure the mitigation of BRDF effects. Many SfM processing software will help to minimize BRDF effects by using the whole of the image overlapping regions to align the images [1], but then use only the central most nadir portion of each individual image for the final mosaic. High image overlap >70% substantially increases the generated image data volume and flight duration. Since for certain sensors time and duration of acquisition is critical, the image overlap settings as well as flight altitude should be reviewed (e.g lowering lateral overlap close to the recommended minimum of 60% and increasing flight altitude) and sensors prioritised during a multi-sensor campaign. For more details refer to [68].

- **Sensor stabilisation (#2 in Fig. 8.2).** Specific instruments, such as uncooled TIR cameras, require thermal stabilisation after take-off to minimize temperature drift that occurs when the camera temperature changes over time. Warming up on the ground, using an external heated shutter [212], hovering, or loitering over 5-10 minutes can minimise these effects. However, this extra flight time has to be considered and will reduce the useful time available for the actual mission [127]. Field spectrometer systems for SIF retrieval theoretically require less warming-up in the field, however, during laboratory calibration, a warming-up time of around 15 - 20 minutes has often yielded the most stable results. Thus, we recommend powering up the instrument approx. 20 minutes prior to critical measurements. When fusing information across different sensors, it is recommended to minimize biases due to drifting of individual sensors by giving each sensor sufficient time to stabilize in the ambient air temperature. The stabilization time may vary depending on sensor type and the environmental conditions. Thermal expansion or contraction of lens materials and mechanical components can alter the physical distance between the lens elements, thereby affecting the focal length. Additionally, temperature variations can affect the properties of electronic components within the camera, such as sensors, circuit boards and calibration materials. This affects the imaging performance and accu-

racy and needs to be taken into account.

8.2.2 Ancillary data

- **Calibration targets (#3 in Fig. 8.2).** Proper radiometric calibration with calibration targets is required for accurate crop trait mapping using imaging spectroscopy data. Different sensor types have unique requirements, and when using multiple sensors, each must be met for high-quality data acquisition. A standard approach for VIS-NIR sensors is the empirical line correction method (ELM) [186]. Here it is recommended to use at least 2 gray-gradient targets with different reflectance factors and a Lambertian surface [135, 43]. Targets for VIS-NIR sensors should be placed on a non-vegetated surface, not too close to each other to minimise adjacency effects, and cover several pixels from the desired flight altitude. This point is especially important when performing multiple sensor campaigns with varying spatial resolutions. For more detailed information on best practices of calibration targets refer to [1]. TIR sensors require temperature calibration plates (TCPs) with a large temperature range and built-in insulation to avoid temperature fluctuations [138, 144]. Standard practice is to place contrasting TCPs at different locations in the field. TCP material should have high emissivity, be stable over time, have a uniform surface and be durable. Certain materials such as painted black and white polypropylene or aluminium plated panels have proven to be satisfy the above requirements [127, 144]. Similar to VIS-NIR sensors, TCPs are used for radiometric calibration with ELM.

  Reference targets to verify SIF retrievals require mimicking the double peak emission of chlorophyll fluorescence, ideally against a spectral signature background that is close to that of vegetation. Active SIF reference targets with LED panels are recommended for signal intensity validation and correction, but they require a time-consuming setup and management [37]. Passive SIF reference targets based on a dye that has a similar spectral shape as chlorophyll fluorescence are easier to set up but they rapidly age under sunlight and require continuous monitoring [168]. Both types have spectral differences compared to SIF in natural vegetation. It is recommended to characterize both types of reference targets on the ground and continuously monitor them during the experiment to consider ambient influences.

- **Ground control points (GCPs; #4 in Fig. 8.2)**. The installation of

GCPs is strongly recommended, even if the UAV is equipped with real time kinematic (RTK) positioning. This is particularly important for wavelength ranges with less reflected or emitted energy like SWIR or TIR, where the spatial contrasts are less sharp and the identification of targets in the image might be challenging. SIF sensors typically require the same GCP characteristics as other hyperspectral sensors do. Suitable GCPs are aluminium panels, which are well visible in the thermal but also in all other spectral domains. In the context of multi-sensor operations GCP dimensions are of high importance. They should be large enough to be discernible from sensors with different spatial resolutions. Covering panels (for example thin wood) with standard household aluminum foil is an economic solution and they are easy to carry and install in the field. It should be noted that aluminum foil possesses highly reflective properties within the visible light spectrum. To mitigate specular reflection, the panels should be positioned in shaded areas, oriented appropriately to minimize direct exposure to sunlight, or be covered with crinkled aluminium foil. Furthermore, it is advisable for the GCPs to have a distinct shape, such as a square, rather than, for example, circles, to facilitate clear identification of positions. In addition, the GCPs should have a visible mark in the center to allow exact coordinate identification in post-processing. Black and white GCPs may also be discernable for VIS-NIR and TIR; if placed in the field 1-2 hours before UAV flights the black and white panels should achieve an adequate temperature differential compared to soil and vegetation. For more detailed information on GCPs refer to [1] and [54].

- **Weather data (#5 in Fig. 8.2)** Local weather data is important for many applications, especially for TIR and SIF. TIR data is often normalised using air temperature, solar irradiance, and wind speed. Normalizing SIF by solar irradiance brings more insight into the crops' physiological status. In the case of optical sensors, the use of a sun photometer can provide aerosol optical depth (AOD) and atmospheric water content for calculating irradiance and determining reflectance. Alternatively, irradiance measurements can be performed in the field [96] using spectroradiometers or cosine irradiance sensors mounted on the UAVs. Monitoring the environmental conditions is also essential for comparing measurements across multiple days or environments. If local weather stations are nearby, their data could be used to characterize weather conditions during the flight. However, due to significant variations in parameters such as wind speed or irradiance over short distances and the typically limited temporal resolution of recorded parameters, it is generally recommended to use portable weather stations to more accurately characterize instantaneous weather conditions.

- **Annotation**. Acquired data must be adequately annotated to make the fusion of various spatial, spectral or temporal resolutions possible. General attention should be paid to the geocoding including the used geographic coordinate system and time of the acquisition. The annotation of measurements with meta-data provides the first level of data products and is crucial for data quality and control and the potential usefulness for further studies. It is also needed to combine the data from the different sensors without mistakes like a mix-up of time or location etc.

8.3 Data analysis

Data analysis encompasses the pre- and post-processing of the imagery, starting from georectification and ending with retrieving crop traits using parametric and non-parametric methods (Figure 8.6). In this process, data products are classified into different levels based on the extent of processing they undergo. These levels, denoted as (Level 0), (Level 1c), and (Level 3), represent distinct grades of pre-processing. Level 0 refers to raw data as digital numbers (DNs) recorded by the sensor and metadata, Level 1c involves radiometrically processed and calibrated data in absolute SI units, while Level 3 corresponds to higher-level information extraction such as SIF and vegetation indices (VI).

The level of pre-processing determines the usability and generality of data products, depending largely on the desired application. Synergistic use of multiple sensors requires a standardization of data products enabling the valid fusion of information. Fusion of raw data (Level 0) from multiple sensors is possible in principle if proper annotation is provided along with complete meta-data. This Level 0 information is sensor specific and therefore, cannot be generalized easily. We recommend pre-processing data to Level 1c, which provides absolute and comparable, physical SI units together with relevant meta-data to enable transferable results. It is advisable to keep a record of the used sensor calibration in the meta-data after processing to Level 1c. Furthermore, we recommend the use of data quality flags, that provide uncertainties and error budgets in the meta-data to filter unstable or biased measurements [49, 109].

One of the prerequisites of hyperspectral and multispectral data fusion across different sensors are spectral re-sampling and convolution [2]. In this context, temporal and spatial aspects need to be considered carefully and may require aggregation methods for combining data of different temporal resolutions and of different spatial extents. For example, to compare datasets pixel-to-pixel, spatial

resampling for matching GSD is necessary as well as pixel-to-pixel co-registration of orthomosaics. Temporal mismatches may be addressed by normalisation such as vegetation indices, or by applying corrections e.g. for changes in PAR, e.g. relevant for data in radiance units such as SIF. Researchers are advised to make sure to always record the appropriate time-stamp, time-zone, field of view, sensor elevation and location with each measurement to ease the combination of information from sub-plots and experiments later on. When combining higher level information (Level 3), for example SIF or VI, from multiple sensors, ensure that the retrieval methods or band combinations for their retrievals were identical or at least as similar as possible.

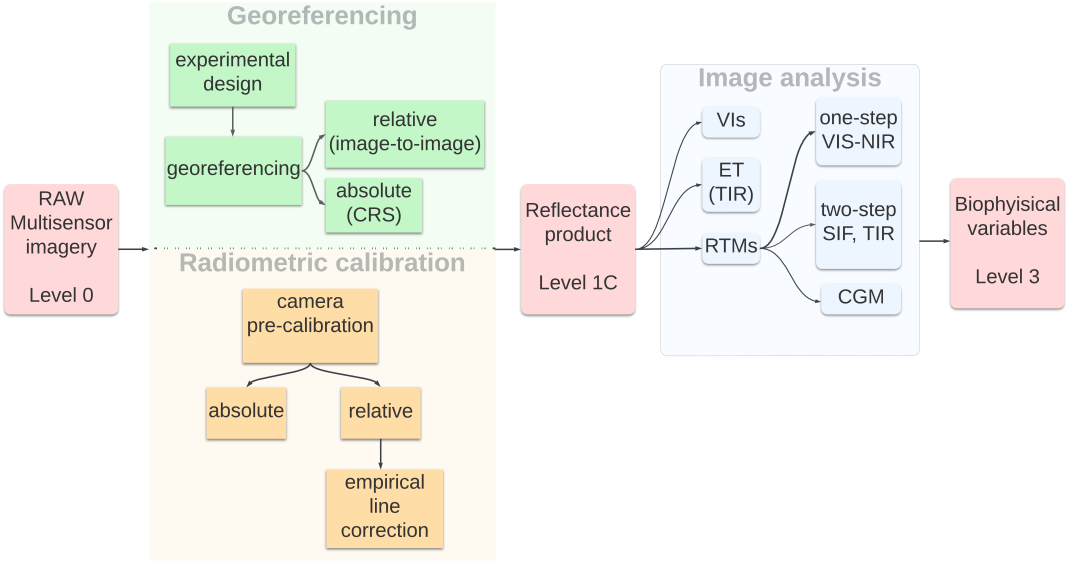

Figure 8.6: Consideration points for pre and post processing of UAV data from several spectral domains; CRS - Coordinate Reference System, RTM - Radiative Transfer Model, VI - Vegetation Index, ET - Evapotranspiration, CGM - Crop Growth Model

8.3.1 Pre-processing: level 0 to level 1c

Georeferencing The synergistic use of image data from multiple sensors with different spectral domains requires careful geometric processing. Different sensors often have varying spatial resolutions and geometric accuracies. Additionally, data may have been acquired at different times or on different days. Two approaches for georeferencing the image data include image-to-image georeferencing and absolute georectification. Image-to-image georeferencing is suitable for sensor fusion with significantly different spatial resolutions or different acquisition times, while georectification is necessary when using other spatially aligned imagery, such as satellite scenes.

Radiometric calibration. To perform accurate multi-temporal crop stress analysis and correct for minor atmospheric influences in UAV data, raw DN pixel values are not sufficient [187] and need to be converted to reflectance. Reflectance calibration slightly differs for visible (RGB), multispectral [164], hyperspectral [134, 106] and thermal sensors [127], due to varying atmospheric attenuation effects. A common and easy-to-use approach is one-point calibration, which involves using a single calibration panel and performing empirical line correction [216]. However, using multiple panels yields more accurate results [43]. For more information on calibration targets refer to subsection 8.2.2. In recent years, standalone physical-based atmospheric correction software, such as DROACOR [180], has emerged, offering a more streamlined approach to atmospheric correction, particularly beneficial for newcomers in the field.

More precise reflectance calibration approaches monitor the atmosphere at all times using downwelling light sensors (DLS) and correct for short-term changes in the atmosphere [159]. Some MS sensors may have a single band broad range DLS, while other sensors may have dedicated DLS band filters for the separate calibration of each band, with the latter providing improved accuracy. However, under certain conditions, DLS mounted on UAVs are biased due to in-flight yaw and pitch angles. When using DLS synergistic application of multiple sensors, assure valid and congruent correction for all used sensors.

For thermal data, it is essential to understand the relationship between acquired DN values and targeted surface temperature [127, 144]. Radiometric correction in the field is done by empirical line calibration regressing the measured TCPs temperature and DN values at the TCPs. This approach assumes high emissivities of TCPs (> 0.98). The validation may be done using linear regression of defined homogeneous regions measured by infrared thermometers. Even if absolute temperature is desirable, it is rather challenging [99]. In some cases, just relative differences are sufficient or a simple correction with the ambient temperature of the closest weather station might be suitable. The calculation of a simplified, image-based version of the CWSI (crop water stress index) [111] can also be an option to combine TIR data with further sensor information (see section 8.3.2.1).

8.3.2 Post-processing: level 1c to level 3

8.3.2.1 VIs

In this section we are going to show how UAV-acquired data from different spectral domains were used together in vegetation studies. The synergies we are going to describe are VIS-NIR, VIS-NIR-SWIR, VIS-NIR-TIR.

The most common example of sensor synergy is the usage of VIS-NIR for vegetation-soil separation with, for example, NDVI and further processing of vegetated pixels. Masking soil pixels with NDVI, [122] retrieved water stress as stomatal conductance from SWIR and [14] retrieved water stress from TIR. The SWIR region is affected by water availability in the vegetated canopy, highlighted in the synergy with NIR in normalized difference water index (NDWI) for vegetation water content [80] and normalized difference infrared index (NDII) for canopy water stress [97]. NIR/SWIR indices were applied for grass [119, 18] and wheat [119] biomass mapping from a UAV NIR/SWIR imaging system [118]. Several attempts were made to reconstruct SWIR regions from VIS-NIR images with machine learning for estimation of fuel moisture content (FMC) [7, 8, 210, 209].

8.3.2.2 ET (TIR)

For VIS-NIR-TIR synergy, the group of trapezoid (also known as triangular) approaches is used to explain the variation in land surface temperature (LST) with a variation in vegetation index, usually NDVI, to estimate the vegetation water stress [131]. The first application was developed for Water Deficit Index (WDI) [151]. Lately, the method was used with UAV-borne data for crop water stress mapping [100] and ET computation [150]. Many ET models (TSEB [157], SEBS [190], METRIC [5]) develop this LST-NDVI relation further, including shortwave albedo.

8.3.2.3 RTMs

One of the advanced methods for making use of VIS-NIR-SWIR synergy is exemplified by the RTMs, most of which function in the shortwave radiation range, 400-2500 nm. The models such as SAIL [203], INFORM [181] and DART [81] upscale leaf reflectance, simulated usually with the PROSPECT model [115], to the canopy level. The inversion of RTMs enables retrieving leaf (chlorophyll and

water content) and canopy (LAI) parameters, which can be further correlated with stress levels [207]. As mentioned earlier, SWIR-carrying UAV systems were developed relatively recently [118, 9], therefore UAV studies that use RTM inversion are limited to the VIS-NIR domain, sampled either hyperspectrally [63, 132, 215, 217, 3, 229] or multispectrally [202, 172, 117, 191, 44, 6, 185]. As a guideline, we advise to degrade the spatial resolution of a UAV image to satisfy turbid-medium models, such as SAIL, or to mask shaded and bare soil pixels before the inversion [44].

The incorporation of the TIR domain in RTMs remains less studied due to challenges with temperature-emissivity separation. Some attempts have been made with codes like SAIL-Thermique [158] and 4SAIL [204]. Although it was shown that the SCOPE model has the potential to use TIR to retrieve leaf biophysical traits (maximum carboxylation capacity of RuBisCO, Vcmax25, related to the photosynthesis rate and Ball-Berry slope, BBS, related to stomatal conductance, photosynthesis and transpiration) [165], the practical attempts required additional constraints with the flux data (GPP, ET) [64, 166] or look-up tables [21]. The main challenge for RTM applications with UAV-borne TIR data is the accurate absolute radiometric calibration of UAV-TIR data, because RTMs work with absolute physical quantities.

In spite of being more temporally dynamic than TIR, SIF was successfully introduced into leaf (FLUSPECT [208]) and canopy (SCOPE, CliMA [217], DART[140]) RTMs. [219] used UAV-borne VIS-NIR-SIF synergistic retrieval of leaf and canopy traits and fluorescence quantum yield (fqe) with the SCOPE model for sugar beet under water stress. Additional TIR constraint was needed as a proxy of stomata closure. The UAV-borne systems suitable for SIF retrievals are being developed actively [24, 45, 201, 218, 235] and we expect more studies to use RTM for SIF data processing.

Overall, the inversion of RTMs in the VIS-NIR-SWIR domains sampled hyperspectrally can be considered a routine operation. In relation to multispectral UAV sensors, the success is limited by the number of bands (constraints) in the UAV system, plant phenological stage, time of the day, spatial resolution, viewing angle etc. The application of RTMs with SIF and TIR data is an emerging field and currently requires a two-step procedure [219]. In the first step, biophysical parameters retrievable from multispectral and hyperspectral are obtained. In the second step, plant physiological parameters such as Vcmax25 and fqe are retrieved from SIF or TIR.

8.3.2.4 Integration with crop models

[29] had elaborately portrayed the advantages and potential of combining crop growth models with remotely sensed data obtained by several types of imaging instruments. While crop models focus on simulating the complex process of crop development and biomass accumulation, some only provide an output of plant and soil properties [107], and other, more complex CGMs, do account for the interaction of soil and plant with radiation by modeling the energy balance in the soil-plant-atmosphere but do not produce output variables directly related to remote sensing measurements (e.g., surface reflectance, etc.). Thus, some important aspects should be considered to assimilate remote sensing data into crop models, specifically data from multiple sensor types.

There are several crop models commonly used in the literature, which vary in aspects such as crop growth driving mechanism, simulated state variables, and model parameters [120]. These differences might determine the adequacy of a certain crop model to benefit from integration of RS data in different domains. For example, canopy cover, used in AquaCrop to describe the canopy development [188], is a property that can be evaluated either from plain RGB images or from VIS-NIR data [234]. More complex crop models, such as DSSAT [121] or APSIM [103], differ from AquaCrop in two major aspects: (a) plant growth is driven by the amount of intercepted radiation, and (b) they simulate more processes including the soil-plant-nitrogen balance [36]. Following the example of canopy development simulation, these two crop models use LAI to describe canopy expansion, which can be obtained, e.g., by empirical relations to vegetation indices [142]. This approach, of using data from one spectral domain to evaluate a single property is straight forward, but still limited to very specific simulated state variables and data types.

To use data from several spectral domains with varying spectral resolution in a synergized way, and to utilize more crop related properties, one can couple the crop model with a radiative transfer model. This means to choose mathematical equations that relate the crop model's state variables with the RTM input parameters. Since crop models are dynamic and usually use daily time steps, while RTMs are instantaneous, one should consider the rate of change of the simulated properties. Most previous studies that used this approach used different versions of SAIL [203] for the choice of RTM [222, 137, 108], but this group of models, along with its diverse capabilities, is limited to the optical domain of the electromagnetic spectrum. Thus, to facilitate the use of SIF and thermal data, a more comprehensive model, such as SCOPE, is recommended, and the coupling relations should be extended to include relations between crop state variables and

RTM parameters that affect thermal emission and SIF.

In previous studies, this framework was mainly used to improve prediction of yield and other crop traits[93], but in the context of this paper, it might as well be used for crop stress detection since GCMs (e.g., APSIM, DSSAT) simulate the daily stresses (water and nitrogen) that impact photosynthesis and growth processes (e.g. expansive growth processes) in a dynamic way. For this purpose, the method for integration of the RS data in the coupled model should be carefully chosen. Due to the dynamic nature of crop models, either a calibration or sequential updating are commonly used. Calibration methods consider the course of a full season, and determine the values of the crop model parameters, which does not directly relate to stress indicators and are less suitable for our purpose. In contrast, sequential updating methods (e.g, Kalman filter or particle filter), usually used to update the state variables, and thus they are more recommended in the context of stress detection. Following this approach, by assimilating RS data, both RTM parameters and stress-related crop model state variables can be evaluated dynamically. Finally, it should be noted, that although most of the previous studies used space-borne RS data because yield prediction does not require very high spatial resolution [107], stress detection requires the use of UAVs to obtain much higher spatial resolution.

8.4 Lessons learnt / Bad Examples

Sensor synergies can be challenging, above all due to inconsistencies arising from differences in overpass time and resolution (spatial, temporal, and spectral). To assist new users and avoid pitfalls and frustration, we compiled recommendations derived from real-world examples where data acquisition did not go as planned by experienced UAV operators using multiple sensors. These recommendations, are not strictly limited to multi-sensor synergies and apply to UAV field campaigns in general.

8.4.1 Checklist, Protocols, Fieldbook

First and foremost, we advise every operator to design/modify checklists and standardized protocols adequate to their respective field campaigns. Besides preventing rather apparent mistakes such as forgetting critical parts of the equipment in the lab, variations due to changing operators are minimized and the procedure can be reproduced at a later time [194, 70, 192] Similarly, we recommend pre-

cisely documenting the metadata such as weather conditions, handling person, time, and any other source of information that appears to be useful while being in the field to comprehend eventual issues occurring when processing the data. Short and precise checklists and metadata documentation are most effective. They should focus on essential information to prevent user frustration. Lengthy checklists are less likely to be thoroughly reviewed by users. Often, noting metadata is overlooked during UAV operations as field campaigns typically require multitasking. To address this, we suggest taking photos of screens, the sky, instruments, and watches, and recording voice messages as reminders. Additionally, a pre-populated text on a mobile phone or tablet, or printed on paper can aid in remembering crucial information during fieldwork. This allows for quick data capture on-site, with more comprehensive documentation completed later in a quieter setting.

8.4.2 Solar illumination

We advise users to critically check their protocols based on daily and seasonal cycles of solar azimuth and zenith angles. Variations of these angles potentially induce uncertainties and change the distribution of direct and diffuse illumination of vegetation. Although not completely avoidable, it is advisable to minimize this effect, quantify the related uncertainties or consider strategies such as BRDF modeling where appropriate. Related to this, variation in illumination leads to variation in shading which can hinder successful analysis but, also allow for easier object detection (e.g. trunks not visible in nadir). Especially for thermal sensors, shaded objects can induce variations in radiometric temperature. These should be treated adequately as they might significantly affect derived variables (e.g. ET).

8.4.3 Test flights, GCP visibility, ROI markers

We also advise performing test flights and quickly analyzing the corresponding data as we encountered cases where we found an insufficient overlap of images, although image acquisition protocols provided by the manufacturer were met. While performing these test flights, we further recommend ensuring that GCP placement is correct and the markers are clearly visible through all spectral domains, with special emphasis on the thermal domain. We encountered problems with permanently placed markers which had poor visibility in certain spectral domains due to dirt accumulation and/or wear due to exposure to UV radiation (see

Fig. 8.7). Additionally, we recommend using additional markers (again, visible in all spectral domains) defining regions of interest as differences in the field of view and spatial resolution can hinder identification, especially in homogeneous environments such as crop rows as shown in Fig. 8.5. From our experience, investing in high-quality reference panels can significantly improve radiometric quality, especially when dealing with narrowband hyperspectral sensors. Therefore, we recommend allocating a budget for suitable reference panels for the corresponding sensors. Lastly, ensure reference targets receive regular cleaning, especially in dry summer conditions when dust accumulates quickly.

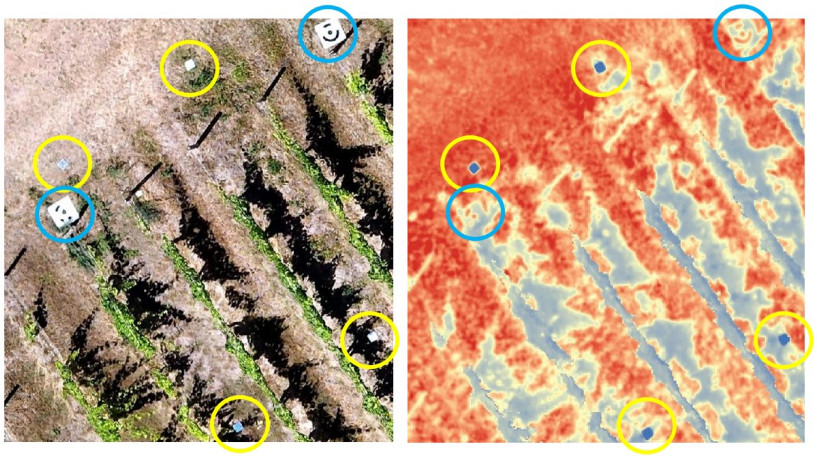

Figure 8.7: Visibility of markers in different spectral domains. Yellow circles show panels made from aluminium foil, while blue circles represent panels with printouts of markers (i.e. white squares with geometric patterns). In RGB (left) both marker types are easy to spot, while the visibility of the standard panels is clearly restricted in the thermal image (right).

8.4.4 Instantaneous weather conditions

Most of us found ourselves tackling problems due to weather conditions during image acquisition on many occasions. As the majority of flights are performed on sunny days, we encountered issues regarding equipment overheating (e.g. tablets for UAV operation, UAV batteries, spectrometers etc.) hindering the successful acquisition of data. Recommended practices are scheduling with breaks to let the equipment cool down, avoiding direct sunlight exposure (e.g. through a parasol) or the usage of active cooling systems in extreme environments. Also, we advise allocating resources carefully: Cancelling or delaying flights due to unfavorable weather conditions is regrettable but often a more prudent decision than collecting inaccurate data, which could result in even greater resource wastage. From our experience, decision-making is often not straightforward and discussions

within teams are common. We, therefore, recommend defining clear criteria (e.g. maximum wind/gust speed thresholds) beforehand which are monitored during the campaign and allow to make an informed decision on campaign cancellation.

8.4.5 Flight and irrigation timing

Crop water status is dependent on the timing of irrigation, not only irrigation dose. When measuring Crop Water Stress Index (CWSI) from thermal imaging, one must take into account when the last irrigation was applied; if irrigation is applied just before or during the imaging, differences between irrigation treatments may be less pronounced compared to taking a thermal measurement before irrigation is applied. Whenever possible, we recommend scheduling the irrigation after the measurement flight. An example is given in Fig. 8.8, where the visibility of the different treatments is strongly reduced in the left panel.

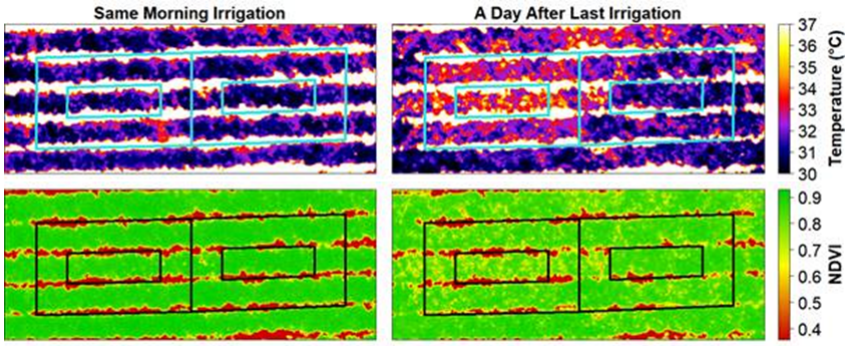

Figure 8.8: Surface temperature and NDVI from UAV observations in two different days of an experiment in processing tomatoes in Israel in the summer of 2020. The figure shows experimental blocks with two different treatments: the right block features full irrigation (i.e., best practice irrigation, the control treatment), while the left block was given 50% of full irrigation. Each block comprises three crop rows (outer boxes), but the irrigation effect was measured only for the middle row (inner boxes), as the outer rows serve as buffers from adjacent treatments. If irrigation is applied just before or during the imaging, differences between irrigation treatments may be less pronounced compared to taking a thermal measurement before irrigation is applied.

8.5 Conclusion and outlook

This manuscript summarises relevant aspects important to consider when exploiting multiple sensors onboard UAVs for crop stress and trait detection. The need for such guidelines has been identified as a result of increased stress occurrence

caused by climate change effects, the increased availability of optical sensors on-board UAVs, and the current lack of existing protocols on how to collect and analyze such data.

The first part of the manuscript covered data acquisition of high-quality multi sensor imagery. The most relevant points to consider were: i) Optimal timing for data acquisition is crucial. The order of the flight is detrimental as some sensors have very specific timing requirements. ii) Sensor characteristics need to be taken into account for mission planning. iii) Sensor from different optical domain require calibration targets with different properties. iv) Use of ground control points that are discernible from every sensor are strongly recommended to ensure accurate image co-registration. v) Use of additional measurements (e.g. weather data) for atmospheric correction is advisable.

The second part of this guideline dealt with the data analysis. The most relevant points to consider were vi) Data fusion for synergistic usage should be done at data level 1c (physical units). vii) Data quality flags should be used to filter unstable or biased measurements. We presented some straightforward methods like vegetation indices to combine information from different spectral domains, along with some more complex processing such as retrieving biophysical variables from RTM inversion. The latter necessitates further research, and it is hoped that numerous studies will be conducted in line with the recommendations made by [29].

Finally, the recommendations are rounded up by bad examples that scientists experienced during their research work. This collection of best practices and lessons learnt can help scientists and practitioners in making informed decisions regarding sensor selection, mission planning and the challenges associated with multiple sensor data acquisition and processing to advance crop stress monitoring with UAVs.

Chapter 9

Synthesis

Uncrewed aerial vehicles have great potential in agriculture research and plant breeding due to their versatility, ability to deliver high-resolution image data, and size that makes them accommodate different sensors. For these reasons, they are perfect phenotyping platforms allowing agriculture practitioners to save time and resources. The crop breeding community is under pressure to develop resilient and productive crop varieties in response to climate change, new sustainable agriculture policies, and growing skepticism towards GMOs. This includes developing crops that can withstand, drought, heat stress, and changing pest and disease pressures. In addition to improving climate resilience, breeders also need to maintain or improve yield, quality, and other important agronomic traits. Monitoring these amount of varieties in the field and studying the effects of the different environmental conditions, be it biotic or abiotic stress is a challenging task and is not feasible if done by manual human labor. This is a niche that UAVs could fill well since they can carry various sensors to retrieve information on plant parameters in a standardised manner.

This thesis aimed to explore the application of UAVs in retrieving crop parameters and exploring sensor synergies for crop stress detection. For this reason, several field experiments have been conducted to acquire image and plant data. These experiments served to ask and answer questions about three main contribution topics that will be discussed below.

9.1 Reflectance Calibration

A well-defined reflectance calibration pipeline served as a foundation of this thesis. In this study we demonstrated the advantage of the ELM to single-panel approach that is often offered by camera manufacturers. We identified errors in surface reflectance derivation using the MicaSense Dual camera system (production date: 2019), particularly in the NIR and red-edge bands, with the most significant inaccuracies occurring for dark panels (reflectance factors lower than 20%). Negative reflectance values were also observed, as reported in other studies. Several points need to be discussed that could not be included in this publication.

The first point involves the linearity assumption between target reflectance and radiance. Our study indeed shows that the relationship of measured panels and at-sensor-radiance is linear. However, the response of each sensor and calibration target is different and might be non-linear. Non-linearity may arise from the sensor itself. To investigate we started to characterize the sensor which proved to be non-trivial as a variety of integration times and sensor gains were used in different datasets. This is why it's recommended to use more than 2 calibration targets to check for the sensor response. ELM comes with limitations one of which is the assumption of constant illumination. During the aerial campaigns, the solar angle changes constantly. It can be assumed that this change is negligible if the campaign is short and around the solar noon when the rate of solar angle change is at its minimum. Additionally flying over the panels more than once during the campaign and averaging the change will mitigate the effects of illumination, but only when it's completely overcast or clear sky day. In our studies we have conducted campaigns on clear sky days, but in reality UAV users in most cases are challenged by suboptimal weather conditions (e.g changing illumination due to the clouds). In such cases irradiance sensors could be used to record irradiance for each image and band during the flight and use that information to normalize the illumination.

Another point that has not been discussed with reflectance calibration is a Bidirectional Reflectance Distribution Function, shortly BRDF effect. The BRDF effect captures how the reflectance of a surface changes with different combinations of light source and sensor viewing geometry. The magnitude of BRDF effect depends on the magnitude of solar and viewing geometry, sensors with narrow field of view having less pronounced BRDF effect [175]. There are models for correcting for BRDF and these corrections have been primarily made and applied to satellite imagery. Such models have been also recently developed for UAV applications [180]. The BRDF effect during the UAV overflight could be mitigated by

increasing side and front overlap. This will ensure that during the SfM processing only the central parts of the images are used for stitching, artificially reducing FOV.

Flight altitude is another point that needs special attention. In our studies we used 20 m as flight altitude, meaning that the atmospheric column between the sensor and the surface was negligible. The multiple panel approach is especially important when performing flights at higher altitudes where the effects of atmospheric scattering will be much higher. We tested our approaches at 20 m height and therefore the differences we found between both approaches may not hold for other heights. In order to understand better the impact of single-panel and multiple panel approach in the future it would beneficial to conduct a study exploring reflectance calibration at different flight altitudes. This will allow to better identify the effect of the atmosphere on both reflectance calibration pipelines.

9.2 Retrieval

The advantage of UAVs over the coarse satellite data, apart from their versatility, when it comes to the retrieval using PROSAIL proved to be the ability to discriminate between different canopy constituents. This enabled successful retrieval exemplified by the 2nd study.

In this study we have demonstrated that with increasing spatial resolution the retrieval accuracy of both structural and biochemical parameters increases. The results for LAI retrieval are comparable with the findings of [191], where authors reported decrease of LAI accuracy with increasing resolution. Our study further demonstrates that soil removal is beneficial for estimating LCC with high precision. Even though soil removal was possible even for 0.48 m data, it is assumed that in more heterogeneous plots it may be more challenging and higher resolution data would deliver better results.

It needs to be noted that UAV operation in airspace is limited to a certain height and that some of the spatial resolutions tested here cannot be flown under certain regulations. We demonstrated that the coarser resolution data that can be acquired from airborne sensors (0.48 m), would still deliver good retrieval results. Flights above 100 m will be significantly influenced by some atmospheric effects, especially in conditions with high aerosol content or humidity. In this project no additional atmospheric effects were applied to the resampled image data. For future research atmospheric simulations or experimental flights could be conducted

at different altitudes, humidity levels and illumination conditions.

Another point that needs to be addressed is the retreival of LCC for chlorophyll-deficient mutant Minngold. The LCC overestimation observed in Minngold with removed soil could be attributed to the constraints of the PROSAIL model: Minngold is characterised by two distinct canopy layers, low LCC in upper leaves and high LCC in lower leaves. This two-layer canopy structure is not accounted for in PROSAIL, leading to overestimation. PROSAIL assumes a homogeneous canopy with uniform leaf properties throughout. This assumption breaks down when dealing with canopies that have distinct vertical stratification. Solution to this problem would be to use more complex models as M-SCOPE, where more than one optical property could be assigned to the plant [225]. Better results for Minngold when using an unmasked orthomosaic can be attributed to the large contribution of soil signal that lowers the LCC values.

While 2nd study explored the impact of resolution on the retrieval, the 3rd study tested the PROSAIL capability in retrieving the same crop parameters in a more complex, maize canopy.

Key point to highlight is the difference in LAI retrieval between the two maize varieties. One of the reasons for the different LAI prediction accuracies achieved for sweet and silage maize might be the particular choice of the ELADP value used for leaf angle distribution during the SunScan measurements. In both maize types, a fixed value was used; however, the leaf angle distribution visually differed between the two maize types. Therefore, the observed overestimation of LAI in the case of silage, and underestimation in the case of sweet maize, could be attributed to the fixed ELADP value chosen for the ground measurements. Additionally, the SunScan measurement results varied strongly depending on the probe placement in the canopy during data acquisition, which had a significant effect on the LAI estimation. Neighboring silage maize plots might also cast shadows on the sugar maize plots, distorting the measurements.

The discrepancy in LAI estimation at early (stem elongation) and late growth stages (flowering, etc.) is another point that requires attention. Better estimation results for early stages can be attributed to the smaller number of leaves compared to later growth stages, when leaf clumping is more pronounced, especially for nadir imagery, where row effects are discernible. It is known that PROSAIL simulations have limited applicability in row crops such as maize which are characterized by large gaps between the rows and rather open canopies. The underestimation observed specifically in sugar maize could be attributed to the absence of leaf clumping correction in the PROSAIL model. While these canopy

characteristics were partially considered when conducting ground measurements, they cannot be parameterized in PROSAIL. PROSAIL assumes a homogeneous and closed canopy, the condition partially met by the satellite and airborne images but not by the high-resolution UAV images. For better estimation of LAI in maize, RTMs that account for leaf clumping and shading can be explored, e.g 3D radiative transfer model such as DART [83]. However, 3D RTMs are computationally demanding compared to simpler 1D models. This high computational cost can limit their use in operational settings. Additionally 3D models require detailed parameterization of canopy properties that may be uknown to the user. This level of detail can be challenging to obtain and may introduce additional sources of uncertainty.

Furthermore, the in-situ, non-destructive measurements may contribute to uncertainties in LCC retrieval. The relationship between SPAD readings and chlorophyll content is often non-linear, particularly at high chlorophyll concentrations [198]. Different species may require different mathematical models (e.g., linear, polynomial or exponential functions) for accurate calibration. The relationship between SPAD values and chlorophyll content could also change throughout a plant's growth cycle, requiring calibrations for different developmental stages. Retrieval accuracy could be improved by deriving separate calibration equations per maize type, and converting SPAD measurements to chlorophyll content in physical units. The constant overestimation of low LCC and underestimation of high LCC values by both approaches for each date may be attributed to the use of a calibration equation that does not reflect the actual relationship between SPAD values and real chlorophyll content.

We used all available spectral bands provided by the MicaSense Dual camera system for the LCC estimation. It is known that chlorophyll retrieval is sensitive in the visible and red edge regions [27]. One of the ways to increase the LCC retrieval accuracy would be to apply a spectral constraint to the model. This would entail removing the spectral bands that are not sensitive to chlorophyll content from the reflectance data.

Another topic that has not been discussed in the papers is the uncertainty estimation in PROSAIL. Uncertainty information serves as a key indicator of data quality, helping to assess the reliability and limitations of RS products. This understanding is essential for determining whether a particular dataset is suitable for a specific application. Moreover, uncertainty estimates provide valuable insights into the sources and magnitudes of errors in RS measurements. There are several sources of uncertainties in the parameter retrieval pipeline. The first is input parameter uncertainties and the errors attributed to measuring them. We

have briefly touched this in case of SPAD value conversion to LCC. The second is model uncertainties: simplifying assumptions in PROSAIL may not fully represent real-world complexity, hence the parameter estimation will not be accurate. Some inversion methods, e.g Bayesian inversion frameworks can provide inversion uncertainties and could be better alternatives for the future use.

9.3 Crop Stress Detection

We demonstrated the potential of synergistic sensor use to detect paraheliotropic leaf movement due to drought stress for the first time. Owing to their versatility, miniature size, and ease of use, UAVs are and will remain the preferred RS platform for phenotyping research. The 4th study presents the first attempt to observe paraheliotropic leaf movement using TLS and optical remote sensing approaches. We characterised leaf movement throughout the dry boreal summer months and evaluated the relationship between the canopy reflectance and the leaf movement.

Together with photosynthetic activity, variations in leaf temperature, and changes in the xanthophyll cycle, leaf movement serves as an important early stress indicator [29, 228]. Unlike leaf-level measurements of photosynthetic activity, which are often labor-intensive, possess limited spatial coverage, or lack sufficient resolution, tracking leaf movement using proximal multispectral imaging can be promising to be used in breeding applications to identify varieties better adapted to higher temperatures and lower water availability. This characteristic makes ALIA particularly compelling as one of the parameters to investigate early stress responses in various crops. A limited number of studies have explored the retrieval of ALIA using imaging spectroscopy data, making the comparison of results rather challenging. This is partly due to the complexity of estimating ALIA and its relatively subtle impact on canopy reflectance. ALIA is a challenging parameter to retrieve from spectral data alone because its effect on canopy reflectance can be confounded with other structural parameters like LAI.

The parametrization of PROSAIL significantly influences the retrieval process. While we explored both constrained and unconstrained ALIA simulations with fixed LAI, future studies should delve into the impact of other parameters, especially those related to leaf chlorophyll content and other leaf pigments. Our findings indicate that Look-Up Table (LUT)-based inversion is sufficient for ALIA retrieval. However, hybrid methods incorporating machine learning approaches could enhance retrieval accuracies, reduce the computing time of the inversion

pipeline and provide uncertainty estimates of the retrieval.

Our study focused exclusively on soybeans for leaf angle retrieval. Soybean was a convenient choice due to its paraheliotropism and its architecture, which is well-suited for reconstruction using TLS data. Soybeans typically exhibit an upright, bushy growth habit with distinct leaves and branches, making it easier to capture the overall plant structure and enhancing visibility of individual plant components. Future research should investigate the application of our method to other crops to determine if the ratio index is transferable. These crops should preferably have leaves of a detectable and discernible size by TLS. For example, it would be challenging to create a 3D model of the wheat using TLS data, due to resolution limitation, density of the crop canopy and susceptibility of cereal crops towards slight wind. Another challenge with other crops may be the lack of significant variation in leaf angle. Crops exhibiting any form of heliotropism would be of particular interest for further study.

With 4th study, we reviewed the advantage of the multiple-sensor approach in studying crop stress. The 5th study emphasized this importance and reviewed important aspects in the form of a guideline that need to be considered when planning multiple sensor campaigns. The need for such guidelines has been identified as a result of increased stress occurrence caused by climate change effects, the increased availability of optical sensors onboard UAVs, and the current lack of existing protocols on how to collect and analyze such data. The recommendations are rounded up by bad examples that scientists experienced during their research work. This collection of best practices and lessons learned can help scientists and practitioners in making informed decisions regarding sensor selection, mission planning and the challenges associated with multiple sensor data acquisition and processing to advance crop stress monitoring with UAVs. In this study the main focus has been on optical RS sensors. In addition to optical sensors that were reviewed in this guideline, UAVs can be equipped with LiDAR, multispectral LiDAR or SAR. These sensors can be used for high-resolution 3D canopy structure mapping, assessing crop moisture, simultaneous measurement of canopy structure and biochemical properties.

Our project explored UAV remote sensing in a direction that had not been previously investigated. While we made significant contributions by applying PROSAIL for UAV use, further research is needed to test its effectiveness with a variety of crops. While ML approaches have gained prominence in today's data-driven landscape, RTMs remain valuable for their grounding in physical principles. Recent advancements in explainable ML and physics-informed ML are bridging the gap between these approaches. Therefore, future UAV studies should integrate

RTMs with ML to harness their combined potential.

Acronyms

aPAR Absorbed Photosynthetically Active Radiation

AOD Aerosol Optical Depth

ALIA Average Leaf Inclination Angle

BBCH Biologische Bundesanstalt, Bundessortenamt und Chemische Industrie

BRDF Bidirectional Reflectance Factor

Cab Chlorophyll a and b

Car Leaf Carotenoid Content

CCC Canopy Chlorophyll Content

CGM Crop Growth Model

DLS Downwelling Light Sensor

DN Digital Numbers

DSM Digital Surface Model

DTM Digital Terrain Model

DWD Deutscher Wetterdienst

ELADP Ellipsoidal Leaf Angle Distribution Parameter

ELM Empirical Line Method

ESU Elementary Sampling Unit

ET Evapotranspiration

ETR Electron Transport Rate

FOV Field of View

GCP Ground Control Point

GF Green Fraction

GNSS Global Navigation Satellite System

GSD Ground Sampling Distance

HS Hyperspectral

LAI Leaf Area Index

LAD Leaf Angle Distribution

LCC Leaf Chlorophyll Content

LHS Latin Hypercube Sampling

LUT Look-up Table

LWC Leaf Water Content

MCA Multispectral Camera Array

ML Machine Learning

MS Multispectral

NDVI Normalized Difference Vegetation Index

NIR Near Infrared

NPQ Non-photochemical Quenching

OZA Observer Zenith Angle

PDA Personal Digital Assistant

PDSI Palmer Drought Severity Index

rRMSE Relative Root Mean Squared Error

RMSE Root Mean Square Error

ROI Region of Interest

RS Remote Sensing

RTK Real-Time Kinematic

RTM Radiative Transfer Model

SfM Structure-from-Motion

SIF Sun-Induced Chlorophyll Fluorescence

SWC Soil Water Content

SWIR Shortwave Infrared

SZA Sun Zenith Angle

TCP Temperature Calibration Plate

TIN Triangular Irregular Networks

TIR Thermal Infrared

TLS Terrestrial Laser Scanner

UAV Uncrewed Aerial Vehicle

VI Vegetation Index

VIS Visible

Bibliography

[1] Helge Aasen and Andreas Bolten. "Multi-temporal high-resolution imaging spectroscopy with hyperspectral 2D imagers – From theory to application". In: *Remote Sensing of Environment* 205 (Feb. 2018), pp. 374–389. ISSN: 00344257. DOI: 10.1016/j.rse.2017.10.043. URL: https://linkinghub.elsevier.com/retrieve/pii/S0034425717305072.

[2] Helge Aasen et al. "Quantitative Remote Sensing at Ultra-High Resolution with UAV Spectroscopy: A Review of Sensor Technology, Measurement Procedures, and Data Correction Workflows". In: *Remote Sensing* 10.7 (July 2018), p. 1091. ISSN: 2072-4292. DOI: 10.3390/rs10071091. URL: http://www.mdpi.com/2072-4292/10/7/1091.

[3] Asmaa Abdelbaki et al. "Comparison of Crop Trait Retrieval Strategies Using UAV-Based VNIR Hyperspectral Imaging". In: *Remote Sens.* 13.9 (2021), p. 1748.

[4] Telmo Adão et al. "Hyperspectral imaging: A review on UAV-based sensors, data processing and applications for agriculture and forestry". In: *Remote Sensing* 9.11 (Nov. 2017). ISSN: 20724292. DOI: 10.3390/RS9111110.

[5] Richard G. Allen, Masahiro Tasumi, and Ricardo Trezza. "Satellite-Based Energy Balance for Mapping Evapotranspiration with Internalized Calibration (METRIC)—Model". In: *Journal of Irrigation and Drainage Engineering* 133 (4 Aug. 2007), pp. 380–394. ISSN: 0733-9437. DOI: 10.1061/(ASCE)0733-9437(2007)133:4(380).

[6] Giulia Antonucci et al. "Evaluating biostimulants via high-throughput field phenotyping: Biophysical traits retrieval through PROSAIL inversion". In: *Smart Agricultural Technology* 3 (Feb. 2023), p. 100067. ISSN: 27723755. DOI: 10.1016/j.atech.2022.100067.

[7] Tito Arevalo-Ramirez et al. "Moisture content estimation of Pinus radiata and Eucalyptus globulus from reconstructed leaf reflectance in the SWIR region". In: *Biosystems Engineering* 193 (May 2020), pp. 187–205. ISSN: 15375110. DOI: 10.1016/j.biosystemseng.2020.03.004.

[8] Tito André Arevalo-Ramirez et al. “Single bands leaf reflectance prediction based on fuel moisture content for forestry applications”. In: *Biosystems Engineering* 202 (Feb. 2021), pp. 79–95. ISSN: 15375110. DOI: 10.1016/j.biosystemseng.2020.12.003.

[9] J. Pablo Arroyo-Mora et al. “Assessing the impact of illumination on UAV pushbroom hyperspectral imagery collected under various cloud cover conditions”. In: *Remote Sensing of Environment* 258 (June 2021), p. 112396. ISSN: 00344257. DOI: 10.1016/j.rse.2021.112396.

[10] Gregory P. Asner, Jonathan MO Scurlock, and Jeffrey A. Hicke. “Global synthesis of leaf area index observations: implications for ecological and remote sensing studies”. In: *Global Ecol. Biogeogr.* 12.3 (2003), pp. 191–205.

[11] Gregory P. Asner et al. “Ecological research needs from multiangle remote sensing data”. In: *Remote Sensing of Environment* 63.2 (1998), pp. 155–165. DOI: https://doi.org/10.1016/S0034-4257(97)00139-9.

[12] Ghassem Asrar et al. “Estimating Absorbed Photosynthetic Radiation and Leaf Area Index from Spectral Reflectance in Wheat”. In: *Agron. J.* 76.2 (1984), pp. 300–306.

[13] Clement Atzberger and Katja Berger. “Spatially constrained inversion of radiative transfer models for improved LAI mapping from future Sentinel-2 imagery”. In: *Remote Sens. Environ.* 120 (May 2012), pp. 208–218.

[14] Idan Bahat et al. “In-Season Interactions between Vine Vigor, Water Status and Wine Quality in Terrain-Based Management-Zones in a ‘Cabernet Sauvignon’ Vineyard”. In: *Remote Sensing* 13.9 (Apr. 2021), p. 1636. ISSN: 2072-4292. DOI: 10.3390/rs13091636.

[15] Brian N. Bailey and Walter F. Mahaffee. “Rapid measurement of the three-dimensional distribution of leaf orientation and the leaf angle probability density function using terrestrial LiDAR scanning”. In: *Remote Sens. Environ.* 194 (2017), pp. 63–76.

[16] Subhajit Bandopadhyay, Anshu Rastogi, and Radosław Juszczak. “Review of top-of-canopy sun-induced fluorescence (Sif) studies from ground, uav, airborne to spaceborne observations”. In: *Sensors (Switzerland)* 20.4 (Feb. 2020). ISSN: 14248220. DOI: 10.3390/S20041144.

[17] Asim Banskota et al. “An LUT-Based Inversion of DART Model to Estimate Forest LAI from Hyperspectral Data”. In: *IEEE J-STARS* 8.6 (2015), pp. 3147–3160.

[18] Nastassia Barber et al. “Estimating Fuel Moisture in Grasslands Using UAV-Mounted Infrared and Visible Light Sensors”. In: *Sensors* 21 (19 Sept. 2021), p. 6350. ISSN: 1424-8220. DOI: 10.3390/s21196350.

[19] Frederic Baret and Samuel Buis. “Estimating Canopy Characteristics from Remote Sensing Observations: Review of Methods and Associated Problems”. In: *Advances in Land Remote Sensing: System, Modeling, Inversion and Application*. Dordrecht: Springer Netherlands, 2008, pp. 173–201. ISBN: 978-1-4020-6450-0.

[20] W.G.M. Bastiaanssen et al. “A remote sensing surface energy balance algorithm for land (SEBAL). 1. Formulation”. In: *Journal of Hydrology* 212-213 (Dec. 1998), pp. 198–212. ISSN: 00221694. DOI: 10.1016/S0022-1694(98)00253-4.

[21] Bagher Bayat, Christiaan van der Tol, and Wouter Verhoef. “Integrating satellite optical and thermal infrared observations for improving daily ecosystem functioning estimations during a drought episode”. In: *Remote Sens. Environ.* 209.March (May 2018), pp. 375–394. ISSN: 00344257. DOI: 10.1016/j.rse.2018.02.027.

[22] Joaquim Bellvert et al. “Remote sensing energy balance model for the assessment of crop evapotranspiration and water status in an almond rootstock collection”. In: *Frontiers in Plant Science* 12 (2021), p. 608967.

[23] Juliane Bendig et al. “Combining UAV-based plant height from crop surface models, visible, and near infrared vegetation indices for biomass monitoring in barley”. In: *International Journal of Applied Earth Observation and Geoinformation* 39 (2015), pp. 79–87.

[24] Juliane Bendig et al. “Solar-Induced Chlorophyll Fluorescence Measured From an Unmanned Aircraft System: Sensor Etaloning and Platform Motion Correction”. In: *IEEE Transactions on Geoscience and Remote Sensing* 58.5 (May 2020). Conference Name: IEEE Transactions on Geoscience and Remote Sensing, pp. 3437–3444. ISSN: 1558-0644. DOI: 10.1109/TGRS.2019.2956194.

[25] Katja Berger et al. “Experimental assessment of the Sentinel-2 band setting for RTM-based LAI retrieval of sugar beet and maize”. In: *Can. J. Remote Sens.* 35.3 (2009), pp. 230–247.

[26] Katja Berger et al. “Evaluation of the PROSAIL model capabilities for future hyperspectral model environments: A review study”. In: *Remote Sens.* 10.1 (2018), p. 85.

[27] Katja Berger et al. “Model-Based Optimization of Spectral Sampling for the Retrieval of Crop Variables with the PROSAIL Model”. In: *Remote Sens.* 10.12 (2018). ISSN: 2072-4292.

[28] Katja Berger et al. “Retrieval of aboveground crop nitrogen content with a hybrid machine learning method”. In: *Int. J. Appl. Earth. Obs. Geoinf.* 92 (2020), p. 102174. ISSN: 0303-2434.

[29] Katja Berger et al. “Multi-sensor spectral synergies for crop stress detection and monitoring in the optical domain: A review”. In: *Remote Sensing of Environment* 280 (2022), p. 113198. ISSN: 0034-4257. DOI: https://doi.org/10.1016/j.rse.2022.113198.

[30] Michael Berger et al. “ESA’s sentinel missions in support of Earth system science”. In: *Remote sensing of environment* 120 (2012), pp. 84–90.

[31] Fausto Bernardini et al. “The ball-pivoting algorithm for surface reconstruction”. In: *IEEE transactions on visualization and computer graphics* 5.4 (1999), pp. 349–359. DOI: DOI:10.1109/2945.817351.

[32] Jose AJ Berni et al. “Thermal and narrowband multispectral remote sensing for vegetation monitoring from an unmanned aerial vehicle”. In: *IEEE Transactions on geoscience and Remote Sensing* 47.3 (2009), pp. 722–738. DOI: DOI:10.1109/TGRS.2008.2010457.

[33] Emanuele Bevacqua et al. “Guidelines for Studying Diverse Types of Compound Weather and Climate Events”. In: *Earth’s Future* 9.11 (2021). DOI: https://doi.org/10.1029/2021EF002340.

[34] Bernhard Biskup et al. “A stereo imaging system for measuring structural parameters of plant canopies”. In: *Plant, Cell & Environment* 30.10 (Oct. 2007), pp. 1299–1308. DOI: 10.1111/j.1365-3040.2007.01702.x.

[35] HR Bogena et al. “Potential of wireless sensor networks for measuring soil water content variability”. In: *Vadose Zone Journal* 9.4 (2010), pp. 1002–1013. DOI: https://doi.org/10.2136/vzj2009.0173.

[36] Kenneth J. Boote, James W. Jones, and Gerrit Hoogenboom. *Simulation of Crop Growth: CROPGRO Model*. CRC Press, Oct. 2018, pp. 651–692. DOI: 10.1201/9781482269765-18.

[37] Andreas Burkart et al. “A Method for Uncertainty Assessment of Passive Sun-Induced Chlorophyll Fluorescence Retrieval Using an Infrared Reference Light”. In: *IEEE Sensors Journal* 15.8 (Aug. 2015), pp. 4603–4611. ISSN: 1530-437X. DOI: 10.1109/JSEN.2015.2422894. URL: http://ieeexplore.ieee.org/document/7086007/.

[38] Carlos Camino et al. “Radiative transfer Vcmax estimation from hyperspectral imagery and SIF retrievals to assess photosynthetic performance in rainfed and irrigated plant phenotyping trials”. In: *Remote Sensing of Environment* 231 (Sept. 2019), p. 111186. DOI: 10.1016/j.rse.2019.05.005.

[39] Benjamin W. Campbell et al. “Identical substitutions in magnesium chelatase paralogs result in chlorophyll-deficient soybean mutants”. In: *G3: Genes, Genomes, Genetics* 5.1 (2015), pp. 123–131. DOI: DOI:10.1534/g3.114.015255.

[40] Gaylon S. Campbell and John M. Norman. “The light environment of plant canopies”. In: *An introduction to environmental biophysics*. Springer, 1998, pp. 247–278.

[41] James B. Campbell and Randolph H. Wynne. *Introduction to remote sensing*. Guilford press, 2011.

[42] Richard J. Campbell et al. “Growing Conditions Alter the Relationship Between SPAD-501 Values and Apple Leaf Chlorophyll”. In: *HortScience* 25.3 (1990), pp. 330–331.

[43] Erekle Chakhvashvili et al. “Comparison of Reflectance Calibration Workflows for a UAV-Mounted Multi-Camera Array System”. In: *2021 IEEE International Geoscience and Remote Sensing Symposium IGARSS*. IEEE. 2021, pp. 8225–8228.

[44] Erekle Chakhvashvili et al. “Retrieval of crop variables from proximal multispectral UAV image data using PROSAIL in maize canopy”. In: *Remote sensing* 14.5 (2022), p. 1247.

[45] Christine Y. Chang et al. “An Unmanned Aerial System (UAS) for concurrent measurements of solar-induced chlorophyll fluorescence and hyperspectral reflectance toward improving crop monitoring”. In: *Agricultural and Forest Meteorology* 294 (Nov. 15, 2020), p. 108145. ISSN: 0168-1923. DOI: 10.1016/j.agrformet.2020.108145. URL: https://www.sciencedirect.com/science/article/pii/S0168192320302471 (visited on 04/17/2023).

[46] Roger N. Clark et al. “Surface reflectance calibration of terrestrial imaging spectroscopy data: a tutorial using AVIRIS”. In: *Proceedings of the 10th Airborne Earth Science Workshop*. Vol. 2. Jet Propulsion Laboratory Pasadena, CA, USA. 2002.

[47] Jan G. P. W. Clevers and Lammert Kooistra. “Using Hyperspectral Remote Sensing Data for Retrieving Canopy Chlorophyll and Nitrogen Content”. In: *IEEE J-STARS* 5.2 (2012), pp. 574–583.

[48] Intergovernmental Panel on Climate Change (IPCC). "Weather and Climate Extreme Events in a Changing Climate". In: (2023), pp. 1513–1766. DOI: 10.1017/9781009157896.013.

[49] Sergio Cogliati et al. "Continuous and long-term measurements of reflectance and sun-induced chlorophyll fluorescence by using novel automated field spectroscopy systems". In: *Remote Sensing of Environment* 164 (July 2015), pp. 270–281. ISSN: 00344257. DOI: 10.1016/j.rse.2015.03.027.

[50] Ismael Colomina and Pere Molina. "Unmanned aerial systems for photogrammetry and remote sensing: A review". In: *ISPRS Journal of photogrammetry and remote sensing* 92 (2014), pp. 79–97.

[51] COST Action SENSECO CA17134. *Optical synergies for spatiotemporal SENsing of Scalable ECOphysiological traits (SENSECO), European Cooperation in Science and Technology (COST) Action.* Available online: https://www.senseco.eu/. (accessed on 21 July 2023). (Visited on 07/21/2023).

[52] Arthur P. Cracknell. *The development of remote sensing in the last 40 years.* 2018.

[53] Holly Croft et al. "Leaf chlorophyll content as a proxy for leaf photosynthetic capacity". In: *Glob. Change. Biol.* 23.9 (2017), pp. 3513–3524.

[54] Andrew Cunliffe and Karen Anderson. "Measuring above-ground biomass with drone photogrammetry: data collection protocol". In: (2019).

[55] Alexander Damm et al. "Response times of remote sensing measured sun-induced chlorophyll fluorescence, surface temperature and vegetation indices to evolving soil water limitation in a crop canopy". In: *Remote Sensing of Environment* 273 (May 2022), p. 112957. DOI: 10.1016/j.rse.2022.112957.

[56] Martin Danner et al. "Retrieval of Biophysical Crop Variables from Multi-Angular Canopy Spectroscopy". In: *Remote Sens.* 9.7 (2017). ISSN: 2072-4292.

[57] Roshanak Darvishzadeh et al. "Inversion of a radiative transfer model for estimating vegetation LAI and chlorophyll in a heterogeneous grassland". In: *Remote Sens. Environ.* 112.5 (2008), pp. 2592–2604. ISSN: 0034-4257.

[58] Jesús Delegido et al. "Remote Estimation of Crop Chlorophyll Content by Means of High-Spectral-Resolution Reflectance Techniques". In: *Agron. J.* 103 (Nov. 2011), pp. 1834–1842.

[59] Deutscher Wetterdienst. *Climate diagram of Cologne/Bonn airport*. [Internet]. Deutscher Wetterdienst. URL: https://www.dwd.de/DWD/klima/beratung/ak/ak_105130_di.pdf. 2023.

[60] A. Devot et al. "The impact of extreme climate events on agriculture production in the EU". In: *Research for AGRI Committee* (2023).

[61] Darren T. Drewry, Praveen Kumar, and Stephen P. Long. "Simultaneous improvement in productivity, water use, and albedo through crop structural modification". In: *Global change biology* 20.6 (2014), pp. 1955–1967. DOI: https://doi.org/10.1111/gcb.12567.

[62] Liping Du et al. "Estimating leaf area index of maize using UAV-based digital imagery and machine learning methods". In: *Scientific Reports* 12.1 (2022), p. 15937. DOI: https://doi.org/10.1038/s41598-022-20299-0.

[63] Si-Bo Duan et al. "Inversion of the PROSAIL model to estimate leaf area index of maize, potato, and sunflower fields from unmanned aerial vehicle hyperspectral data". In: *Int. J. Appl. Earth. Obs. Geoinf.* 26 (2014), pp. 12–20. ISSN: 0303-2434.

[64] Debsunder Dutta et al. "Optimal inverse estimation of ecosystem parameters from observations of carbon and energy fluxes". In: *Biogeosciences* 16.1 (Jan. 2019), pp. 77–103. ISSN: 1726-4189. DOI: 10.5194/bg-16-77-2019.

[65] James Ehleringer and Irwin Forseth. "Solar Tracking by Plants". In: *Science* 210.4474 (Dec. 1980), pp. 1094–1098. DOI: 10.1126/science.210.4474.1094.

[66] Elmer Kanjo Ekinzog et al. "Revisiting crop water stress index based on potato field experiments in Northern Germany". In: *Agricultural Water Management* 269 (July 2022), p. 107664. ISSN: 03783774. DOI: 10.1016/j.agwat.2022.107664. URL: https://linkinghub.elsevier.com/retrieve/pii/S0378377422002116.

[67] R. Escadafal, A. Belghith, and H. Ben Moussa. "Indices spectraux pour la teledetection de la degradation des milieux naturels en tunisie aride". In: *6. Symp. Int. Mesures Physiques et Signatures en Teledetection, ISPRS-CNES*. Val d'Isère, France, 1994, pp. 253–259.

[68] Roghieh Eskandari et al. "Meta-analysis of unmanned aerial vehicle (UAV) imagery for agro-environmental monitoring using machine learning and statistical models". In: *Remote Sensing* 12.21 (2020), p. 3511.

[69] Maria España et al. "A dynamic model of maize 3D architecture: application to the parameterisation of the clumpiness of the canopy". In: *Agronomie* 18.10 (1998), pp. 609–626.

[70] European Commission. *Standardized protocol for UAV data acquisition*. Last accessed on 01.09.2023. URL: https://ec.europa.eu/research/participants/documents/downloadPublic?documentIds=080166e5bd3dfa4f&appId=PPGMS.

[71] Shah Fahad et al. "Crop Production under Drought and Heat Stress: Plant Responses and Management Options". In: *Frontiers in Plant Science* 8 (2017). ISSN: 1664-462X. DOI: 10.3389/fpls.2017.01147. URL: https://www.frontiersin.org/articles/10.3389/fpls.2017.01147.

[72] FAO. "The Future of Food and Agriculture—Trends and Challenges. Rome". In: (2017).

[73] FAO. "AOSTAT: Production: Crops and livestock products". In: (2022).

[74] Dominic Fawcett and Karen Anderson. "Investigating impacts of calibration methodology and irradiance variations on lightweight drone-based sensor derived surface reflectance products". In: *Remote Sensing for Agriculture, Ecosystems, and Hydrology XXI*. Vol. 11149. SPIE. 2019, pp. 101–114.

[75] Jean-Baptieste Féret et al. "PROSPECT-D: towards modeling leaf optical properties through a complete lifecycle". In: *Remote Sens. Environ.* 193 (2017), pp. 204–215.

[76] Jean-Baptiste Féret et al. "PROSPECT-PRO for estimating content of nitrogen-containing leaf proteins and other carbon-based constituents". In: *Remote Sensing of Environment* 252 (2021), p. 112173.

[77] Jose A. Fernandez-Gallego et al. "Automatic wheat ear counting using machine learning based on RGB UAV imagery". In: *The Plant Journal* 103.4 (2020), pp. 1603–1613.

[78] I. N. Forseth and J. R. Ehleringer. "Ecophysiology of two solar tracking desert winter annuals". In: *Oecologia* 54.1 (1982), pp. 41–49. DOI: 10.1007/bf00541105.

[79] Cyrus Foster, Henry Hallam, and James Mason. "Orbit determination and differential-drag control of Planet Labs CubeSat constellations". In: *arXiv preprint arXiv:1509.03270* (2015).

[80] Bo-cai Gao. "NDWI—A normalized difference water index for remote sensing of vegetation liquid water from space". In: *Remote Sensing of Environment* 58.3 (Dec. 1996), pp. 257–266. ISSN: 00344257. DOI: 10.1016/S0034-4257(96)00067-3.

[81] Jean-Philippe Gastellu-Etchegorry et al. *Modeling Radiative Transfer in Heterogeneous 3-D Vegetation Canopies*. 1995, pp. 131–156.

[82] Jean-Philippe Gastellu-Etchegorry et al. “Discrete Anisotropic Radiative Transfer (DART 5) for Modeling Airborne and Satellite Spectroradiometer and LIDAR Acquisitions of Natural and Urban Landscapes”. In: *Remote Sensing* 7.2 (Feb. 2015), pp. 1667–1701. DOI: 10.3390/rs70201667.

[83] Jean-Philippe Gastellu-Etchegorry et al. “DART: Recent Advances in Remote Sensing Data Modeling With Atmosphere, Polarization, and Chlorophyll Fluorescence”. In: *IEEE J. STARS* 10.6 (2017), pp. 2640–2649.

[84] Jakob Geipel, Johanna Link, and Wilhelm Claupein. “Combined spectral and spatial modeling of corn yield based on aerial images and crop surface models acquired with an unmanned aircraft system”. In: *Remote Sens.* 6.11 (2014), pp. 10335–10355.

[85] L Genesio et al. “A chlorophyll-deficient, highly reflective soybean mutant: radiative forcing and yield gaps”. In: *Environmental Research Letters* 15.7 (2020), p. 074014. DOI: 10.1088/1748-9326/ab865e.

[86] Max Gerhards et al. “Challenges and Future Perspectives of Multi-Hyperspectral Thermal Infrared Remote Sensing for Crop Water-Stress Detection: A Review”. In: *Remote Sensing* 11.10 (May 2019), p. 1240. DOI: 10.3390/rs11101240.

[87] Anatoly A. Gitelson. “Wide Dynamic Range Vegetation Index for Remote Quantification of Biophysical Characteristics of Vegetation”. In: *J. Plant Physiol.* 161.2 (2004), pp. 165–173. ISSN: 0176-1617.

[88] Anatoly A. Gitelson, Yuri Gritz †, and Mark N. Merzlyak. “Relationships between leaf chlorophyll content and spectral reflectance and algorithms for non-destructive chlorophyll assessment in higher plant leaves”. In: *J. Plant Physiol.* 160.3 (2003), pp. 271–282. ISSN: 0176-1617. URL: https://www.sciencedirect.com/science/article/pii/S0176161704704034.

[89] Anatoly A. Gitelson, Galina P. Keydan, and Mark N. Merzlyak. “Three-band model for noninvasive estimation of chlorophyll, carotenoids, and anthocyanin contents in higher plant leaves”. In: *Geophysical Research Letters* 33.11 (June 2006). DOI: 10.1029/2006gl026457.

[90] Anatoly A. Gitelson and Mark N. Merzlyak. “Remote sensing of chlorophyll concentration in higher plant leaves”. In: *Advances in Space Research* 22.5 (Jan. 1998), pp. 689–692. DOI: 10.1016/s0273-1177(97)01133-2.

[91] Anatoly A. Gitelson et al. “Remote estimation of canopy chlorophyll content in crops”. In: *Geophys. Res. Lett.* 32.8 (2005).

[92] Michael Gräf et al. “Water-Stressed Plants Do Not Cool: Leaf Surface Temperature of Living Wall Plants under Drought Stress”. In: *Sustainability 2021, Vol. 13, Page 3910* 13 (7 Apr. 2021), p. 3910. ISSN: 2071-1050. DOI: 10.3390/SU13073910. URL: https://www.mdpi.com/2071-1050/13/7/3910/htm%20https://www.mdpi.com/2071-1050/13/7/3910.

[93] Caili Guo et al. “Integrating remote sensing information with crop model to monitor wheat growth and yield based on simulation zone partitioning”. In: *Precision agriculture* 19 (2018), pp. 55–78.

[94] Driss Haboudane et al. “Integrated narrow-band vegetation indices for prediction of crop chlorophyll content for application to precision agriculture”. In: *Remote Sens. Environ.* 81.2 (2002), pp. 416–426. ISSN: 0034-4257.

[95] Driss Haboudane et al. “Hyperspectral vegetation indices and novel algorithms for predicting green LAI of crop canopies: Modeling and validation in the context of precision agriculture”. In: *Remote Sens. Environ.* 90.3 (2004), pp. 337–352. ISSN: 0034-4257.

[96] Teemu Hakala et al. “Direct Reflectance Measurements from Drones: Sensor Absolute Radiometric Calibration and System Tests for Forest Reflectance Characterization”. In: *Sensors* 18.5 (May 2018), p. 1417. DOI: 10.3390/s18051417.

[97] Michael A. Hardisky et al. “Remote sensing of biomass and annual net aerial primary productivity of a salt marsh”. In: *Remote Sensing of Environment* 16.2 (Oct. 1984), pp. 91–106. ISSN: 00344257. DOI: 10.1016/0034-4257(84)90055-5.

[98] Wolfgang Haupt and Robert W. Scheurlein. “Chloroplast movement”. In: *Plant, Cell and Environment* 13.7 (Sept. 1990), pp. 595–614. DOI: 10.1111/j.1365-3040.1990.tb01078.x.

[99] Sascha Heinemann et al. “Land surface temperature retrieval for agricultural areas using a novel UAV platform equipped with a thermal infrared and multispectral sensor”. In: *Remote sensing* 12.7 (2020), p. 1075.

[100] Helene Hoffmann et al. “Crop water stress maps for an entire growing season from visible and thermal UAV imagery”. In: *Biogeosciences* 13.24 (Dec. 2016), pp. 6545–6563. ISSN: 1726-4189. DOI: 10.5194/bg-13-6545-2016. URL: https://bg.copernicus.org/articles/13/6545/2016/.

[101] Brent Holben and Chris Justice. “An examination of spectral band ratioing to reduce the topographic effect on remotely sensed data”. In: *International journal of remote sensing* 2.2 (1981), pp. 115–133. DOI: https://doi.org/10.1080/01431168108948349.

[102] Fenner H. Holman et al. “High Throughput Field Phenotyping of Wheat Plant Height and Growth Rate in Field Plot Trials Using UAV Based Remote Sensing”. In: *Remote Sens.* 8.12 (2016). ISSN: 2072-4292.

[103] Dean P. Holzworth et al. “APSIM – Evolution towards a new generation of agricultural systems simulation”. In: *Environmental Modelling & Software* 62 (Dec. 2014), pp. 327–350. ISSN: 13648152. DOI: 10.1016/j.envsoft.2014.07.009.

[104] Rasmus Houborg et al. “Joint leaf chlorophyll content and leaf area index retrieval from Landsat data using a regularized model inversion system (REGFLEC)”. In: *Remote Sens. Environ.* 159 (2015), pp. 203–221. ISSN: 0034-4257.

[105] Stuart Mark Howden et al. “Adapting agriculture to climate change”. In: *Proceedings of the national academy of sciences* 104.50 (2007), pp. 19691–19696.

[106] Ryan Hruska et al. “Radiometric and geometric analysis of hyperspectral imagery acquired from an unmanned aerial vehicle”. In: *Remote Sensing* 4.9 (Sept. 2012), pp. 2736–2752. ISSN: 20724292. DOI: 10.3390/RS4092736.

[107] Jianxi Huang et al. “Assimilation of remote sensing into crop growth models: Current status and perspectives”. In: *Agricultural and forest meteorology* 276 (2019), p. 107609.

[108] Jianxi Huang et al. “Evaluation of regional estimates of winter wheat yield by assimilating three remotely sensed reflectance datasets into the coupled WOFOST–PROSAIL model”. In: *European Journal of Agronomy* 102 (Jan. 2019), pp. 1–13. ISSN: 11610301. DOI: 10.1016/j.eja.2018.10.008.

[109] Andreas Hueni et al. “Field and Airborne Spectroscopy Cross Validation—Some Considerations”. In: *IEEE Journal of Selected Topics in Applied Earth Observations and Remote Sensing* 10.3 (Mar. 2017), pp. 1117–1135. ISSN: 1939-1404. DOI: 10.1109/JSTARS.2016.2593984.

[110] Nikolai Ivanov et al. “Computer stereo plotting for 3-D reconstruction of a maize canopy”. In: *Agricultural and Forest Meteorology* 75.1-3 (June 1995), pp. 85–102. DOI: 10.1016/0168-1923(94)02204-w.

[111] Ray D. Jackson et al. “Canopy temperature as a crop water stress indicator”. In: *Water resources research* 17.4 (1981), pp. 1133–1138.

[112] Stéphane Jacquemoud. “Inversion of the PROSPECT+ SAIL canopy reflectance model from AVIRIS equivalent spectra: theoretical study”. In: *Remote sensing of environment* 44.2-3 (1993), pp. 281–292. DOI: https://doi.org/10.1016/0034-4257(93)90022-P.

[113] Stéphane Jacquemoud and Frédéric Baret. "PROSPECT: A model of leaf optical properties spectra". In: *Remote sensing of environment* 34.2 (1990), pp. 75–91. DOI: https://doi.org/10.1016/0034-4257(90)90100-Z.

[114] Stéphane Jacquemoud et al. "Comparison of Four Radiative Transfer Models to Simulate Plant Canopies Reflectance: Direct and Inverse Mode". In: *Remote Sens. Environ.* 74.3 (2000), pp. 471–481. ISSN: 0034-4257.

[115] Stéphane Jacquemoud et al. "PROSPECT+SAIL models: A review of use for vegetation characterization". In: *Remote Sens. Environ.* 113 (2009), S56–S66. ISSN: 0034-4257.

[116] Růžena Janoutová et al. "Detailed reconstruction of trees from terrestrial laser scans for remote sensing and radiative transfer modelling applications". In: *isP* 3.2 (Aug. 2021).

[117] Sylvain Jay et al. "Exploiting the centimeter resolution of UAV multispectral imagery to improve remote-sensing estimates of canopy structure and biochemistry in sugar beet crops". In: *Remote Sens. Environ.* 231 (2019), p. 110898. ISSN: 0034-4257.

[118] Alexander Jenal et al. "Development of a VNIR/SWIR Multispectral Imaging System for Vegetation Monitoring with Unmanned Aerial Vehicles". In: *Sensors* 19.24 (Dec. 2019), p. 5507. ISSN: 1424-8220. DOI: 10.3390/s19245507.

[119] Alexander Jenal et al. "Investigating the Potential of a Newly Developed UAV-Mounted VNIR/SWIR Imaging System for Monitoring Crop Traits—A Case Study for Winter Wheat". In: *Remote Sensing* 13.9 (Apr. 2021), p. 1697. ISSN: 2072-4292. DOI: 10.3390/rs13091697. URL: https://www.mdpi.com/2072-4292/13/9/1697.

[120] Xiuliang Jin et al. "A review of data assimilation of remote sensing and crop models". In: *European Journal of Agronomy* 92 (2018), pp. 141–152.

[121] James.W Jones et al. "The DSSAT cropping system model". In: *European Journal of Agronomy* 18 (3-4 Jan. 2003), pp. 235–265. ISSN: 11610301. DOI: 10.1016/S1161-0301(02)00107-7.

[122] Zacharias Kandylakis et al. "Water Stress Estimation in Vineyards from Aerial SWIR and Multispectral UAV Data". In: *Remote Sensing* 12.15 (Aug. 2020), p. 2499. DOI: 10.3390/rs12152499.

[123] Martin Kanning et al. "High-resolution UAV-based hyperspectral imagery for LAI and chlorophyll estimations from wheat for yield prediction". In: *Remote Sensing* 10.12 (2018), p. 2000. DOI: https://doi.org/10.3390/rs10122000.

[124] Wen-Yuan Kao and I.N Forseth. "Responses of gas exchange and phototropic leaf orientation in soybean to soil water availability, leaf water potential, air temperature, and photosynthetic photon flux". In: *Environmental and Experimental Botany* 32.2 (1992), pp. 153–161. DOI: https://doi.org/10.1016/0098-8472(92)90040-9.

[125] Gregoriy Kaplan and Offer Rozenstein. "Spaceborne Estimation of Leaf Area Index in Cotton, Tomato, and Wheat Using Sentinel-2". In: *Land* 10.5 (May 2021), p. 505. ISSN: 2073-445X. DOI: 10.3390/land10050505. URL: https://www.mdpi.com/2073-445X/10/5/505.

[126] Teja Kattenborn et al. "Linking plant strategies and plant traits derived by radiative transfer modelling". In: *J. Veg. Sci.* 28.4 (2017), pp. 717–727.

[127] Julia Kelly et al. "Challenges and best practices for deriving temperature data from an uncalibrated UAV thermal infrared camera". In: *Remote Sensing* 11.5 (Mar. 2019). ISSN: 20724292. DOI: 10.3390/RS11050567.

[128] Benjamin Koetz et al. "Use of coupled canopy structure dynamic and radiative transfer models to estimate biophysical canopy characteristics". In: *Remote Sens. Environ.* 95.1 (2005), pp. 115–124. ISSN: 0034-4257. URL: https://www.sciencedirect.com/science/article/pii/S0034425704003736.

[129] Frank J. Kriegler. "Preprocessing transformations and their effects on multspectral recognition". In: *Proceedings of the Sixth International Symposium on Remote Sesning of Environment*. 1969, pp. 97–131.

[130] Angela Kross et al. "Assessment of RapidEye vegetation indices for estimation of leaf area index and biomass in corn and soybean crops". In: *Int. J. Appl. Earth. Obs. Geoinf.* 34 (2015), pp. 235–248. ISSN: 0303-2434.

[131] E. F. Lambin and D. Ehrlich. "The surface temperature-vegetation index space for land cover and land-cover change analysis". In: *International Journal of Remote Sensing* 17.3 (1996), pp. 463–487.

[132] Qinan Lin et al. "Detection of Pine Shoot Beetle (PSB) Stress on Pine Forests at Individual Tree Level using UAV-Based Hyperspectral Imagery and Lidar". In: *Remote Sensing* 11 (21 Oct. 2019), p. 2540. ISSN: 2072-4292. DOI: 10.3390/rs11212540.

[133] Shulin Liu et al. "Toward a "green revolution" for soybean". In: *Molecular plant* 13.5 (2020), pp. 688–697. DOI: https://doi.org/10.1016/j.molp.2020.03.002.

[134] Arko Lucieer et al. “HyperUAS-Imaging Spectroscopy from a Multirotor Unmanned Aircraft System”. In: *Journal of Field Robotics* 31.4 (July 2014), pp. 571–590. ISSN: 15564959. DOI: 10.1002/rob.21508. URL: https://onlinelibrary.wiley.com/doi/10.1002/rob.21508.

[135] Arko Lucieer et al. “HyperUAS—Imaging spectroscopy from a multirotor unmanned aircraft system”. In: *Journal of Field Robotics* 31.4 (2014), pp. 571–590.

[136] Mervyn M. Ludlow and Olle Björkman. “Paraheliotropic leaf movement in Siratro as a protective mechanism against drought-induced damage to primary photosynthetic reactions: damage by excessive light and heat”. In: *Planta* 161.6 (1984), pp. 505–518. DOI: 10.1007/bf00407082.

[137] Miriam Machwitz et al. “Enhanced biomass prediction by assimilating satellite data into a crop growth model”. In: *Environmental Modelling & Software* 62 (Dec. 2014), pp. 437–453. ISSN: 13648152. DOI: 10.1016/j.envsoft.2014.08.010.

[138] Wouter H. Maes, Alfredo R. Huete, and Kathy Steppe. “Optimizing the processing of UAV-based thermal imagery”. In: *Remote Sensing* 9.5 (2017), p. 476.

[139] Zbyněk Malenovskỳ et al. “Variability and uncertainty challenges in scaling imaging spectroscopy retrievals and validations from leaves up to vegetation canopies”. In: *Surv. Geophys.* 40.3 (2019), pp. 631–656.

[140] Zbyněk Malenovskỳ et al. “Discrete anisotropic radiative transfer modelling of solar-induced chlorophyll fluorescence: Structural impacts in geometrically explicit vegetation canopies”. In: *Remote sensing of environment* 263 (2021), p. 112564.

[141] John Markwell, John C. Osterman, and Jennifer L. Mitchell. “Calibration of the Minolta SPAD-502 leaf chlorophyll meter”. In: *Photosynthesis research* 46.3 (1995), pp. 467–472.

[142] Ali Masjedi et al. “Sorghum Biomass Prediction Using Uav-Based Remote Sensing Data and Crop Model Simulation”. In: IEEE, July 2018, pp. 7719–7722. ISBN: 978-1-5386-7150-4. DOI: 10.1109/IGARSS.2018.8519034.

[143] Filipe Inácio Matias, Maria V. Caraza-Harter, and Jeffrey B. Endelman. “FIELDimageR: An R package to analyze orthomosaic images from agricultural field trials”. In: *TTPJ* 3.1 (2020), e20005.

[144] Gaetano Messina and Giuseppe Modica. “Applications of UAV thermal imagery in precision agriculture: State of the art and future research outlook”. In: *Remote Sensing* 12.9 (May 2020). ISSN: 20724292. DOI: 10.3390/RS12091491.

[145] Wayne S. Meyer and Sue Walker. "Leaflet Orientation in Water-stressed Soybeans 1". In: *Agronomy Journal* 73.6 (1981), pp. 1071–1074. DOI: https://doi.org/10.2134/agronj1981.00021962007300060039x.

[146] *MicaSense RedEdge and Altum image processing tutorials, https://delta-t.co.uk/wp-content/uploads/2017/02/SSI-UM_v3.3.pdf, Accessed: 2021-10-15.*

[147] Kimball Milton and Julian Schwinger. *Classical electrodynamics*. CRC Press, 2024.

[148] Thomas Miraglio et al. "Monitoring LAI, Chlorophylls, and Carotenoids Content of a Woodland Savanna Using Hyperspectral Imagery and 3D Radiative Transfer Modeling". In: *Remote Sens.* 12.1 (2020). ISSN: 2072-4292.

[149] Gina H. Mohammed et al. "Remote sensing of solar-induced chlorophyll fluorescence (SIF) in vegetation: 50 years of progress". In: *Remote Sensing of Environment* 231 (Sept. 2019), p. 111177. DOI: 10.1016/j.rse.2019.04.030.

[150] Ali Mokhtari et al. "Actual Evapotranspiration from UAV Images: A Multi-Sensor Data Fusion Approach". In: *Remote Sensing* 13.12 (June 2021), p. 2315. ISSN: 2072-4292. DOI: 10.3390/rs13122315.

[151] M.S. Moran et al. "Estimating crop water deficit using the relation between surface-air temperature and spectral vegetation index". In: *Remote Sensing of Environment* 49.3 (Sept. 1994), pp. 246–263. ISSN: 00344257. DOI: 10.1016/0034-4257(94)90020-5. URL: https://linkinghub.elsevier.com/retrieve/pii/0034425794900205.

[152] Patricia Müller, Xiao-Ping Li, and Krishna K. Niyogi. "Non-Photochemical Quenching. A Response to Excess Light Energy". In: *Plant Physiology* 125.4 (Apr. 2001), pp. 1558–1566. DOI: 10.1104/pp.125.4.1558.

[153] Mark Müller-Linow et al. "The leaf angle distribution of natural plant populations: assessing the canopy with a novel software tool". In: *Plant methods* 11 (2015), pp. 1–16. DOI: https://doi.org/10.1186/s13007-015-0052-z.

[154] E. H. Murchie and P. Horton. "Acclimation of photosynthesis to irradiance and spectral quality in British plant species: chlorophyll content, photosynthetic capacity and habitat preference". In: *Plant, Cell and Environment* 20.4 (Apr. 1997), pp. 438–448. DOI: 10.1046/j.1365-3040.1997.d01-95.x.

[155] Héctor Nieto et al. “Evaluation of TSEB turbulent fluxes using different methods for the retrieval of soil and canopy component temperatures from UAV thermal and multispectral imagery”. In: *Irrigation Science* 37.3 (Sept. 2019), pp. 389–406. DOI: 10.1007/s00271-018-0585-9.

[156] Erik T. Nilsen and Irwin N. Forseth. “The role of leaf movements for optimizing photosynthesis in relation to environmental variation”. In: *The leaf: a platform for performing photosynthesis* (2018), pp. 401–423. DOI: https://doi.org/10.1007/978-3-319-93594-2.

[157] John M. Norman, W.P. Kustas, and K.S. Humes. “Source approach for estimating soil and vegetation energy fluxes in observations of directional radiometric surface temperature”. In: *Agricultural and Forest Meteorology* 77 (3-4 Dec. 1995), pp. 263–293. ISSN: 01681923. DOI: 10.1016/0168-1923(95)02265-Y.

[158] Albert Olioso. “Simulating the relationship between thermal emissivity and the normalized difference vegetation index”. In: *International Journal of Remote Sensing* 16.16 (1995), pp. 3211–3216. ISSN: 13665901. DOI: 10.1080/01431169508954625.

[159] Per-Ola Olsson et al. “Radiometric correction of multispectral uas images: Evaluating the accuracy of the parrot sequoia camera and sunshine sensor”. In: *Remote Sensing* 13.4 (2021), p. 577.

[160] Derrick M. Oosterhuis, Sue Walker, and Judy Eastham. “Soybean Leaflet Movements as an Indicator of Crop Water Stress 1”. In: *Crop science* 25.6 (1985), pp. 1101–1106. DOI: https://doi.org/10.2135/cropsci1985.0011183X002500060048x.

[161] Javier Pacheco-Labrador et al. “senSCOPE: Modeling mixed canopies combining green and brown senesced leaves. Evaluation in a Mediterranean Grassland”. In: *Remote Sensing of Environment* 257 (May 2021), p. 112352. DOI: 10.1016/j.rse.2021.112352.

[162] Cinzia Panigada et al. “Fluorescence, PRI and canopy temperature for water stress detection in cereal crops”. In: *International Journal of Applied Earth Observation and Geoinformation* 30 (Aug. 2014), pp. 167–178. DOI: 10.1016/j.jag.2014.02.002.

[163] Claudio Pastenes. “Leaf movements and photoinhibition in relation to water stress in field-grown beans”. In: *Journal of Experimental Botany* 56.411 (Nov. 2004), pp. 425–433. DOI: 10.1093/jxb/eri061.

[164] Aurelie M. Poncet et al. “Multispectral UAS data accuracy for different radiometric calibration methods”. In: *Remote Sensing* 11.16 (2019). ISSN: 20724292. DOI: 10.3390/RS11161917.

[165] Egor Prikaziuk and Christiaan Van der Tol. "Global sensitivity analysis of the SCOPE model in Sentinel-3 Bands: Thermal domain focus". In: *Remote Sensing* 11.20 (Nov. 2019). ISSN: 20724292. DOI: 10.3390/rs11202424.

[166] Egor Prikaziuk et al. "Simulation of ecosystem fluxes with the SCOPE model: Sensitivity to parametrization and evaluation with flux tower observations". In: *Remote Sensing of Environment* 284 (Jan. 2023), p. 113324. ISSN: 00344257. DOI: 10.1016/j.rse.2022.113324.

[167] Sabrina Raddi et al. "Monitoring drought response and chlorophyll content in Quercus by consumer-grade, near-infrared (NIR) camera: a comparison with reflectance spectroscopy". In: *New Forests* 53 (2 Mar. 2022), pp. 241–265. ISSN: 15735095. DOI: 10.1007/S11056-021-09848-Z/METRICS. URL: https://link.springer.com/article/10.1007/s11056-021-09848-z.

[168] Uwe Rascher et al. "FLEXSense: Technical Assistance for Airborne Measurement during the FLEX Sentinel Tandem Experiment". In: (Mar. 24, 2022).

[169] *RedEdge camera radiometric calibration model , https://support.micasense.com/hc/en-us/articles/115000351194-RedEdge-Camera-Radiometric-Calibration-Model, Accessed: 2021-10-15.*

[170] R. Reed and R. L. Travis. "Paraheliotropic Leaf Movements in Mature Alfalfa Canopies". In: *Crop Science* 27.2 (Mar. 1987), pp. 301–304. DOI: 10.2135/cropsci1987.0011183x002700020036x.

[171] Andrew D. Richardson, Shane P. Duigan, and Graeme P. Berlyn. "An evaluation of noninvasive methods to estimate foliar chlorophyll content". In: *New Phytol.* 153.1 (2002), pp. 185–194.

[172] Peter P.J. Roosjen et al. "Improved estimation of leaf area index and leaf chlorophyll content of a potato crop using multi-angle spectral data – potential of unmanned aerial vehicle imagery". In: *Int. J. Appl. Earth. Obs. Geoinf.* 66 (2018), pp. 14–26. ISSN: 0303-2434.

[173] Luis M. Rosa, Lucia R. Dillenburg, and Irwin N. Forseth. "Responses of soybean leaf angle, photosynthesis and stomatal conductance to leaf and soil water potential". In: *Annals of Botany* 67.1 (1991), pp. 51–58. DOI: https://doi.org/10.1093/oxfordjournals.aob.a088099.

[174] John Wilson Rouse et al. "Monitoring vegetation systems in the Great Plains with ERTS". In: *NASA Spec. Publ* 351.1 (1974), p. 309.

[175] David P. Roy et al. “A general method to normalize Landsat reflectance data to nadir BRDF adjusted reflectance”. In: *Remote Sensing of Environment* 176 (2016), pp. 255–271. ISSN: 0034-4257. DOI: https://doi.org/10.1016/j.rse.2016.01.023. URL: https://www.sciencedirect.com/science/article/pii/S0034425716300220.

[176] Jerome Sacks et al. “Design and analysis of computer experiments”. In: *Stat. Sci.* 4.4 (1989), pp. 409–423.

[177] Karolina Sakowska et al. “Leaf and canopy photosynthesis of a chlorophyll deficient soybean mutant”. In: *Plant, cell & environment* 41.6 (2018), pp. 1427–1437. DOI: https://doi.org/10.1111/pce.13180.

[178] Sindhuja Sankaran et al. “Low-altitude, high-resolution aerial imaging systems for row and field crop phenotyping: A review”. In: *Eur. J. Agron.* 70 (2015), pp. 112–123. ISSN: 1161-0301.

[179] Gretchen F. Sassenrath-Cole. “Dependence of canopy light distribution on leaf and canopy structure for two cotton (Gossypium) species”. In: *Agricultural and Forest Meteorology* 77.1-2 (1995), pp. 55–72. DOI: https://doi.org/10.1016/0168-1923(95)02238-S.

[180] D Schläpfer et al. “DROACOR®-THERMAL: Automated Temperature Emissivity Retrieval for Drone Based Hyperspectral Imaging Data”. In: *The International Archives of the Photogrammetry, Remote Sensing and Spatial Information Sciences* 43 (2022), pp. 429–434.

[181] Martin Schlerf and Clement Atzberger. “Inversion of a forest reflectance model to estimate structural canopy variables from hyperspectral remote sensing data”. In: *Remote Sensing of Environment* 100 (3 Feb. 2006), pp. 281–294. ISSN: 00344257. DOI: 10.1016/j.rse.2005.10.006.

[182] Bastian Siegmann and Thomas Jarmer. “Comparison of different regression models and validation techniques for the assessment of wheat leaf area index from hyperspectral data”. In: *Int. J. Remote Sens.* 36.18 (2015), pp. 4519–4534.

[183] Bastian Siegmann et al. “The high-performance airborne imaging spectrometer HyPlant—From raw images to top-of-canopy reflectance and fluorescence products: Introduction of an automatized processing chain”. In: *Remote sensing* 11.23 (2019), p. 2760. DOI: https://doi.org/10.3390/rs11232760.

[184] Bastian Siegmann et al. “Downscaling of far-red solar-induced chlorophyll fluorescence of different crops from canopy to leaf level using a diurnal data set acquired by the airborne imaging spectrometer HyPlant”. In: *Remote Sensing of Environment* 264 (Oct. 1, 2021), p. 112609. ISSN: 0034-4257. DOI: 10.1016/j.rse.2021.112609. URL: https://www.sciencedirect.com/science/article/pii/S0034425721003291 (visited on 04/14/2023).

[185] Prachi Singh et al. “High resolution retrieval of leaf chlorophyll content over Himalayan pine forest using Visible/IR sensors mounted on UAV and radiative transfer model”. In: *Ecological Informatics* 75 (July 2023), p. 102099. ISSN: 15749541. DOI: 10.1016/j.ecoinf.2023.102099.

[186] Geoffrey M. Smith and Edward J. Milton. “The use of the empirical line method to calibrate remotely sensed data to reflectance”. In: *Int. J. Remote Sens.* 20.13 (1999), pp. 2653–2662.

[187] Conghe Song et al. “Classification and Change Detection Using Landsat TM Data”. In: *Remote Sensing of Environment* 75.2 (Feb. 2001), pp. 230–244. ISSN: 00344257. DOI: 10.1016/S0034-4257(00)00169-3. URL: https://linkinghub.elsevier.com/retrieve/pii/S0034425700001693.

[188] P. Steduto et al. “AquaCrop the FAO crop model to predict yield response to water. I Concepts. Special issue on “Yield Response to Water: Examination of the Role of Crop Models in Predicting Water Use Efficiency””. In: *Agron J* 101 (2009), pp. 426–437.

[189] Wei Su et al. “Phenotyping of Corn Plants Using Unmanned Aerial Vehicle (UAV) Images”. In: *Remote Sens.* 11.17 (2019). ISSN: 2072-4292.

[190] Zhongbo Su. “The Surface Energy Balance System (SEBS) for estimation of turbulent heat fluxes”. In: *Hydrology and Earth System Sciences* 6 (1 Feb. 2002), pp. 85–100. ISSN: 1607-7938. DOI: 10.5194/hess-6-85-2002.

[191] Bo Sun et al. “Retrieval of rapeseed leaf area index using the PROSAIL model with canopy coverage derived from UAV images as a correction parameter”. In: *Int. J. Appl. Earth. Obs. Geoinf.* 102 (2021), p. 102373. ISSN: 0303-2434.

[192] TERN. *Field Survey Protocols*. Terrestrial Ecosystem Research Network (TERN). 2023. URL: %7Bhttps://www.tern.org.au/field-survey-protocols/%7D.

[193] David Tilman. “Global environmental impacts of agricultural expansion: the need for sustainable and efficient practices”. In: *Proceedings of the national Academy of Sciences* 96.11 (1999), pp. 5995–6000.

[194] Goran Tmušić et al. “Current practices in UAS-based environmental monitoring”. In: *Remote Sensing* 12.6 (2020), p. 1001.

[195] Carlo Tomasi and Takeo Kanade. “Shape and motion from image streams under orthography: a factorization method”. In: *International journal of computer vision* 9 (1992), pp. 137–154.

[196] Kumar Puran Tripathy and Ashok Kumar Mishra. “How unusual is the 2022 European compound drought and heatwave event?” In: *Geophysical Research Letters* 50.15 (2023), e2023GL105453. DOI: https://doi.org/10.1029/2023GL105453.

[197] Yu-Hsuan Tu et al. “Optimising drone flight planning for measuring horticultural tree crop structure”. In: *ISPRS Journal of Photogrammetry and Remote Sensing* 160 (Feb. 2020), pp. 83–96. DOI: 10.1016/j.isprsjprs.2019.12.006.

[198] Johan Uddling et al. “Evaluating the relationship between leaf chlorophyll concentration and SPAD-502 chlorophyll meter readings”. In: *Photosynthesis research* 91 (2007), pp. 37–46.

[199] *User manual for the SunScan Canopy Analysis System type SS1, https://delta-t.co.uk/wp-content/uploads/2017/02/SSI-UM_v3.3.pdf, Accessed: 2021-10-27.*

[200] Christian Van der Tol et al. “An integrated model of soil-canopy spectral radiances, photosynthesis, fluorescence, temperature and energy balance”. In: *Biogeosciences* 6.12 (Dec. 2009), pp. 3109–3129. ISSN: 1726-4189. DOI: 10.5194/bg-6-3109-2009. URL: https://bg.copernicus.org/articles/6/3109/2009/.

[201] Juan Quirós Vargas et al. “Unmanned Aerial Systems (UAS)-Based Methods for Solar Induced Chlorophyll Fluorescence (SIF) Retrieval with Non-Imaging Spectrometers: State of the Art”. In: *Remote Sensing* 12.10 (2020). ISSN: 2072-4292. DOI: 10.3390/rs12101624. URL: https://www.mdpi.com/2072-4292/12/10/1624.

[202] Aleixandre Verger et al. “Green area index from an unmanned aerial system over wheat and rapeseed crops”. In: *Remote Sensing of Environment* 152 (Sept. 2014), pp. 654–664. ISSN: 00344257. DOI: 10.1016/j.rse.2014.06.006.

[203] Wout Verhoef. “Light scattering by leaf layers with application to canopy reflectance modeling: The SAIL model”. In: *Remote Sensing of Environment* 16 (2 Oct. 1984), pp. 125–141. ISSN: 00344257. DOI: 10.1016/0034-4257(84)90057-9.

[204] Wout Verhoef et al. “Unified Optical-Thermal Four-Stream Radiative Transfer Theory for Homogeneous Vegetation Canopies”. In: *IEEE TRANSACTIONS ON GEOSCIENCE AND REMOTE SENSING* 45.6 (2007), pp. 1808–1822.

[205] Jochem Verrelst, Erika Romijn, and Lammert Kooistra. “Mapping Vegetation Density in a Heterogeneous River Floodplain Ecosystem Using Pointable CHRIS/PROBA Data”. In: *Remote Sen.* 4.9 (2012), pp. 2866–2889. ISSN: 2072-4292.

[206] Jochem Verrelst et al. “Machine learning regression algorithms for biophysical parameter retrieval: Opportunities for Sentinel-2 and -3”. In: *Remote Sens. Environ.* 118 (2012), pp. 127–139. ISSN: 0034-4257.

[207] Jochem Verrelst et al. “Quantifying vegetation biophysical variables from imaging spectroscopy data: a review on retrieval methods”. In: *Surveys in Geophysics* 40 (2019), pp. 589–629.

[208] Nastassia Vilfan et al. “Fluspect-B: A model for leaf fluorescence, reflectance and transmittance spectra”. In: *Remote Sensing of Environment* 186 (2016), pp. 596–615. ISSN: 00344257. DOI: 10.1016/j.rse.2016.09.017. URL: http://dx.doi.org/10.1016/j.rse.2016.09.017.

[209] Juan Villacrés and Fernando A. Auat Cheein. “Construction of 3D maps of vegetation indices retrieved from UAV multispectral imagery in forested areas”. In: *Biosystems Engineering* 213 (Jan. 2022), pp. 76–88. ISSN: 15375110. DOI: 10.1016/j.biosystemseng.2021.11.025.

[210] Juan Villacrés et al. “Retrieval of Vegetation Indices Related to Leaf Water Content from a Single Index: A Case Study of Eucalyptus globulus (Labill.) and Pinus radiata (D. Don.)” In: *Plants* 10 (4 Apr. 2021), p. 697. ISSN: 2223-7747. DOI: 10.3390/plants10040697.

[211] Robert K Vincent. *An ERTS multispectral scanner experiment for mapping iron compounds*. Tech. rep. 1972.

[212] Jacob Virtue et al. “Thermal sensor calibration for unmanned aerial systems using an external heated shutter”. In: *Drones* 5.4 (2021), p. 119.

[213] Michael Vohland, S. Mader, and Wouter Dorigo. “Applying different inversion techniques to retrieve stand variables of summer barley with PROSPECT+SAIL”. In: *Int. J. Appl. Earth. Obs. Geoinf.* 12.2 (2010), pp. 71–80. ISSN: 0303-2434.

[214] Charles Walthall et al. “A comparison of empirical and neural network approaches for estimating corn and soybean leaf area index from Landsat ETM+ imagery”. In: *Remote Sens. Environ.* 92.4 (2004). 2002 Soil Moisture Experiment (SMEX02), pp. 465–474. ISSN: 0034-4257.

[215] Liang Wan et al. “Unmanned aerial vehicle-based field phenotyping of crop biomass using growth traits retrieved from PROSAIL model”. In: *Computers and Electronics in Agriculture* 187 (Aug. 2021), p. 106304. ISSN: 01681699. DOI: 10.1016/j.compag.2021.106304.

[216] Chuyuan Wang and Soe W Myint. “A simplified empirical line method of radiometric calibration for small unmanned aircraft systems-based remote sensing”. In: *IEEE Journal of selected topics in applied earth observations and remote sensing* 8.5 (2015), pp. 1876–1885.

[217] Li Wang et al. “Phenology Effects on Physically Based Estimation of Paddy Rice Canopy Traits from UAV Hyperspectral Imagery”. In: *Remote Sensing* 13 (9 May 2021), p. 1792. ISSN: 2072-4292. DOI: 10.3390/rs13091792.

[218] Na Wang et al. “Diurnal variation of sun-induced chlorophyll fluorescence of agricultural crops observed from a point-based spectrometer on a UAV”. In: *International Journal of Applied Earth Observation and Geoinformation* 96 (Apr. 1, 2021), p. 102276. ISSN: 1569-8432. DOI: 10.1016/j.jag.2020.102276. URL: https://www.sciencedirect.com/science/article/pii/S0303243420309193 (visited on 04/14/2023).

[219] Na Wang et al. “Decoupling physiological and non-physiological responses of sugar beet to water stress from sun-induced chlorophyll fluorescence”. In: *Remote Sensing of Environment* 286 (Mar. 2023), p. 113445. ISSN: 00344257. DOI: 10.1016/j.rse.2022.113445.

[220] Michelle Watt et al. “Phenotyping: New Windows into the Plant for Breeders”. In: *Annu. Rev. Plant Biol.* 71.1 (2020), pp. 689–712.

[221] M. Weiss, F. Jacob, and G. Duveiller. “Remote sensing for agricultural applications: A meta-review”. In: *Remote Sens. Environ.* 236 (2020), p. 111402. ISSN: 0034-4257.

[222] Marie Weiss et al. “Coupling canopy functioning and radiative transfer models for remote sensing data assimilation”. In: *Agricultural and Forest Meteorology* 108 (2 June 2001), pp. 113–128. ISSN: 01681923. DOI: 10.1016/S0168-1923(01)00234-9.

[223] David M. Woebbecke et al. “Color indices for weed identification under various soil, residue, and lighting conditions”. In: *Transactions of the ASAE* 38.1 (1995), pp. 259–269. DOI: doi:10.13031/2013.27838.

[224] Guijun Yang et al. “Unmanned aerial vehicle remote sensing for field-based crop phenotyping: current status and perspectives”. In: *Frontiers in plant science* 8 (2017), p. 1111.

[225] Peiqi Yang, Wout Verhoef, and Christiaan van der Tol. "The mSCOPE model: A simple adaptation to the SCOPE model to describe reflectance, fluorescence and photosynthesis of vertically heterogeneous canopies". In: *Remote sensing of environment* 201 (2017), pp. 1–11.

[226] Peiqi Yang et al. "Fluorescence Correction Vegetation Index (FCVI): A physically based reflectance index to separate physiological and non-physiological information in far-red sun-induced chlorophyll fluorescence". In: *Remote Sensing of Environment* 240 (Apr. 1, 2020), p. 111676. ISSN: 0034-4257. DOI: 10.1016/j.rse.2020.111676. URL: http://www.sciencedirect.com/science/article/pii/S0034425720300456 (visited on 05/28/2020).

[227] Peiqi Yang et al. "SCOPE 2.0: a model to simulate vegetated land surface fluxes and satellite signals". In: *Geoscientific Model Development* 14.7 (July 2021), pp. 4697–4712. ISSN: 1991-9603. DOI: 10.5194/gmd-14-4697-2021. URL: https://gmd.copernicus.org/articles/14/4697/2021/.

[228] Xi Yang et al. "Leaf angle as a leaf and canopy trait: Rejuvenating its role in ecology with new technology". In: *Ecology Letters* (2023). DOI: https://doi.org/10.1111/ele.14215.

[229] Shiyun Yin et al. "Estimating the Horizontal and Vertical Distributions of Pigments in Canopies of Ginkgo Plantation Based on UAV-Borne LiDAR, Hyperspectral Data by Coupling PROSAIL Model". In: *Remote Sensing* 14 (3 Feb. 2022), p. 715. ISSN: 2072-4292. DOI: 10.3390/rs14030715.

[230] Bradley M. Zamft and Robert J. Conrado. "Engineering plants to reflect light: strategies for engineering water-efficient plants to adapt to a changing climate". In: *Plant biotechnology journal* 13.7 (2015), pp. 867–874. DOI: https://doi.org/10.1111/pbi.12382.

[231] Pablo J. Zarco-Tejada et al. "Previsual symptoms of Xylella fastidiosa infection revealed in spectral plant-trait alterations". In: *Nature Plants* 4.7 (June 2018), pp. 432–439. DOI: 10.1038/s41477-018-0189-7.

[232] Yelu Zeng et al. "Estimating near-infrared reflectance of vegetation from hyperspectral data". In: *Remote Sensing of Environment* 267 (Dec. 15, 2021), p. 112723. ISSN: 0034-4257. DOI: 10.1016/j.rse.2021.112723. URL: https://www.sciencedirect.com/science/article/pii/S0034425721004430 (visited on 02/17/2022).

[233] Chunhua Zhang and John M. Kovacs. "The application of small unmanned aerial systems for precision agriculture: a review". In: *Precision agriculture* 13 (2012), pp. 693–712. DOI: https://doi.org/10.1007/s11119-012-9274-5.

[234] Tianxiang Zhang et al. “Bayesian calibration of AquaCrop model for winter wheat by assimilating UAV multi-spectral images”. In: *Computers and Electronics in Agriculture* 167 (2019), p. 105052.

[235] Xiaokang Zhang et al. “Influences of fractional vegetation cover on the spatial variability of canopy SIF from unmanned aerial vehicle observations”. In: *International Journal of Applied Earth Observation and Geoinformation* 107 (Mar. 1, 2022), p. 102712. ISSN: 1569-8432. DOI: 10.1016/j.jag.2022.102712. URL: https://www.sciencedirect.com/science/article/pii/S0303243422000381 (visited on 04/14/2023).

[236] Chuang Zhao et al. “Temperature increase reduces global yields of major crops in four independent estimates”. In: *Proceedings of the National Academy of sciences* 114.35 (2017), pp. 9326–9331.

[237] Guang Zheng and L. Monika Moskal. “Leaf Orientation Retrieval From Terrestrial Laser Scanning (TLS) Data”. In: *IEEE Transactions on Geoscience and Remote Sensing* 50.10 (Oct. 2012), pp. 3970–3979. DOI: 10.1109/tgrs.2012.2188533.

[238] Qian-Yi Zhou, Jaesik Park, and Vladlen Koltun. “Open3D: A Modern Library for 3D Data Processing”. In: *arXiv:1801.09847* (2018).

[239] Matthias Zink et al. “The German drought monitor”. In: *Environmental Research Letters* 11.7 (2016), p. 074002. DOI: DOI:10.1088/1748-9326/11/7/074002.

[240] Xiaochen Zou and Matti Mõttus. “Retrieving crop leaf tilt angle from imaging spectroscopy data”. In: *Agricultural and Forest Meteorology* 205 (2015), pp. 73–82. DOI: https://doi.org/10.1016/j.agrformet.2015.02.016.

[241] Xiaochen Zou et al. “Photographic measurement of leaf angles in field crops”. In: *Agricultural and Forest Meteorology* 184 (2014), pp. 137–146. DOI: https://doi.org/10.1016/j.agrformet.2013.09.010.